



**HAL**  
open science

## MeMoVolc consensual document: a review of cross-disciplinary approaches to characterizing small explosive magmatic eruptions

Lucia Gurioli, D. Andronico, Patrick Bachèlery, Hélène Balcone-Boissard, Jean Battaglia, G. Boudon, Alain Burgisser, M. Burton, Katharine Cashman, Sarah B. Cichy, et al.

### ► To cite this version:

Lucia Gurioli, D. Andronico, Patrick Bachèlery, Hélène Balcone-Boissard, Jean Battaglia, et al.. MeMoVolc consensual document: a review of cross-disciplinary approaches to characterizing small explosive magmatic eruptions. *Bulletin of Volcanology*, 2015, 77, pp.49. 10.1007/s00445-015-0935-x . hal-01170133

**HAL Id: hal-01170133**

**<https://uca.hal.science/hal-01170133>**

Submitted on 17 Nov 2021

**HAL** is a multi-disciplinary open access archive for the deposit and dissemination of scientific research documents, whether they are published or not. The documents may come from teaching and research institutions in France or abroad, or from public or private research centers.

L'archive ouverte pluridisciplinaire **HAL**, est destinée au dépôt et à la diffusion de documents scientifiques de niveau recherche, publiés ou non, émanant des établissements d'enseignement et de recherche français ou étrangers, des laboratoires publics ou privés.



Distributed under a Creative Commons Attribution - NonCommercial 4.0 International License

# MeMoVolc consensual document: a review of cross-disciplinary approaches to characterizing small explosive magmatic eruptions

L. Gurioli<sup>1</sup>, D. Andronico<sup>2</sup>, P. Bachelery<sup>1</sup>, H. Balcone-Boissard<sup>3</sup>, J. Battaglia<sup>1</sup>, G. Boudon<sup>4</sup>, A. Burgisser<sup>5</sup>, S.B. M.R. Burton<sup>6</sup>, K. Cashman<sup>7</sup>, S. Cichy<sup>1</sup>, R. Cioni<sup>8</sup>, A. Di Muro<sup>9</sup>, L. Dominguez<sup>10</sup>, C. D’Orlando<sup>6</sup>, T. Druitt<sup>1</sup>, A.J.L Harris<sup>1</sup>, M. Hort<sup>11</sup>, K. Kelfoun<sup>1</sup>, J.C. Komorowski<sup>4</sup>, U. Kueppers<sup>12</sup>, J.L. Le Pennec<sup>1</sup>, T. Menand<sup>1</sup>, R. Paris<sup>1</sup>, L. Pioli<sup>10</sup>, M. Pistolesi<sup>13</sup>, M. Polacci<sup>6</sup>, M. Pompilio<sup>6</sup>, M. Ripepe<sup>8</sup>, O. Roche<sup>1</sup>, E. Rose-Koga<sup>1</sup>, A. Rust<sup>7</sup>, F. Schiavi<sup>1</sup>, L. Sharff<sup>11</sup>, R. Sulpizio<sup>14</sup>, J. Taddeucci<sup>15</sup>, T. Thordarson<sup>16</sup>

<sup>1</sup> Laboratoire Magmas et Volcans, Université Blaise Pascal - CNRS - IRD, OPGC, 5 rue Kessler, 63038 Clermont Ferrand, France

<sup>2</sup> INGV, Osservatorio Etneo, Sezione di Catania, 95125 Catania, Italy

<sup>3</sup> Sorbonne Universités, UPMC Univ Paris 06, UMR 7193, Institut des Sciences de la Terre Paris (iSTeP) and CNRS, F-75005 Paris, France

<sup>4</sup> Institut de Physique du Globe (IPGP), Sorbonne Paris-Cité, Université Paris Diderot, CNRS UMR-7154, 1 rue Jussieu, 75238 Paris Cedex 05, France

<sup>5</sup> ISTerre Université de Savoie CNRS, 73376 Le Bourget du lac, France

<sup>6</sup> INGV, Sezione di Pisa, 56126 Pisa, Italy

<sup>7</sup> School of Earth Sciences, University of Bristol, United Kingdom

<sup>8</sup> Dipartimento di Scienze della Terra, Università degli Studi di Firenze, 50121 Florence, Italy

<sup>9</sup> Institut de Physique du Globe (IPGP), Sorbonne Paris-Cité, CNRS UMR-7154, Université Paris Diderot, Observatoire Volcanologique du Piton de la Fournaise (OVPF), Bourg Murat, France

<sup>10</sup> Département de Minéralogie, Université de Genève, Switzerland

<sup>11</sup> Klimacampus, CEN, University of Hamburg, Germany

<sup>12</sup> Ludwig-Maximilians-Universitaet (LMU), Munich, Germany

<sup>13</sup> Dipartimento Scienze della Terra, Università degli Studi di Pisa, Italy

<sup>14</sup> Dipartimento di Scienze della Terra e Geo-Ambientali, Università degli Studi di Bari, Italy

<sup>15</sup> INGV, Sezione di Roma, 00143 Roma, Italy

<sup>16</sup> Institute of Earth Sciences (IES), University of Iceland, Reykjavík, Iceland

**Abstract** A workshop entitled “*Tracking and understanding volcanic emissions through cross-disciplinary integration: A textural working group.*” was held at the Université Blaise Pascal (Clermont-Ferrand, France) on the 6-7 November 2012. This workshop was supported by the European Science Foundation (ESF). The main objective of the workshop was to

38 establish an initial advisory group to begin to define measurements, methods, formats and  
39 standards to be applied in the integration of geophysical, physical and textural data collected  
40 during volcanic eruptions. This would homogenize procedures to be applied and integrated  
41 during both past and ongoing events. The workshop comprised a total of 35 scientists from six  
42 countries (France, Italy, Great Britain, Germany, Switzerland and Iceland). The four main  
43 aims were to discuss and define:

- 44 • Standards, precision and measurement protocols for textural analysis
- 45 • Identification of textural, field deposit, chemistry and geophysical parameters that can  
46 best be measured and combined
- 47 • The best delivery formats so that data can be shared between, and easily used by  
48 different groups;
- 49 • Multi-disciplinary sampling and measurement routines currently used, and  
50 measurement standards applied, by each community

51 The group agreed that community-wide, cross-disciplinary integration, centered on defining  
52 those measurements and formats that can be best combined, is an attainable and key global  
53 focus. Consequently, we prepared this paper to present our initial conclusions and  
54 recommendations, along with a review of the current state of the art in this field that  
55 supported our discussions.

56

## 57 **Introduction**

58

59 A major goal of modern volcanology is to relate conditions of magma ascent to the resulting  
60 eruption style using information preserved in volcanic deposits. Because it is impossible to  
61 directly observe magma ascent, vesiculation and fragmentation, one way to obtain  
62 quantitative information on magma-ascent dynamics is through textural quantification of the  
63 sampled particles. Textural quantification involves full description of the vesicle and crystal  
64 properties of erupted products (e.g., Sparks 1978; Sparks and Brazier 1982; Whitham and  
65 Sparks 1986; Houghton and Wilson 1989; Marsh 1988, 1998; Cashman and Marsh 1988,  
66 Toramaru 1989, 1990; Cashman and Mangan 1994; Higgins 2000; 2006; Blower et al. 2002;  
67 Burgisser and Gardner 2005; Shea et al. 2010a; Rust and Cashman 2011; Baker et al. 2012  
68 and references therein). Magma viscosity, ascent rate, vesiculation processes, fragmentation  
69 style and explosion dynamics all imprint characteristic and measurable properties on the  
70 textures of volcanic particles, as shown by theoretical and experimental studies (e.g., Rust and

71 Cashman 2011; Gonnerman and Houghton 2012; Degruyter et al. 2012; Nguyen et al. 2013  
72 and references therein). The main assumption is that most of the pyroclast properties are  
73 acquired during ascent in the conduit, with few changes occurring after fragmentation or in  
74 the atmosphere, if the pyroclasts are lapilli size or smaller (e.g., Houghton and Wilson 1989;  
75 Nguyen et al. 2013). Specifically, the textural parameters of the pyroclastic components can  
76 yield insights into the dynamics of explosive eruptions, as reviewed in Table 1.

77 However, the physical characteristics of individual pyroclasts must not be considered in  
78 isolation from detailed studies of (i) the deposits from which they were collected, (ii) their  
79 chemical properties, (iii) geophysical signatures of the related explosive event, or (iv)  
80 petrological and/or analogue experiments. Indeed, attempts to understand eruption dynamics  
81 have been increasingly coupled to traditional fieldwork and geophysical measurements made  
82 synchronously with sample collection. In 2004, a special issue of the *Journal of Volcanology  
83 and Geothermal Research* (Volume 137) focused on multidisciplinary approaches, proposing  
84 “*simultaneous collection of multiple geophysical data sets, such as seismic, infrasonic,  
85 thermal and deformation data, as well as sampling of ejecta and detailed mapping*”. The  
86 argument was that “*complete constraint of a volcanic system is not possible using one data  
87 set, so that an integrated multiparametric approach involving simultaneous collection of  
88 multiple geophysical and petrological data sets will increase our ability to reach tightly  
89 constrained and confident conclusions regarding the mechanics and dynamics of volcanic  
90 systems and eruptions*” (Harris et al. 2004). Since 2004, numerous studies have borne these  
91 predictions out, combining textural data with:

- 92 i. Field deposits (e.g., Polacci et al. 2006a; Rust and Cashman 2007; 2011; Mattsson  
93 2010);
- 94 ii. Petrological data (e.g., Larsen 2008; Shea et al. 2009; 2010b; Burgisser et al. 2010;  
95 Bai et al. 2011);
- 96 iii. Chemical analyses (e.g., Piochi et al. 2005, 2008; Shimano and Nakada 2006;  
97 Noguchi et al. 2006; Costantini et al. 2010; Schipper et al. 2010a; b; c; 2011; 2012;  
98 2013; Balcone-Boissard et al. 2010, 2011, 2012; Shea et al. 2012; 2014)
- 99 iv. Geophysical measurements (e.g., Burton et al. 2007; Gurioli et al. 2008, 2013;  
100 2014; Polacci et al. 2009b; Andronico et al. 2008; 2009a; 2009b; 2013a, 2013b;  
101 Miwa et al. 2009; Miwa and Toramaru 2013; Colò et al. 2010; Landi et al. 2011;  
102 Pistolesi et al. 2011; Leduc et al. 2015)

103 Together, these studies have delivered complete pictures of explosive eruptions and their  
104 dynamics (Fig. 1).

105 Despite this progress, we remain far from establishing the best protocols for sampling  
106 pyroclasts and for correlating and comparing the many parameters that can be measured using  
107 individual clasts and field deposits. Only a few papers address some of these issues (e.g.,  
108 Bonadonna et al 2013; Engwell et al. 2013; Klawon et al. 2014). In addition, no study has yet  
109 attempted to correlate all derivable textural parameters with the full range of multidisciplinary  
110 data available. To partially resolve these issues, a working group funded by the European  
111 Science Foundation, through the MeMoVolc program (<http://www.memovolc.fr/>), was set up.  
112 The group was composed of experts actively working on integration of textural, deposit and  
113 geophysical data, equally balanced between four theme areas: (i) particle-texture studies, (ii)  
114 deposit analysis, (iii) chemistry and (iv) geophysics. The priorities of the meeting were  
115 discussion and definition of:

- 116 • Improved standards, precision and measurement protocols needed by the particle-  
117 texture studies.
- 118 • Best practices for particle-texture studies in order to have comparable datasets from  
119 different types of eruptions.
- 120 • Parameters obtained from particle-texture, deposit, geochemical and geophysical data  
121 that need to be measured, and the best delivery format if each discipline's output is to  
122 be of use to all workers.
- 123 • Multi-disciplinary sampling and measurement routines, as well as measurement  
124 standards.

125 The core communal issues to be explored were agreed on:

- 126 1. What are the best sampling and measurement strategies for the quantification of  
127 pyroclast textural features, and what are their precision and uncertainty?
- 128 2. What are the best sampling and measurement strategies for pyroclastic deposits to  
129 allow textural characterization of their particles?
- 130 3. How can we link chemistry and particle-texture properties?
- 131 4. How can we link geophysical data and the particle-texture quantification?
- 132 5. What is the best multi-disciplinary strategy for combining output from each field in a  
133 meaningful way?

134 The paper reviews these topics in the light of a workshop consensus. Because of the time  
135 constraints and the complexity of the arguments, the paper focuses only on the study of  
136 explosive subaerial magmatic eruptions that generate sustained columns or fountains, and the  
137 associated fallout deposits (Fig. 1). Further workshop or working groups should be organized

138 to synthesise and integrate all work in progress, and already completed, in the areas of  
139 phreatic, phreatomagmatic and submarine explosions, as well as pyroclastic density current  
140 and lava flow deposits (Table 1).

141 The final objective of this paper is to ensure that data collected in the field and laboratory  
142 can be shared effectively and ingested in a multi-disciplinary sense into experiments,  
143 modeling and monitoring. In the longer term, the objective is to publish and update standards,  
144 as well as to propose, support and organize field meetings to test integrated collection  
145 methodologies. The ultimate aim is to increase the number of open-access data-bases of  
146 standard and community-accepted quality, thereby increasing resources available for cross-  
147 disciplinary correlations.

148

### 149 **Sampling of pyroclasts and quantification of their textural features**

150

#### 151 (i) Representative samples

152

153 Pyroclasts reflect degassing of the parent magma, from the conduit to the plume. Part of the  
154 textural signature is assumed to reflect the fragmentation (or explosion) zone. Consequently,  
155 texture can be used as an indicator of magma properties (composition, porosity, connectivity,  
156 permeability, vesicle and crystal content, size, shape and distribution) at that time (Table 1).

157 This assumption has two requirements:

158 i. The textural signature that was quenched immediately at the fragmentation level can  
159 be distinguished from the textural effects of post-fragmentation processes, including  
160 microlite formation and bubble nucleation, expansion, collapse, coalescence and  
161 Ostwald ripening that will change clast vesicularity or vesicle size and shapes once the  
162 pyroclast has been formed (e.g., Thomas et al. 1994; Cashman et al. 1994; Herd and  
163 Pinkerton 1997; Larsen and Gardner 2000; Gurioli et al. 2008; Costantini et al. 2010;  
164 Stovall et al. 2011, 2012). The time window for post-fragmentation changes depends  
165 on magma composition, viscosity and fragmentation depth.

166 ii. Because clast density is also a function of clast size (Houghton and Wilson 1989), only  
167 clasts of similar sizes must be used in order to avoid non-uniform grain-size effects on  
168 textural parameters.

169 We thus recommend choosing samples that are representative of the studied explosion, or  
170 unit, in terms of:

- 171 i. Timing: This requires sampling of narrow stratigraphic intervals (Houghton and  
172 Wilson 1989) in which juvenile clasts of similar dimensions can be assumed to  
173 represent those parts of the magma fragmented at a particular time (n.b. conduit  
174 processes can change over short timescales);
- 175 ii. Distribution: This requires selection of more than one outcrop for each event;
- 176 iii. Degree of fragmentation: This requires selection of a sampling methods that is  
177 appropriate for the the full range of grain sizes in the deposit;
- 178 iv. Componentry: If the juvenile fraction is heterogeneous, then sampling should be done  
179 based on preliminary componentry analysis of the clasts analyzed (e.g., Wright et al.  
180 2011, Eychenne et al 2015)

181 In previous studies, only clast sizes of 16-32 mm, i.e. coarse lapilli (White and Houghton  
182 2006) have been considered for textural purposes. Such clasts were considered to be large  
183 enough to be easily sampled and studied, while being fully representative of the density  
184 variation of the majority of erupted pyroclasts and unaffected by significant post-  
185 fragmentation phenomena (Houghton and Wilson 1989). These requirements are not always  
186 met. In basaltic magma, post-fragmentation effects can be a complication even for these sizes  
187 (e.g., Cashman et al. 1994; Szramek et al. 2006; Costantini et al. 2010; Gurioli et al. 2008;  
188 Pioli et al. 2014; Pistolesi et al. 2008; 2011; Stovall et al. 2011; 2012). In these cases, the  
189 challenge is to identify, quantify and remove post-fragmentation effects in order to isolate  
190 textures preserved across the fragmentation zone. For example, the original shapes of vesicles  
191 may be reconstructed by de-coalescing large vesicles using the presence of broken, or  
192 partially retracted, glassy septa.

193 However, if we study an ash-dominated or a bomb-dominated event, particle-texture  
194 analyses must be performed on the fine or coarse juvenile fragments, respectively. Ash size  
195 particles (<2 mm) have been investigated recently in terms of vesicle and crystal size  
196 distributions (Taddeucci et al. 2002, 2004; Cioni et al. 2008; D’Oriano et al. 2011a, b; Miwa  
197 et al. 2009; 2013; Miwa and Toramaro 2013; Proussevitch et al. 2011; Genareau et al. 2012;  
198 2013; Colucci et al. 2013, Schipper et al. 2013), and an extensive work has been done in the  
199 last 40 years in characterizing ash morphology and deposit componentry (Table 1). For the  
200 ash fraction, post-fragmentation expansion can be excluded (e.g., Proussevitch et al. 2011;  
201 Genareau et al. 2012; 2013; Colucci et al. 2013). Consequently, analyses allow comparison  
202 between morphological and textural features of clasts sampled in proximal and distal areas.  
203 Ash particles can record most of the information related to magma ascent dynamics (e.g.,  
204 decompression-driven microlite crystallization) and fragmentation (Cioni et al. 2008;

205 D’Oriano et al. 2005; D’Oriano et al. 2011a, b; Proussevitch et al. 2011; Genareau et al. 2012;  
206 2013; Colucci et al. 2013). Advantages of studying ash are that it can also be statistically more  
207 representative of the variability of the magma properties and is less affected by density-driven  
208 settling within the plume. However, ash fragments record only small-scale vesicularity. The  
209 integration of observations made on the external shapes of clasts may give information about  
210 the presence and importance of a coarser vesicularity which drives magma fragmentation  
211 (e.g., Proussevitch et al. 2011; Genareau et al. 2012; 2013; Colucci et al. 2013). However,  
212 they cannot provide complete information about the abundance and size of the full vesicle  
213 population, if the magma included bubbles larger than the ash particles. Furthermore, ash  
214 particles are not suitable for permeability studies, as they are often smaller than the bubbles  
215 forming the permeability network. However, the presence of coalesced vesicles in a preferred  
216 direction, and an abundance of ash clasts with an elongate shape, have been interpreted as an  
217 indication of the development of a permeable bubble network (D’Oriano et al. 2011a).

218 Bombs may provide a plethora of information regarding pre-eruptive degassing and ascent  
219 rate (e.g. Hoblitt and Harmon 1993; Wright et al. 2007), timing and degree of thermal  
220 interaction of magma with wall-rock material prior to ejection (Rosseel et al. 2006; Sottili et  
221 al. 2009; 2010), post-fragmentation changes due to bubble growth, coalescence or shape  
222 changes (e.g. Herd and Pinkerton 1997, Shin et al. 2005) and mingling between stagnant and  
223 fresh magma (Gurioli et al. 2014; Leduc et al. 2015).

224

## 225 (ii) Bulk measurements of particle characteristics

226

227 The fastest and most straightforward textural measurement of individual pyroclasts is density  
228 (vesicularity), which provides basic information on processes related to gas exsolution and  
229 escape (Houghton and Wilson 1989). The densities of lapilli and small bombs can be  
230 determined by comparing their weights in water and air following the Archimedes principle.  
231 Clasts can be made impermeable with silicone waterproofing spray, by immersion in cellulose  
232 acetate, or by using Parafilm<sup>TM</sup> wax. This technique is fairly rapid and yields large arrays of  
233 data with a reproducibility within 10-30 kg m<sup>-3</sup> and accuracy within 30 kg m<sup>-3</sup> (Barker et al.  
234 2012). Quicker, more timely and precise, density measurements can now be performed using  
235 a commercial envelope-density measurement device ([http://www.micromeritics.com/Product-  
236 Showcase/GeoPyc-1360-Envelope-Density-Analyzer.aspx](http://www.micromeritics.com/Product-Showcase/GeoPyc-1360-Envelope-Density-Analyzer.aspx)). Following the same principles, a  
237 battery-powered device has been used to vacuum-seal pumice or scoria in plastic bags in the  
238 field (Kueppers et al. 2005).



239 For pyroclasts characterized by fine vesiculation (with largest vesicles smaller than 2-3  
240 mm), the density can be measured with the glass-bead method (Nakamura et al. 2008) that  
241 allows the calculation of the density as well as the volume of an object of irregular size. For  
242 large bombs (from 15 to 40 cm in diameter), a "natural waterproofing" effect was exploited  
243 (Gurioli et al. 2013). Extensive tests showed that decimetric size bombs collected at Stromboli  
244 acquired a "natural waterproofing" from their quenched margins and thus could be weighed in  
245 water without waterproofing. This represents an easy, precise and fast strategy for large  
246 bombs.

247 The derived density distributions, coupled with external morphology variation, can be  
248 used as filters to select a few clasts, representative of the low, modal and high density values,  
249 from each subpopulation observed (e.g., Shea et al. 2010a). Selected clasts are then used for  
250 textural quantification.

251 Other bulk particle-texture measurements include vesicle connectivity, permeability (Klug  
252 and Cashman 1996; Klug et al. 2002; Formenti and Druitt 2003; Rust and Cashman 2004; and  
253 references in Table 1) and electrical conductivity (Le Pennec et al. 2001; Bernard et al. 2007;  
254 Wright et al. 2009; Wright and Cashman 2014). The connectivity measurements are mostly  
255 performed using gas-displacement helium pycnometers, and they deliver first-order  
256 information on the outgassing capacity (i.e., potential for gas loss) of the magma near  
257 fragmentation (Klug et al. 2002; Formenti and Druitt 2003; Giachetti et al. 2010; Shea et al.  
258 2011; 2012). Permeability controls the rate at which magma outgases during decompression.  
259 Several methods exist for permeability measurements in volcanology. Rust and Cashman  
260 (2004) used a commercial permeameter to perform systematic steady-state gas-flow  
261 experiments using porous samples, and the relationship between flow rate and pressure  
262 gradient was determined. They also introduced the Forchheimer equation into volcanology,  
263 which is a modified form of Darcy's law that includes the inertial effect of gas flow, and  
264 specified the importance of this effect in volcanic degassing processes. Mueller et al. (2005)  
265 used gas-pressure decay with time after sudden decompression in a fragmentation bomb for  
266 the permeability measurements, without measuring gas-flow rate. A falling head permeameter  
267 developed by Burbié and Zinszner (1985) has also been used to measure the permeability of  
268 volcanic porous materials (Jouniaux et al. 2000; Bernard et al. 2007). Recently, a low-cost gas  
269 permeameter was developed (Takeuchi and Nakashima, 2005) and improved (Takeuchi et al.,  
270 2008), to measure permeability of natural samples and experimental products. Finally,  
271 electrical conductivity measures how well a material transports electric charge. Rocks, in  
272 general, are poor conductors, whereas ionic fluids are good conductors. Therefore a

273 measurement of conduction through fluid-saturated rocks provides information about the  
274 connected pore pathway through the sample. Although the influence of pathway tortuosity  
275 and pore shape on permeability is useful for numerical simulations on gas percolation, it has  
276 been the object of only a few studies (Table 1).

277

278 (iii) Comparison between 2D and 3D particle-texture measurements

279

280 Two different methods are currently available for extracting vesicle and crystal sizes, shapes  
281 and distributions in pyroclasts. The first is by conversion of 2D data from a planar surface  
282 (such as a thin section or photograph) to 3D data through stereology. The second method  
283 derives 3D data directly from X-ray tomographic reconstructions and visualization of clast  
284 textures without the need of stereological conversions (Song et al. 2001; Shin et al. 2005;  
285 Polacci et al. 2006b; 2008; 2009a, b; 2010; Degruyter et al. 2010b; Gualda et al. 2010;  
286 Giachetti et al. 2011; Baker et al. 2012), using computer software especially developed for  
287 geo-textural purposes (e.g. Ketcham and Carlson 2001; Ketcham 2005; Friese et al. 2013).  
288 Other 3D methods include serial sectioning (e.g. Bryon et al. 1995), serial focusing with  
289 optical microscope (Manga 1998), serial grinding (e.g., Marschallinger 1998a, b, c; Mock and  
290 Jerram 2005), and constructing digital elevation models of individual ash grains to calculate  
291 vesicle volume (Proussevitch et al. 2011). Two-D and 3D observations have different  
292 limitations and potential, and the two methods are becoming complementary, not competitive  
293 (e.g., Giachetti et al. 2011; Baker et al. 2011).

294

295 *2D method*

296 Standard procedures for the 2D method have been recently published for vesicles (Shea et al.  
297 2010a) and crystals (Higgins 2000; 2006). Two-D techniques can yield high-quality data and  
298 account for both vesicle and crystal sizes in the sample and can be applied to particles ranging  
299 in size from bombs (e.g., Gurioli et al. 2014, Leduc et al. 2015) to ash (Miwa et al. 2009;  
300 2013; Miwa and Toramaru 2013). These measurements are best used when there is a broad  
301 size distribution to be measured. The main limitation of the method is that is based on the  
302 assumption of spherical shape of the textural objects, following Sahagian and Proussevitch  
303 (1998). When this conversion is simply obtained by dividing the number of vesicles per unit  
304 area by the median value of diameter of each size class (Cheng and Lemlich 1983), no shape  
305 assumption is made. However, the 3D conversion is more precise when a shape is defined.  
306 Empirical corrections are commonly used for crystal analyses (Higgins 2000 and 2006), but

307 for vesicles, whose shapes are less uniform, they risk introducing systematic, uncontrolled  
308 errors in the data (Sahagian and Proussevitch 1998; Proussevitch et al. 2007a; 2007b).

309

### 310 *3D method*

311 X-ray-computed microtomography is the only available high-resolution, non-invasive 3D  
312 technique that allows reconstruction, visualization and processing of samples. Data  
313 acquisition is generally relatively straightforward, and several scales can be examined and  
314 combined, ranging from centimeters to <1 micron, depending on the resolution (Giachetti et  
315 al. 2011). In addition, the so-called ‘local area’ tomography technique (e.g., Lak et al. 2008)  
316 enables high resolutions to be attained, even with samples larger than the field of view of the  
317 camera. However, 3D quantification of textures can also be labor intensive, depending on the  
318 size of the volume that needs to be analyzed and on the textural parameters required. The  
319 results show the internal structures of samples, highlighting how objects and apertures are  
320 linked together. This information provides an excellent suite of data for studies of vesicle size,  
321 shape and distribution, collapse, deformation, coalescence, permeability, and tortuosity, as  
322 well as for determining crystal volume, size and distribution and visualizing crystal  
323 aggregates in 3D (Polacci et al. 2009a, b; 2012; Bai et al. 2010, 2011; Degruyter et al. 2010a,  
324 b; Zandomeneghi et al. 2010; Gualda 2010a, b; Baker et al. 2012; Castro et al. 2012;  
325 Okumura et al. 2013). Vesicles with complex shapes are easily identified, while in a 2D  
326 section they might be interpreted as two or more vesicles, thus biasing vesicle size distribution  
327 (VSD) and vesicle number density ( $N_v$ ) (e.g. Giachetti et al. 2011). The 3D method is  
328 particularly effective for determining  $N_v$  if the study is focused on a specific size range;  
329 vesicle number densities over a wide range of sizes is achieved with nested studies in which a  
330 series of scans are done at different sizes and resolutions (e.g. Giachetti et al. 2011; Pardo et  
331 al. 2014b). However, the resolution of the reconstruction is still critical. Klug et al. (2002)  
332 showed that vesicle walls may be as thin as 0.1 $\mu$ m. To achieve this sort of spatial resolution  
333 using tomography requires very small samples. When the attained resolution is 5-15  $\mu$ m, thin  
334 vesicle walls are not resolved.

335 There is currently no unique protocol for 3D measurements of different types of  
336 pyroclastic (or lava) samples; however the SYRMEP group of the Elettra Synchrotron Light  
337 Source (Trieste, Italy), together with researchers at McGill University of Montreal and INGV  
338 Pisa (M. Polacci), are developing protocols for volcanic samples of different vesicularities  
339 and crystallinities.

340

341 (iv) Crystal size distribution

342

343 Crystal size distribution (CSD) is a well-established tool for interpreting the physical  
344 processes and environmental variables that drive differentiation and crystallization in magma  
345 chambers and conduits (e.g., Marsh 1988; Cashman and Marsh 1988; Cashman 1992;  
346 Hammer et al. 1999; Cashman and McConnell 2005, Armienti 2008; also see references in  
347 Table 1). CSD, coupled with vesicle distribution data, yield deeper insights into the physical  
348 processes operating in the conduit (e.g., Gurioli et al. 2005; D’Oriano et al. 2005; Piochi et al.  
349 2005; 2008; Noguchi et al. 2006; Giachetti et al. 2010; D’Oriano et al. 2011a; Vinkler et al.  
350 2012). The CSD method has been well tested and widely applied (Table 1), so that it is now  
351 quite straightforward to quantify CSD (Higgins 2000; 2006; and references in Table 1).

352 However, we must keep in mind that crystals are commonly anisotropic, and therefore  
353 shape cannot be ignored. Most studies use the Higgins technique to account for shape.  
354 However, the Higgins method assumes that all crystals are the same shape. This is clearly not  
355 true, as small crystals are often more anisotropic than large crystals. Treating all crystals in the  
356 same way can introduce artifacts (see Castro et al. 2003). In addition, there are still resolution  
357 issues for microlites, as well as problems in both back-scattered electron (BSE) and cathode  
358 ray tube (CRT) analyses when the crystals have a density (*Z* number) near that of the glass.  
359 Several methods can be used to facilitate the extraction and quantification of crystals. CSDs  
360 of larger crystals (phenocrysts, antecrysts, etc.) can be measured from transmitted light  
361 microscopy images of thin sections and analyzed with digital image analysis to automate and  
362 hence speed up the quantification process (e.g., Armienti et al. 1994; Launeau et al. 1994;  
363 Lumberras and Serrat 1996; Goodchild and Fueten 1998; Launeau and Cruden 1998; De  
364 Keyser 1999; Heilbronner 2000; Armienti and Tarquini 2002; Boorman et al. 2004). Tarquini  
365 and Favalli (2010) used a slide scanner to acquire input imagery in transmitted light from thin  
366 sections and GIS software to analyze the data.

367 Crystals can also be identified using a scanner and a polarizing filter placed at different  
368 angles (Pioli et al. 2014). Three pictures are then combined, and their correlation allows the  
369 individual grains to be classified by their characteristic orientation. To measure smaller  
370 crystals (microphenocrysts and microlites), a scanning electron microscope is commonly used  
371 in backscattered electron (BSE) mode (Cashman 1992; Hammer et al. 1999; Cashman and  
372 McConnell 2005; Nakamura 2006; Ishibashi and Sato 2007; Salisbury et al. 2008; Blundy and  
373 Cashman 2008; Wright et al. 2012). Development of rapid x-ray mapping techniques now  
374 allows CSD analysis of x-ray element maps, which provide information on crystal

375 compositions, textures (crystal size, orientation, shape) and modes of minerals (e.g., Muir et  
376 al. 2012; Leduc et al 2015). Another new technique uses an electron backscatter diffraction  
377 detector (EBSD) attached to the SEM to obtain crystal orientations, which can provide  
378 insights into shearing, accumulation and degassing processes (Prior 1999; Prior et al. 1999;  
379 Hammer et al. 2010). Chemical mapping is now routinely and widely used (e.g., Leduc et al.  
380 2015). In contrast, EBSD is more difficult to use and interpreting the data is harder than the  
381 chemical maps. As described in the references cited, it produces a wealth of information on  
382 various minerals, although the monocline structure of the feldspar can be problematic.

383 Crystal size distribution can also be obtained directly in 3D via X-ray computed  
384 microtomography. Using this approach, it is possible to obtain the total crystal volume, as  
385 well as the crystal volume of each mineral phase present: crystallinity, crystal size and crystal  
386 shape (e.g., Zandomeneghi et al. 2010; Voltolini et al. 2011). Again, resolution can be a  
387 problem. First, crystals may span a large size range, which requires imaging at several  
388 different resolutions (e.g., Pamukcu et al. 2010; 2012). Additionally, as in BSE analysis, the  
389 compositional similarity between some crystal phases, such as alkali feldspars, and silicic  
390 matrix glass can make automated analysis challenging (e.g., Baker et al. 2012). However,  
391 excellent results can be obtained by working in phase-contrast tomographic mode (Polacci et  
392 al. 2010), and applying a procedure known as phase retrieval to the reconstructed sample  
393 volumes (Arzilli et al. 2013).

394

#### 395 (v) Errors in particle-texture analyses

396

397 Uncertainties in textural analysis are due to several factors. Any textural parameter, such as  
398 porosity or crystal size, has intrinsic measurement errors. These are linked to the apparatus  
399 used and are generally easy to quantify using standards. A good practice, when a new method  
400 is introduced, is to assess its intrinsic error with synthetic samples of well-known particles,  
401 having textural components (e.g. crystals, vesicles/voids) with known size and distribution  
402 (e.g., see review of Rust and Cashman 2004 for permeability, and Baker et al. 2011 for 3D  
403 data from X-ray microtomography). Another type of uncertainty is linked to natural  
404 variability, which is generally approached by using the concept of Representative Elementary  
405 Volume (REV, Bear 1972). Parameters measured in small, neighboring, regions within a  
406 sample have a large variability. As the analyzed regions become larger, this variability  
407 decreases until a steady value is reached at the REV size. One complication is that the REV  
408 should be significantly smaller than the sample (not guaranteed for ash, or even lapilli,

409 particles), and that some parameters have an REV at the deposit scale, which means that many  
410 clasts have to be analyzed. If the sample location is such that eruptive parameters were steady  
411 during deposition, application of REV at the deposit scale allows analysis of magma at the  
412 point of fragmentation in the conduit. Taking porosity as an example, one 2D SEM image will  
413 yield one porosity measurement with a typically small (~1 %) intrinsic error due to  
414 thresholding of the grayscale values that represent vesicles. Several 2D images of the same  
415 sample taken at different locations and/or different resolutions (larger than the REV) typically  
416 yield larger (~10 %) uncertainties that are caused by small-scale spatial heterogeneity. Finally,  
417 if we assume that – or if we have a – very well sorted deposit, then the density distribution of  
418 all clasts at that location indicates the variability of porosity at the conduit scale, which can be  
419 quite large (e.g., Houghton and Wilson 1998). The situation is more complex with poorly  
420 sorted deposits in which particles range from bombs through lapilli to ash.

421 Raw data in terms of size (area, long axis, short axis, perimeter) and orientation of crystals  
422 and vesicles yield negligible intrinsic errors, because they are computed with programs on 2D  
423 binary images with high resolution ( $>10^6$  pixels). In this phase, the uncertainty is due to the  
424 image clean-up process, which is generally unquantified (because it takes too long to have  
425 four people complete the task independently and then take the average for every image).

426 The greatest source of intrinsic error here is thresholding, which is set by the operator  
427 (Baker et al. 2011). When converting 2D data to a 3D projection, however, the error depends  
428 on the stereological model used (i.e. particle shapes have to be assumed, Cashman 1988) and  
429 is thus harder to estimate.

430 Most 2D textural parameters have well-established techniques and protocols to quantify  
431 intrinsic errors, including:

- 432 • VSD (Toramaru 1990; Mangan et al. 1993; Klug and Cashman 1994; 1996; Klug  
433 et al. 2002; Adams et al. 2006b; Shea et al. 2010a),
- 434 • CSD (Higgins 2006), fabric indicators (Launeau et al. 1990),
- 435 • vesicle shape (Moitra et al. 2013),
- 436 • clast shape (Marshall 1987; Capaccioni and Sarocchi 1996; Dellino and Liotino  
437 2002; Riley et al. 2003; Ersoy et al. 2006).

438 However, conversion from 2D to 3D distributions introduces errors linked to stereological  
439 assumptions. The Cheng and Lemlich (1983) method does not involve assumptions of object  
440 shape, but it does not take into account a truncation effect (e.g. Pickering et al. 1995).  
441 Truncation is related to the sensitivity of the measurement process; smaller objects are

442 increasingly difficult to detect. On the other hand, large-scale truncation occurs under several  
443 circumstances related to sample-size (volume and area) limitations. The Sahagian and  
444 Proussevitch (1998) conversion assumes spherical shapes and corrects for the cut effect (this  
445 being the effect induced by rarely cutting a spherical object through its exact center).  
446 Giachetti et al. (2011) found that  $N_v$  obtained by 2D and 3D methods for the same lapilli  
447 agreed within 15 %, and that VSD were also very similar. They recommended the Cheng and  
448 Lemlich (1983) method for 2D vesicle analysis, as the Sahagian and Proussevitch (1998)  
449 method may generate negative values for some size classes.

450 In terms of parameters that we can derive from textural analyses, decompression rate is  
451 probably one of the most important to quantify due to its implications for eruption dynamics.  
452 To achieve this, microlite shape,  $N_v$  and size distribution have been used in combination with  
453 experimental data for low-mass flux and effusive eruptions (Couch et al. 2003; Cashman and  
454 McConnell 2005; Szramek et al. 2006; Clarke et al. 2007; Martel 2012; Wright et al. 2012).  
455 Martel et al. (2006) consider this approach to be highly reliable, because different generations  
456 of microlites (nucleated pre-eruptively in the reservoir or syn-eruptively in the conduit) can be  
457 distinguished on the basis of chemical composition. Decompression rates deduced from  $N_v$   
458 (e.g., Toramaru 2006), however, tend to be maximum estimates, because there could be more  
459 nucleation events during ascent that add to the signature left by decompression. Maximum  
460 decompression rates associated with the final, rapid, stages of ascent could be calculated  
461 directly from the smallest bubbles formed during the final fragmentation event (Giachetti et  
462 al. 2010; Shea et al. 2011; 2012). Another developing method is to use chemical gradients of  
463 volatiles in melt inclusions in crystal embayments to infer rise rates (Ferguson et al. 2013).

464 However, the relationships between bubble shape, nucleation, coalescence, deformation  
465 and/or fragmentation are not well established yet.

466

## 467 **Quantification and sampling of pyroclastic deposits for the textural characterization of** 468 **their components**

469

### 470 (i) Preliminary field studies and sampling strategy

471

472 Field-based studies of pyroclastic deposits aim to relate both the whole-deposit characteristics  
473 (thickness and grain size) and the physical properties of the constituent particles to the  
474 eruption conditions. Particle-texture studies are time consuming, especially when they provide  
475 complete size distributions of the vesicle and crystal population. For these measurements, the

476 choice of a limited number of “representative” clasts selected for the analysis is critical,  
477 particularly when using these data to model eruption processes and their variability in time  
478 and space. Obtaining such clasts requires a cautious sampling strategy with well-defined  
479 scientific goals during field work. These studies are best performed only on well-documented  
480 deposits, supported by a robust stratigraphic reconstruction and correlation, as well as an  
481 accurate compositional stratigraphic framework. When not familiar with the deposit, a  
482 preliminary survey at different locations is useful to evaluate the significance of the outcrops  
483 used for detailed analysis. Well-defined sublayers (or units) should be identified in the deposit  
484 on the basis of clear, unequivocal lithologic and sedimentologic features and cross-correlated  
485 over the whole dispersal area of the deposit. Stratigraphic data are critical for placing each  
486 studied layer within an appropriate temporal framework within the stratigraphic sequence.

487 Pyroclasts can be collected after the eruption, from fall deposits of old (unobserved) or  
488 recent (observed) eruptions, for which sampling is done preferably within hours to days of the  
489 event (e.g., Gurioli et al. 2008; 2013). Sampling may also take place during eruptive activity,  
490 with samples collected using sampling device placed inside the fallout field. Three simple  
491 collection methods that can be applied to active fallout, as currently used, are: (1) the hand  
492 collection method involves collecting (and quenching) bombs or lapilli as they fall out of the  
493 plume by people standing in the active fallout field (e.g., Lautze and Houghton, 2007, 2008;  
494 Gurioli et al. 2014); (2) the “clean surface” strategy, whereby plastic sheets are laid out close  
495 to the vent, or a preexisting surface is cleaned before the eruption. In both cases the pyroclasts  
496 falling in a known area are collected (e.g., Rose et al. 2008; Andronico et al. 2009a; 2013a  
497 and b; Eychenne et al. 2012; Houghton et al. 2013, Harris et al. 2013b, Schipper et al. 2013);  
498 (3) the bucket strategy, in which a large number of buckets are distributed across a discrete  
499 area of fallout for a certain period of time (e.g., Yoshimoto et al. 2005; Swanson et al. 2009;  
500 Bustillos and Mothes 2010). When possible, the aims are to collect a sufficient number of  
501 samples to estimate the magnitude of the event through the mass load per unit area; and to  
502 obtain a sufficient number of clasts for chemical and textural characterization. Other  
503 promising methods are just coming on-line, such as automatic ash sampling collectors (e.g.,  
504 Bernard 2013; Shimano et al. 2013, Marchetti et al. 2013).

505

506 (ii) Definition of essential, basic physical properties of the deposit to the study

507

508 Most particle and deposit texture studies aim at characterizing magma heterogeneity and  
509 ascent dynamics, and at understanding the fragmentation process, beginning with the size,



510 morphology and componentry of the particles (Table 1). Clasts selected for particle-texture  
511 analysis are usually sampled in a deposit at a single location (reference section). Lateral  
512 variability across the deposit is filtered by transport and sedimentation processes, which  
513 primarily depend on eruption intensity, along with related plume dynamics and other dynamic  
514 effects such as wind direction and velocity and rainfall. Therefore, clast properties can differ  
515 both in time (from the base to the top of a vertical sequence) and in space (from the main axis  
516 of dispersal to lateral outcrops at the edge of the fallout zone across the cloud, and from  
517 proximal to distal sites). Volcanic plumes (and clouds) are thus complex systems, the  
518 properties of which do not vary linearly with the main eruption parameters. They are also  
519 affected by external variables, such as wind direction and velocity. The external variables add  
520 additional complexity to the clast-type distribution. For this reason, the deposit should be  
521 preliminarily characterized at least in terms of stratigraphy, dispersal, thickness variation and  
522 volume before more detailed study is initiated (e.g., Fisher and Schmincke 1984; Cas and  
523 Wright 1987; Thordarson et al. 2009; Cioni et al. 2011). Estimation of plume height, eruption  
524 duration, volume and magma eruption rate can then also be derived for past eruptions from  
525 such analyses (e.g., Carey and Sparks 1986; Pyle 1989; Fierstein and Nathenson 1992; Sparks  
526 et al. 1997; Bonadonna et al. 1998; Freundt and Rosi 1998; Bonadonna and Costa 2012;  
527 Fagents et al. 2013).

528

529 (iii) Selecting the outcrop

530

531 There are three basic criteria for sample outcrop selection. First: minimize the effect of wind  
532 dispersal. Outcrops located along the main dispersal axis are preferred to lateral exposures,  
533 unless the effect of wind is the target of study. If wind direction or eruption intensity changes  
534 during different phases of the same eruption, it is more appropriate to sample each tephra  
535 layer at different 'equivalent' locations rather than to collect all samples at a single type  
536 outcrop. If sampling is restricted to a single location, the inferred dispersal pattern and  
537 distance from the main dispersal axis of each layer should be noted and taken into account  
538 when analyzing clast variability among different layers.

539 A second criterion for selecting the outcrop is that clear textural variations among the  
540 juvenile clasts, in terms of color, general morphology, vesicularity, vesicle shape, and  
541 crystallinity should be evaluated in the preliminary field survey, so that any lateral and  
542 vertical variability within the deposit is already defined following field reconnaissance. This

543 ensures that, when clast types are chosen in the laboratory, the main textural types are easily  
544 identified and separated.

545 The third criterion for outcrop selection, if one of the goals of the study is quantification  
546 of the proportion of distinct textural clast types, is to remember that sedimentation from the  
547 volcanic plume is affected by clast density, shape and size (Bonadonna et al. 1998; Pfeiffer et  
548 al. 2005; Barsotti et al. 2008; Eychenne et al. 2013, and references therein). This is especially  
549 relevant when a single explosion produces a juvenile population with a wide range of textural  
550 and other physical features: their relative proportions within the deposit can vary laterally in  
551 the deposit as well as with distance from the vent. Thus, at any single site, the sample is not  
552 necessarily representative of the abundance within the eruption mixture. This is especially  
553 true in the case of small plumes and mid-intensity eruptions (e.g., Rose et al. 2008; Cioni et  
554 al. 2008; 2011; D’Oriano et al. 2011a; Andronico et al. 2013a and references therein). While  
555 the textural features of the different clast types can be studied at a single outcrop, the relative  
556 proportions between clast types need to be determined across the whole deposit by integrating  
557 componentry data on samples collected at outcrops at differing azimuths and distances from  
558 the source.

559

#### 560 (iv) Sampling

561

562 After identification of the outcrops where the deposit shows the best and most complete  
563 exposure, a suitable approach is random collection of a statistically relevant number of clasts  
564 from a single layer. Several techniques can be used, ranging from sieving in the field to find  
565 the dominant clast size (for coarse clasts), or sampling the bulk deposit for later clast selection  
566 in the laboratory (for small clasts). In the case of fine-grained deposits, it can be useful to  
567 apply sampling techniques that preserve structural and textural characteristics of the whole  
568 deposit. Samples can be retrieved using tubes or boxes manually pressed into the deposits, or  
569 carefully carved out and surround-wrapped deposit blocks. In situ and/or laboratory  
570 impregnation techniques of deposits exist for a broad range of grain sizes and compositions  
571 (Bouma 1969), some of which are applicable to fragile or loose volcanic deposits (e.g. Fiske  
572 et al 2009). The applicability of such techniques to fine-to-medium grained volcanic deposits  
573 should be tested, since they would allow both 2D (e.g., X-ray radiography and thin section  
574 analysis) and 3D analysis (X-ray tomography and anisotropy of magnetic susceptibility) to be  
575 applied to deposits, rather than single pyroclasts; these, techniques are frequently used for  
576 hard rocks (e.g., Lanza and Meloni 2006).

577           The number of samples should be defined depending on the purpose of the study.  
578 Fixing the number of samples per stratigraphic layer based on the layer characteristics (e.g.,  
579 extent of zoning/fluctuations in grain-size, componentry, etc.) for characterizing eruption  
580 dynamics, or focusing on the layer thickness for conduit dynamic characterizations, are two  
581 examples of such pre-selection decisions. Before selecting clasts, basic grain-size studies  
582 (when the bulk deposit is collected) on each sampled layer (median and sorting of grain-size  
583 distribution) and componentry analysis should be carried out to ensure effective sub-sampling  
584 for textural studies. Following White and Houghton (2006) componentry analysis is the  
585 subdivision of the sample into three broad components: juvenile, non-juvenile particles and  
586 composite clasts. The juvenile components are vesicular or dense fragments, as well as  
587 crystals, that represent the primary magma involved in the eruption; non-juvenile material  
588 includes accessory and accidental fragments, as well as crystals, that predate the eruption  
589 from which they are deposited. Finally, the composite clasts are mechanical mixtures of  
590 juvenile and non-juvenile (and/or recycled juvenile) clasts. More-detailed componentry can  
591 subdivide the juvenile and non-juvenile materials into subpopulations that have important  
592 dynamic meanings (e.g., Eychenne et al. 2015).

593           Finally, after choosing the size intervals of the clasts for physical and textural  
594 measurements (i.e., bulk and solid density, vesicularity, microtextures, permeability), it is  
595 useful to compare the grain-size distribution of each interval with the total grain-size  
596 distribution of the sampled layers, especially when the grain-size distribution is highly  
597 variable within the sampled stratigraphy. This strategy allows checking of sample  
598 representativeness. For example, sampling may be from (i) bimodal or complex multimodal  
599 distributions, or (ii) anomalous, poorly sorted deposits. In the second case, sampling should  
600 avoid features that can be indicative of contamination from other sources, such as ballistic  
601 components, elutriated ash from pyroclastic density currents or from reworking (e.g., Fierstein  
602 et al. 1997, Eychenne et al. 2012). It is useful, whenever possible, to show variance, or  
603 invariance, of the textural features by comparing data collected in the selected size class with  
604 textural data for different size classes. This should, at least, be carried out for a few selected  
605 samples.

606

## 607 **How to link petrological, geochemistry and textural quantifications**

608

609 (1) Initial parameters and conduit processes

610

611 Geochemical and petrological analysis of pyroclastic products can constrain the initial  
612 conditions in the shallow crustal holding chamber through to the surface via the conduit  
613 system (Fig. 1). In transit through this system, the textural features are imprinted on the  
614 pyroclasts quenched upon eruption. The geochemical and petrologic analysis can help:

- 615 • Define pre-eruptive P-T storage conditions from mineral-melt equilibria or  
616 disequilibria (e.g., Rutherford et al. 1985; Scaillet and Evans 1999; Pichavant et al.  
617 2002; Blundy and Cashman 2008; Schipper et al. 2010b);
- 618 • Assess initial viscosity, temperature, melt composition and volatile budget, including  
619 input of gases from deeper sources (e.g., Wallace 2001; Blundy and Cashman 2008;  
620 Métrich et al. 2010);
- 621 • Define the evolution of volatile contents (specifically Cl, F, S, H<sub>2</sub>O, CO<sub>2</sub>) using  
622 electron probe, ion probe (SIMS), Raman and FTIR in melt inclusions and host  
623 minerals, while combining results with vesiculation studies and gas release  
624 measurements (e.g., Wallace 2005; Métrich and Wallace 2008, Schipper et al. 2010c).  
625 In such a way we can determine whether the magma was saturated, over-saturated or  
626 under-saturated at a certain depth, and how these conditions affect vesiculation in the  
627 conduit (e.g., Anderson 1991; Hurwitz and Navon 1994; Dixon 1997; Roggensack et  
628 al. 1997; Schipper et al. 2012);
- 629 • Measure residual volatiles in glasses and bulk-rock samples to reveal how degassed  
630 the magma is (Newman et al. 1988; Villemant and Boudon 1998; Shea et al. 2014);
- 631 • Provide variable diffusion of stable elements (<sup>6</sup>Li, <sup>7</sup>Li, H/D, <sup>10</sup>B, <sup>11</sup>B) or radiogenic  
632 isotopes (<sup>210</sup>Pb-<sup>226</sup>Ra), which are used as tracers for melt degassing and interaction  
633 with hydrothermal fluids (e.g., Berlo et al. 2004; Kent et al. 2007; Humphreys et al.  
634 2008b; Schiavi et al. 2010; Berlo and Turner 2010; Vlastélic et al. 2011);
- 635 • Measure mineral diffusion profiles and derive pre-eruptive residence times, ascent  
636 rates and cooling rates (e.g., Kahl et al. 2011);
- 637 • Provide crystal shapes, zoning schemes, and dissolution stages, while determining  
638 which magmatic process and physical parameters control crystal shape/zoning (e.g.,  
639 Hammer and Rutherford 2002; Rutherford and Devine 2003; Blundy et al. 2006; Costa  
640 et al. 2008; Streck 2008);

641 In addition, laboratory petrological investigations can provide:

- 642 - Experimental observations on phase equilibria (mineral-melt-vapor), crystallization  
643 paths and liquid line of descent (e.g., Hammer and Rutherford 2002; Couch et al.  
644 2003; Blundy et al. 2006; Hammer 2008);
- 645 - Calibration of decompression rates. While this has been carried out for rhyolitic  
646 systems (e.g., Mourtada-Bonnefoi and Laporte 2002, 2004; Mangan and Sisson 2005;  
647 Gardner 2007; Cichy et al. 2011; Cluzel et al. 2008) and phonolitic systems (e.g.,  
648 Larsen 2008; Shea et al. 2010b), there are ongoing studies on basaltic systems (Bai et  
649 al. 2008; Lesne et al. 2011; Pichavant et al. 2013);
- 650 - Diffusion coefficients of relevant chemical elements, including volatiles, to improve  
651 kinetic modeling (Dohmen et al. 2007; Chakraborty 2008);
- 652 - Relationships between crystal morphologies, cooling rates and degree of undercooling  
653 (e.g., growth of crystals with hopper and swallow tail shapes experiencing rapid late-  
654 stage crystallization; Faure et al. 2003, 2007);
- 655 - Surface flux of volatiles (i.e. what leaves the system; see reviews by Fischer 2008;  
656 Pyle and Mather 2009) compared with melt inclusion data (i.e. what is in the system  
657 initially; e.g., Le Voyer et al. 2010; Rose-Koga et al. 2012; Schiavi et al. 2012).

658

659 2) Where geochemistry can help textural study

660

661 Measurements of volatile contents in quenched, phenocryst-hosted melt inclusions provide  
662 estimates of initial (shallow crustal) values (e.g., Kent 2008). These are minimum estimates,  
663 because H<sub>2</sub>O can leak from melt inclusions during ascent by intracrystalline diffusion as the  
664 far-field environment of the crystal evolves (Chen et al. 2011, 2013). Melt inclusion volatile  
665 contents can be inverted to equivalent saturation pressures using multi-species (e.g., H<sub>2</sub>O-  
666 CO<sub>2</sub>; H<sub>2</sub>O-Cl) solubility laws (using, for example, VOLATILCALC, Newman and  
667 Lowenstern 2002; MELTS, Ghiorso and Sack 1995; Asimow and Ghiorso 1998). These, in  
668 turn, can be used to calculate total pressures (and hence depth) by assuming volatile  
669 saturation, or minimum pressures if the sample is under-saturated in volatiles. Progressive  
670 closure of melt inclusion networks in growing phenocrysts can result in zone-dependent melt  
671 inclusion volatile contents that record the evolution of pressure conditions as magmas migrate  
672 from depth (Blundy and Cashman 2008, and references therein). Combining major element  
673 and volatile compositions of the melt with phenocryst contents allows calculation of initial  
674 magma physical properties (viscosity, density, surface tension, and others). Derivations of

675 such parameters are necessary for modeling magma ascent, vesiculation and groundmass  
676 crystallization.

677 Pre-ascent storage conditions can also be inferred from phase-equilibria studies of natural  
678 compositions. Comparison of natural and experimental phase abundances and compositions,  
679 combined with constraints of volatile content (from melt inclusions) and temperature (from  
680 e.g., Fe-Ti oxides) allows estimation of total pressure if the degree of volatile saturation is  
681 established through use of mixed-volatile experiments (Pichavant et al. 2007; Cadoux et al.  
682 2014).

683 Residual volatile content (e.g., H<sub>2</sub>O, CO<sub>2</sub>, SO<sub>2</sub>, Cl, F) measured in the glass or directly  
684 from gases emitted at the vent can be correlated with textures (e.g., Piochi et al. 2005; 2008;  
685 Schipper et al. 2010a; Balcone-Boissard et al. 2011, 2012; Shea et al. 2012, 2014; Burton et  
686 al. 2007; Polacci et al. 2009b; Miwa and Toramaru 2013). The residual volatile contents can  
687 also be compared with pre-eruptive volatile contents obtained from melt inclusion to evaluate  
688 both the extent and efficiency of syn-eruptive degassing (e.g., Shimano and Nakada 2006;  
689 Noguchi et al. 2006, Métrich et al. 2001; 2010). Residual water content or Cl content (when  
690 Cl partitions into a H<sub>2</sub>O vapor phase, so that it can thus be used as an indicator of degassing  
691 processes; Balcone-Boissard et al. 2010) is typically plotted against  $V_g/V_l$ , where  $V_g$  is the  
692 volume of vesicles corrected for phenocrysts and  $V_l$  is the volume of melt and microlites  
693 (Villemant and Boudon 1998, Balcone-Boissard et al. 2011, 2012). An important issue is to  
694 assess the extent of post-eruption hydration. Recently, thermal gravimetric studies have  
695 proved to be quite effective in allowing this correction based on oxygen or hydrogen isotopic  
696 compositions (e.g., Giachetti and Gonnerman 2013; Shea et al. 2014). Studies of hydrogen  
697 isotopes, correlated with SEM glass textures, permit distinction of magmatic water from  
698 meteoric water generated by re-hydration (Kyser and O'Neil 1984). Hydration can also be  
699 assessed from the ratio of water species (molecular H<sub>2</sub>O vs. OH) in residual glass, as  
700 determined by FTIR data or Raman analyses (Hammer et al. 1999; Le Losq et al. 2012).

701 Ascent and decompression in the conduit can result in chemical changes that can be  
702 quantified by a range of microbeam analytical techniques (e.g., EPMA, LA-ICPMS, FTIR,  $\mu$ -  
703 Raman). As the pressure drops, H<sub>2</sub>O will migrate out of melt inclusions and crystals (Le  
704 Voyer et al 2010; Hamada et al 2010), and light elements (Li, B) will try to re-establish  
705 equilibrium between crystals, host melt and any vapor or brine phase present (Berlo et al.  
706 2004). At the same time, H<sub>2</sub>O and CO<sub>2</sub> migrating out of melt inclusions will become apparent  
707 as re-entrant tubes at the edges of crystals (Liu et al. 2007; Humphreys et al. 2008a). Each of  
708 these processes will establish diffusive gradients frozen into the pyroclast that can be

709 measured and modelled using experimentally determined kinetic laws to infer decompression  
710 rates during ascent (e.g. Gonnermann and Manga 2013). These decompression rates can then  
711 be compared with values derived from other approaches, including those based on analyses of  
712 microlite sizes and shapes, vesicle number densities, and hornblende-breakdown reactions  
713 (e.g., Martel 2012; Cluzel et al. 2008; Giachetti et al 2010; Shea et al. 2011).

714

### 715 3) Contentious points

716

717 Care needs to be taken when converting decompression rate to magma ascent rate, and  
718 especially when comparing decompression rates obtained using different methods. Pressure  
719 gradients in conduits are highly nonlinear due to the strong effect of dissolved H<sub>2</sub>O on magma  
720 viscosity, particularly at low H<sub>2</sub>O contents (Gonnermann and Manga 2013). Moreover,  
721 different processes will likely record different decompression rates, according to the time  
722 available for the process to take place. For example, microlite growth is relatively slow, so  
723 that microlite size and shape distributions are likely to record an average decompression rate  
724 during ascent (Martel 2012). Bubble nucleation and growth, on the other hand, can occur very  
725 rapidly, so that  $N_v$  may record just the peak decompression rate immediately beneath the  
726 fragmentation zone (Cluzel et al. 2008; Giachetti et al 2010). Comparison of rate calculations  
727 from different methods therefore requires caution. However, integration of decompression  
728 rates as obtained from different textural and chemical characterizations, when combined with  
729 mass eruption rate estimation from deposit analysis or direct observations, can provide  
730 quantitative insights into the processes involved in magma ascent from the deep source to the  
731 surface.

732 Another outstanding issue is the role of dense clasts. That is, did they originate (i) from  
733 magma quenched at depth prior vesiculation, (ii) by vesicle collapse in an originally vesicular  
734 clast, (iii) from volatile-poor magma or from recycling? It is important to provide a correct  
735 interpretation, because the three conclusions relate to very different mechanisms. In several  
736 eruptions it has been found that the densest clasts were depleted in water through syneruptive  
737 bubble collapse and coalescence (Rust and Cashman 2007; Piochi et al. 2008, Shea et al.  
738 2014). In Plinian eruptions at Vesuvius (Pompeii and Avellino), the densest clasts have been  
739 interpreted as magma that lost water during transition from closed-to open-system degassing  
740 (Balcone-Boissard et al. 2011; 2012). Water depletion can also result from syn-eruptive  
741 processes, such as clast recycling at magmatic temperature (Gurioli et al. 2014) and intrinsic  
742 magmatic redox conditions, as shown by the experiments of D’Oriano et al. (2012). No study

743 has yet have demonstrated that dense clasts retain all of their original gas and were quenched  
744 at great pressure.

745 Another key question is whether the measured compositions (including volatile content)  
746 of bulk rock, glass, or minerals represent equilibrium or disequilibrium processes, and if  
747 equilibrium or disequilibrium conditions pertain to local subsystems or to the whole magmatic  
748 body under investigation (see for example Pichavant et al. 2007). Chemical species with  
749 different diffusivities, for example, record equilibrium or non-equilibrium conditions in the  
750 same sample (e.g. De Campos et al. 2008; Schipper et al. 2012). Equilibrium kinetics is also  
751 composition-dependent, because it is dictated in part by melt viscosity which is itself related  
752 to viscosity. This issue will generally affect silicic to intermediate magmas more than basaltic  
753 magmas. However, we note that even for basaltic systems crystal-fluid-bubble magma  
754 mixtures can achieve apparent viscosities that range over six orders of magnitude, up to  $10^6$   
755 Pa s (e.g., Gurioli et al. 2014), depending on the degree of cooling, degassing and  
756 crystallization. Such rheological variation even within a single composition, and its effect on  
757 eruption mechanisms, deserves increased attention.

758

### 759 **How to link the geophysical data with pyroclast textural quantification**

760

761 A wide array of remote sensing and geophysical approaches can be used to parameterize an  
762 explosive event, both within and outside the conduit (Fig. 1). Geophysical signals are  
763 generated by fluid and gas flow in the magma-filled part of the conduit and during  
764 fragmentation. Magma-gas ascent dynamics and conduit conditions extracted from  
765 geophysical data for this part of the system are particularly difficult to validate because the  
766 system cannot be directly observed. They are thus effectively “invisible” to direct observation.  
767 Measurements outside the conduit can be made of the emitted mixture of gas and particles as  
768 it (i) exits the vent, (ii) ascends above the vent as a plume, and then (iii) drifts away from the  
769 vent as the cloud. Models and dynamic parameters extracted for geophysical and remote  
770 sensing data outside the conduit are a little easier to validate because they can be directly  
771 observed.

772 The invisible part of the system is the realm of studies using seismic, pressure  
773 (infrasonic), and deformation data. All three data sets have long been shown capable of  
774 detecting the geophysical signature of explosive events spanning weakly explosive Hawaiian-  
775 to-Strombolian through Plinian events. Seismic data sets are available, for example, for gas-  
776 pistonning events, puffing, fountains, and strombolian eruptions at mafic systems (e.g.,



777 Goldstein and Chouet 1994; Ripepe et al. 1996; Sciotto et al. 2011; Ripepe and Braun 1994),  
778 as well as for events that generate somewhat larger plumes during silicic eruptions, as at  
779 Santiaguito, Soufriere Hills, and Redoubt. Associated pressure impulses (typically recorded  
780 by infrasound and barometers) have long been recorded for such energetic events, famous  
781 examples including the pressure response to the 1883 eruption of Krakatoa and the 1967  
782 caldera-forming eruption of Fernandina (Simkin and Howard 1970). Magma-gas ascent has  
783 also been shown to generate rapid, but recordable, deformation signals detected by tiltmeters  
784 (Aoyama and Oshima 2008; Genco and Ripepe 2010; Iguchi et al. 2008; Zobin et al 2007).

785 Velocities, masses and size distributions of particles leaving the vent have typically been  
786 measured by visible and thermal video (e.g., Chouet et al. 1974; Ripepe et al. 1993; Harris et  
787 al. 2012; Delle Donne and Ripepe 2012; Taddeucci et al. 2012; Bombrun et al. 2014; Gaudin  
788 et al., 2014a, b) and Doppler radar (e.g., Dubosclard et al 1999; Hort and Seyfried 1998; Vöge  
789 et al 2005; Gouhier and Donnadieu 2008; 2011; Gerst et al 2013). Infrasonic array methods  
790 are also available to locate the emission in x,y space (Ripepe and Marchetti 2002). Plume  
791 front velocities, density and entrainment rates have also been successfully tracked using  
792 visible and thermal cameras, as well as radiometers, for a few stronger, ash-rich, buoyant  
793 plumes at Stromboli, Santiaguito and Eyjafjallajökull (Patrick 2007; Sahetapy-Engel and  
794 Harris 2009; Bjornsson et al. 2013; Valade et al. 2014); See Chapter 9 of Harris (2013) for  
795 review.

796 Satellite remote sensing has long been used to track and measure properties of the  
797 eruption cloud as it drifts and disperses. These data are available for all cloud sizes, from  
798 those associated with small Strombolian and fountaining events (e.g., Heiken and Pitts 1975;  
799 Dehn et al. 2000; 2002) to sub-Plinian and Plinian events (e.g., Holasek and Self 1995;  
800 Koyaguchi and Tokuno 1993; Holasek et al. 1996). Cloud dispersion dynamics are especially  
801 well revealed by geostationary satellite data with nominal imaging of one image every 15  
802 minutes and higher. Basic cloud properties that can be measured by satellite data include  
803 cloud dimensions, drift velocity and height (e.g., Robock and Matson 1982; Denniss et al.  
804 1998; Aloisi et al. 2002; Zakšek et al 2013). Prata (1989) and Wen and Rose (1994)  
805 introduced a method to potentially extract particle size distribution and mass from “split  
806 window” (10-12  $\mu\text{m}$ ) thermal data. While specially modified ground-based thermal cameras  
807 were adapted to extract ash particle size and plume mass (Prata and Bernardo 2009), newly  
808 available technology such as LiDAR and PLUDIX were shown of value in detecting, tracking  
809 and measuring fine particles in the Eyjafjallajökull cloud (e.g., Bonadonna et al. 2011).  
810 Disdrometers and ash collectors, however, currently show greater potential for measuring

811 particle size and terminal velocity (Marchetti et al. 2013; Shimano et al. 2013) than PLUDIX,  
812 which was designed more for meteorological applications (Caracciolo et al. 2006; Prodi et al.  
813 2011).

814 For the gas content of the cloud, satellite-based sensors such as TOMS, AIRS, OMI,  
815 MODIS, GOME and IASI have been used to obtain the SO<sub>2</sub> content in the far field, once the  
816 gas cloud has decoupled from the ash cloud (e.g., Krueger et al. 1990; Carn et al. 2003; 2005;  
817 Watson et al. 2004; Yang et al. 2007; Thomas et al. 2011; Rix et al. 2012; Walker et al. 2012).  
818 Ground-based sensors, such as COSPEC, FLYSPEC and DOAS (e.g., Caltabiano et al. 1994;  
819 Horton et al. 2005; Oppenheimer et al. 2011), have been used to measure SO<sub>2</sub> fluxes relatively  
820 close to the source; see Williams-Jones et al (2008) for full review. These approaches have  
821 been recently supplemented by SO<sub>2</sub> camera systems, which allow 2D images of SO<sub>2</sub>  
822 concentrations to be collected at ~1 Hz rates (Mori and Burton 2006). Such studies have,  
823 though, tended to focus on passive degassing and gas-puffing systems, because the presence  
824 of ash interferes with UV-light transmission on which the technique relies, making  
825 measurements problematic. Recently, SO<sub>2</sub> cameras have been used to measure the gas masses  
826 and fluxes involved in discrete explosive events (Mori and Burton 2009; Holland et al 2011;  
827 Barnie et al. 2014).

828 However, none of these remote sensing techniques directly collects or makes contact with  
829 the magma or particles they measure. Thus the need exists for quality ground-truth data to  
830 validate particle velocities and sizes extracted from what is, basically, an electronic response,  
831 as well as to test the assumptions and models used to convert received “power” to a more  
832 meaningful and useful parameter (such as mass). At the same time, any single data set can be  
833 inverted to support a conduit or plume dynamic model; but results need to fall within  
834 constraints provided by ground-truth data. In this case, ground truth is provided by analyses of  
835 the magma and particles themselves to extract parameters such as magma temperature,  
836 chemistry, density, crystallinity and vesicle content, as well as vesicle shape and size and  
837 particle density, size, shape and roughness. Magma ascent, explosion-source and  
838 fragmentation models based on geophysical data likewise need to be consistent with  
839 independent measurements made for physical volcanology for the same processes if they are  
840 to be valid. We explore below these needs, mostly focusing on weakly explosive, basaltic  
841 cases, the usual targets because they provide a reliable and easy-to-measure source for testing  
842 new technology, methods and algorithms for ground-based geophysical enquiry.

843

844 *The basic need: Realistic assumptions and validation*

845 The basic response of a remote sensing instrument is a voltage which, through calibration, can  
846 be converted at higher level physical value, such as spectral radiant intensity or power. The  
847 conversion of this value to higher level and more volcanologically useful parameters (such as  
848 particle-size distribution, mass flux or plume density) requires an increasingly complex  
849 system of assumption stacking. Thus, to adequately reduce geophysical data, a number of  
850 input parameters are required and many assumptions need to be made, all of which can be  
851 provided by the physical volcanological community. Data sets from this community,  
852 especially if provided simultaneously with geophysical data collection during an active event,  
853 or provided as a library typical of that event, can also be used to “ground truth” or check the  
854 precision and reality of the geophysically applied input or generated output.

855 Seismic signals that accompany explosions are primarily short period (SP; high frequency  
856  $> 1$  Hz) signals which are typically termed “explosion quakes”. These usually have high  
857 amplitudes and mostly include frequencies up to a few hertz, with a possible higher frequency  
858 acoustic phase (McNutt 1986, Mori et al. 1989, Braun and Ripepe, 1993). Below these  
859 frequencies, short period (SP) signals are often hidden by very-long period (VLP) components  
860 with much lower amplitudes (Neuberg et al. 1994; Kaneshima et al. 1996). In spite of an  
861 enormous amount of work, it remains unclear as to how we can explain the VLP seismic  
862 component, which itself is only one part of the seismic signal. It also remains unclear as to  
863 whether, and/or how, SP and VLP components are related to the magnitude and intensity of an  
864 explosion, although attempts have been made using tremor (Brodsky et al. 1999; Nishimura  
865 and McNutt 2008; Prejean and Brodsky 2011). Clearly, better coupling with the physical  
866 volcanology community could help narrow down much uncertainty and allow progress  
867 towards better models to untangle the seismic signal associated with discrete explosive events.

868 Delay times in the arrival of seismic, infrasonic and thermal signals have been commonly  
869 used to assess the depth at which various physical processes occur in explosive basaltic  
870 systems (e.g., Ripepe and Braun 1994; Ripepe et al. 2001; 2002; Harris and Ripepe 2007).  
871 However, the sound speed in the conduit needs to be assumed if, for example, the thermal-  
872 infrasound delay is to be used to obtain the fragmentation depth. This will vary strongly with  
873 conditions in the empty portion of the conduit, including mixture density, gas-to-particle ratio,  
874 and temperature of the mixture through which the sound is propagating. Thus we need to  
875 know these variables if we are to provide a realistic sound speed value and hence infer a  
876 plausible depth. We thus need to constrain two fundamental parameters to strengthen  
877 geophysical modelling of the shallow explosion mechanism and depth. First, the magma  
878 crystal and bubble content (as well as size, shape and distribution), plus fluid chemistry and

879 temperature, are needed to define magma rheology properties and bubble ascent dynamics.  
880 Second, the exact proportions and character of the mixture of gas and particles that ascends  
881 the final section of the conduit to exit the vent and feed the emission must be known.

882 Velocities, mass fluxes and particle size distributions (PSDs) for lapilli through bomb-size  
883 particles have been derived from high spatial and temporal resolution video data obtained  
884 using both near-infrared and thermal cameras (Chouet et al. 1974; Ripepe et al. 1993; Harris  
885 et al. 2012; Delle Donne and Ripepe 2012; Bombrun et al. 2014).

886 Generally, these studies have focused on Stromboli. For such camera data, the lower limit  
887 of a particle size that can be extracted is limited by pixel size. This is typically about one  
888 centimeter in dimension, depending on the detector's instantaneous field of view and distance  
889 to the target (Harris 2013). A pixel-mixture model can be applied to obtain the size of a sub-  
890 pixel particle, but it needs to assume a temperature for the particle and then uses the pixel-  
891 integrated temperature to solve for the pixel portion occupied by that particle (Harris et al.  
892 2013a). Symmetry then needs to be assumed to convert from particle area to particle volume,  
893 and a density needs to be assumed to derive particle mass (Bombrun et al. 2014). For ash-rich  
894 plumes, methods have been applied to extract total plume mass and air entrainment properties  
895 from ascent dynamics of buoyant thermals (Wilson and Self 1980; Patrick 2007; Valade et al.  
896 2014). However, all methods need particle shape, particle density, plume density and/or size  
897 distribution data to: (i) determine whether the input assumptions are valid; and (ii) ground  
898 truth the remote-sensing-data-derived size and mass data (Harris et al. 2013a and b). The  
899 advantage is, if a validated method can be developed, particle size distribution, mass and mass  
900 flux data for the plume leaving the vent can potentially be provided multiple times per second  
901 using camera data (e.g., Taddeucci et al. 2012; Bombrun et al. 2014).

902 Deducing the erupted mass from Doppler radar data requires the assumption of a particle  
903 size distribution for the eruption. Because this distribution is unknown, an average particle  
904 size can be constrained from the Doppler radar measurement, typically using the eruption  
905 velocities themselves deduced from either terminal fall velocities (Hort et al 2003) or by  
906 discriminating between lapilli (larger than a few millimeters or 1 cm, depending on the radar  
907 wavelength) and fine ash particles (<1 mm) using their temporal velocity evolution (Valade  
908 and Donnadieu 2011). Both methods can be used to obtain an estimate for the erupted mass of  
909 ballistics. We thus need to know whether the constrained average particle size can be used for  
910 mass calculation, whether the assumption is a good approximation, and what the difference  
911 between the derived value and true value is.

912 The radar is able to measure particles of all sizes, provided enough particles are available  
913 to return a signal. The relationship between particle size and number of particles required for  
914 a signal that exceeds the noise level is not linear, however. It also depends on the radar  
915 wavelength and the distance between the radar and target. The smaller the radar wavelength,  
916 and/or the smaller the distance between the radar and target, the smaller the number of fine  
917 particles needed for a return signal. For particles <1 mm, halving the particle size increases  
918 the number of required particles by a factor of 64. Doubling the size of particles to >1 cm  
919 means that only  $\frac{1}{4}$  of the number of particles is needed to return the same signal amplitude. In  
920 addition, radar can measure at points (gates) across the entire plume thickness. Currently,  
921 radar's best role is to provide radial velocity measurements, with well-stated limits as to the  
922 particle size to which these data relate, through the entire plume thickness.

923

#### 924 *Questions, points and issues*

925 The main question from the geophysical community to the textural community is: “*What*  
926 *does the magma look like at the point of fragmentation?*” Geophysical analysts need to know  
927 everything possible about the fragments physically in order to reduce and model the data  
928 correctly. To help with this, we concluded that:

- 929 - Measurements of basic geophysical parameters (such as seismic energy, acoustic  
930 energy, energy partitioning, spectral radiance, and radar power) are the most  
931 straightforward to consider for correlations with parameters derived from physical  
932 volcanology.
- 933 - Multi-disciplinary correlations lead to improved understanding of explosion dynamics,  
934 and only a complete set of measurements can enable a complete and well-constrained  
935 understanding of the system (e.g., Gurioli et al. 2013; 2014; Leduc et al 2015).
- 936 - A wealth of textural and geophysical data exist for Strombolian events, and some data  
937 for larger events. They have been used to define the characteristic geophysical and  
938 textural signatures that allow distinguishing each event type (e.g. Patrick et al. 2007;  
939 Leduc et al 2015). Focus on such relatively low energy events is appropriate, because  
940 they are frequent and approachable (Harris and Ripepe 2007).
- 941 - There is an unfortunate, but understandable, lack of multi-disciplinary data for larger  
942 (Vulcanian-to-Plinian) events; because they are rare. With multi-disciplinary  
943 approaches becoming more routine, this situation is improving.

944 Thermal and SO<sub>2</sub> sensor arrays are becoming increasingly common components of permanent  
945 monitoring arrays at many persistently active sites (Harris 2013). However, such technology

946 will probably never be installed on every potentially active volcano, all of which give seismic  
947 and pressure signals detectable by distant stations. From a practical point of view, it is more  
948 realistic to push forward with operational correlations between seismic-infrasonic metrics and  
949 deposit and particle textural deliverables to understand the ongoing progression of global  
950 volcanic events. In doing so, we must remember that many geophysical signals tend to be  
951 time-averages (e.g., tremor amplitude). We need to consider, however, geophysical  
952 measurements that describe single, discrete explosions if we are to reasonably compare the  
953 data with textural variations between many individual emission events, or emission phases,  
954 that characterize the total eruption total energy is one prime example (e.g., Marchetti et al  
955 2009).

956 We are at an exciting point in our ability to track and understand explosive volcanic  
957 emissions through true cross-disciplinary integration of deposit, geochemical, textural and  
958 geophysical data. Studies are increasingly bringing together multiple approaches in the field  
959 (e.g., Rosi et al. 2006), in the laboratory (Clarke et al. 2009), at large-scale experiments  
960 (Sonder et al. 2013) and during field deployments (Harris et al. 2013b). As a community, we  
961 appear to be converging on the correct, multi-disciplinary approach. We are at the beginning  
962 of a new age, one which links particle texture to seismology (Miwa et al. 2009; Miwa and  
963 Toramaru 2013; Gurioli et al. 2014; Leduc et al. 2015) and infrasound (Colò et al. 2010,  
964 Landi et al. 2011); as well as petrology to geophysics (Saunders et al. 2012; Martí et al. 2013).  
965 Continuation of this trajectory can be aided by further support for pan-disciplinary workshops,  
966 meetings and working groups, the objectives of which are to totally understand the system and  
967 to constrain measurements with the least uncertainty.

968

## 969 **Questions, needs and recommendations**

970

971 Tables 2–4 summarize the main results from the previous discussions. Table 2 is the summary  
972 of major conclusions to date from cross-disciplinary approaches. Table 3 suggests  
973 improvements to methods to facilitate cross-disciplinary approaches. Finally, Table 4 groups  
974 outstanding questions that might be addressed if the recommended methods are used.

975 The list of key issues and questions defined allows us to distil the following community-  
976 wide points and initiatives as priorities:

- 977 1. We need to define, and adhere to, standard sampling, data collection, experimental and  
978 methodological procedures to allow full integration of the four disciplines;

- 979 2. In doing this, we need to understand each other's needs, and then follow each other's  
980 well-recognized sampling etiquette in order to work together as a truly integrated  
981 team;
- 982 3. We should aim to collate all data and measurements that can be provided by each  
983 discipline at some central host site and evaluate whether we need more from each  
984 field;
- 985 4. Quantification and statement of the precision of the measurements must always be  
986 made, and a set of standards must be produced to allow data quality control has to be  
987 followed;
- 988 5. The community needs to explore and discuss the best means to improve the quality of  
989 the measurements and the amount of data available;
- 990 6. Guidelines should be agreed on regarding essential key parameters that need to be  
991 extracted, versus those that are less important. Common standards need to be  
992 established that allow these key parameters to be shared by all groups;
- 993 7. Central to this is creation of an open access data bank to support essential  
994 geophysical, deposit, textural and geochemical data integration and sharing. This  
995 means creation of a repository of data grouped by eruptive style and/or geographic  
996 location into which members can make deposits and withdrawals;
- 997 8. All of this should ideally be integrated into a GIS platform to allow for easy cross-  
998 correlation and comparison of different types of parameters.

999

## 1000 **DynVolc: an integrated database**

1001

1002 Inspired by this effort, a database – DynVolc (Dynamics of Volcanoes) – is now operative  
1003 at <http://wwwobs.univ-bpclermont.fr/SO/televolc/dynvolc/index.php>. This database is part of  
1004 an observation system within the services provided by Observatoire de Physique du Globe de  
1005 Clermont-Ferrand (OPGC). It is an attempt to provide an integrated and accessible library for  
1006 all multi-disciplinary data sets for explosive eruptive events. This database is an integrated  
1007 collection of data from physical and geophysical observations of dynamic volcanic processes.

1008 DynVolc database spans the full range of explosive and effusive activity. Its intent is to  
1009 provide a library of standards for eruptive styles, for each of which the data base provides:

- 1010 • field data (i.e., results of field mapping, outcrop and sample descriptions)
- 1011 • key deposit features (thickness, areal dispersion, sedimentary structure, grain size)
- 1012 • clast characterization (componentry, morphology, density, porosity, permeability)

- 1013 • clast texture (connectivity, vesicle and crystal size and size distributions)
- 1014 • chemical analyses of samples (bulk and glass chemistry)
- 1015 • associated geophysical measurements (e.g., fragmentation depth, ejection and ascent
- 1016 velocity, fragment and gas mass, seismic and acoustic energies)

1017 Integration of these data allows improved, better constrained, insights into the dynamics  
1018 driving each eruptive style. It also allows improved definition of the rheological and  
1019 degassing conditions associated with each activity style. At the same time it provides a library  
1020 of key physical parameters that need to be assumed by geophysical data reduction methods, as  
1021 well as during model-based enquiry.

1022 Central to this initiative will be the transformation of this database into a communal  
1023 databank, involving a web-based GIS platform to allow huge amounts of cross-correlation and  
1024 comparison between parameters relating to different processes and cross-correlation of  
1025 different datasets obtained for the same eruption. It is intended as an open database into which  
1026 anyone can input, and withdraw, citable cross-disciplinary information for scientific analysis.  
1027 At the same time, through this library, we can provide cross-community time series, baseline  
1028 and monitoring data for the full range volcanic activity.

1029

### 1030 **Acknowledgements**

1031 L Gurioli thanks the MeMoVolc, European Science Foundation grant (ref. n. 4253). G  
1032 Valentine D Swanson and the editor, J White are thanked for their constructive reviews. This  
1033 research was financed by the French Government Laboratory of Excellence initiative no  
1034 ANR-10-LABX-0006, the Région Auvergne, and the European Regional Development Fund.  
1035 This is Laboratory of Excellence ClerVolc contribution number XXX

1036

### 1037 **References**

1038 Adams NK, Houghton BF, Hildreth W (2006a) Abrupt transitions during sustained explosive  
1039 eruptions: examples from the 1912 eruption of Novarupta, Alaska. *Bull Volcanol* 69:189–206

1040

1041 Adams NK, Houghton BF, Fagents S, Hildreth W (2006b) The transition from explosive to  
1042 effusive eruptive regime: The example of the 1912 Novarupta eruption, Alaska. *GSA Bulletin*  
1043 118 (5/6):620–634. doi: 10.1130/B25768.1

1044



1045 Alfano F, Bonadonna C, Volentik ACM, Connor CB, Watt SFL, Pyle DM, Connor LJ (2011)  
1046 Tephra stratigraphy and eruptive volume of the May, 2008, Chaiten eruption, Chile. Bull  
1047 Volcanol 73 (5):613–630  
1048

1049 Alfano F, Bonadonna C, Gurioli L (2012) Insights on rhyolitic eruption dynamic from textural  
1050 analysis: the example of the May Chaitén eruption (Chile). Bull Volcanol 74(9):2095-2108. doi  
1051 10.1007/s00445-012-0648-3  
1052

1053 Aloisi M, D’Agostino M, Dean KG, Mostaccio A and Neri G (2002). Satellite analysis and  
1054 PUFF simulation of the eruptive cloud generated by the Mount Etna paroxysm of 22 July  
1055 1998. J Geophys Res 107(B12): 2373. doi: 10.1029/2001JB000630  
1056

1057 Anderson AT (1991) Hourglass inclusions: theory and application to the Bishop Rhyolitic  
1058 Tuff. Am Min 76:530-547  
1059

1060 Andronico D, Corsaro RA, Cristaldi A, Polacci M (2008) Characterizing high energy  
1061 explosive eruptions at Stromboli volcano using multidisciplinary data: an example from the 9  
1062 January 2005 explosion. J Volcanol Geotherm Res 176:541–550.  
1063 doi:10.1016/j.jvolgeores.2008.05.011  
1064

1065 Andronico D, Scollo S, Cristaldi A, Ferrari F (2009a), Monitoring ash emission episodes at  
1066 Mt. Etna: The 16 November 2006 case study. J Volcanol Geotherm Res 180 (2–4):123–134.  
1067 doi:10.1016/j.jvolgeores.2008.10.019  
1068

1069 Andronico D, Cristaldi A, Del Carlo P, Taddeucci J (2009b) Shifting styles of basaltic  
1070 explosive activity during the 2002-03 eruption of Mt Etna, Italy. J Volcanol Geotherm Res  
1071 180(2-4):110-122. doi:10.1016/j.jvolgeores.2008.07.026  
1072

1073 Andronico D, Lo Castro MD, Sciotto M, Spina L (2013a) The 2010 ash emissions at the  
1074 summit craters of Mt Etna: Relationship with seismo-acoustic signals. J Geophys Res 118:51–  
1075 70. doi:10.1029/2012JB009895  
1076

1077 Andronico D, Taddeucci J, Cristaldi A, Miraglia L; Scarlato P, Gaeta M (2013b) The 15  
1078 March 2007 paroxysm of Stromboli: video-image analysis, and textural and compositional  
1079 features of the erupted deposit. *Bull Volcanol* 75:733. doi 10.1007/s00445-013-0733-2  
1080

1081 Aoyama H and Oshima H (2008) Tilt change recorded by broadband seismometer prior to  
1082 small phreatic explosion of Meakan-dake volcano, Hokkaido, Japan. *Geophys Res Lett* 35.  
1083 doi:10.1029/2007GL032988  
1084

1085 Armienti P (2008) Decryption of igneous textures: crystal size distribution tools. *Rev Mineral*  
1086 *Geochem* 69:623-649  
1087

1088 Armienti P, Tarquini S (2002) Power law olivine crystal size distributions in lithospheric  
1089 mantle xenoliths. *Lithos* 65:273–285  
1090

1091 Armienti P, Pareschi M, Innocenti F, Pompilio M (1994) Effects of magma storage and ascent  
1092 on the kinetics of crystal growth. The case of the 1991-92 Mt.Etna eruption. *Contrib Mineral*  
1093 *Petr* 115:402–414  
1094

1095 Arzilli F, Voltolini M, Mancini L, Cicconi MR, Giuli G, Carroll MR (2013) Spherulites in  
1096 trachytic melts. *Mineral Mag* 77(5):622  
1097

1098 Asimow PD, Ghiorso MS (1998) Algorithmic modifications extending MELTS to calculate  
1099 subsolidus phase relations. *Am Mineral* 83:1127–1131  
1100

1101 Bai L, Baker DR, Rivers M (2008) Experimental study of bubble growth in Stromboli basalt  
1102 melts at 1 atmosphere. *Earth Planet Sci Lett* 267:533–547. doi:10.1016/j.epsl.2007.11.063  
1103

1104 Bai L, Baker DR, Hill RJ (2010) Permeability of vesicular Stromboli basaltic glass: Lattice  
1105 Boltzmann simulations and laboratory measurements. *J Geophys Res* 115:B07201.  
1106 doi:10.1029/2009JB007047  
1107

1108 Bai L, Baker DR, Polacci M, Hill RJ (2011) In-situ degassing study on crystal-bearing  
1109 Stromboli basaltic magmas: implications for Stromboli explosions. *Geophys Res Lett*  
1110 38:L17309. doi.org/10.1029/2011GL048540

1111

1112 Baker DR, Polacci M, LaRue A (2011) A study on the reproducibility of counting vesicles in  
1113 volcanic rocks. *Geosphere* 7:70-78

1114

1115 Baker DR, Mancini L, Polacci M, Higgins MD, GAR. Gualda, R.J. Hill, M.L. Rivers (2012)  
1116 An introduction to the application of X-ray microtomography to the three-dimensional study  
1117 of igneous rocks. *Lithos* 148:262-276

1118

1119 Balcone-Boissard H, Villemant B, Boudon G (2010) Behavior of halogens during the  
1120 degassing of felsic magma. *Geochem Geophys Geosyst* 11(9):477–485.  
1121 doi:10.1002/2010GC003028

1122

1123 Balcone-Boissard H, Boudon G, Villemant B (2011) Textural and geochemical constraints on  
1124 eruptive style of the 79AD eruption at Vesuvius. *Bull Volcanol.* doi 10.1007/s00445-010-  
1125 0409-0

1126 Balcone-Boissard H, Boudon G, Ucciani G, Villemant B, Cioni R, Civetta L, Orsi G (2012).  
1127 Magma degassing and eruption dynamics of the Avellino Pumice Plinian eruption of Somma-  
1128 Vesuvius (Italy). Comparison with the Pompeii eruption. *Earth Planet Sci Lett* 331-332:257-  
1129 268. doi: 10.1016/j.epsl.2012.03.011

1130

1131 Barsotti S, Neri A, Scire JS (2008). The VOL-CALPUFF model for atmospheric ash  
1132 dispersal: 1. Approach and physical formulation. *J Geophys Res* 113:B03208.  
1133 doi:10.1029/2006JB004623

1134

1135 Barker SJ, Rotella MD, Wilson CJN, Wright IC, Wysoczanski RJ (2012) Contrasting  
1136 pyroclast density spectra from subaerial and submarine silicic eruptions in the Kermadec arc:  
1137 implications for eruption processes and dredge sampling *Bull Volcanol* 74:1425–1443.  
1138 doi:10.1007/s00445-012-0604-2

1139

1140 Barrie T, Bombrun M, Burton MR, Harris A and Sawyer G (2014) Quantification of gas and  
1141 solid emissions during Strombolian explosions using simultaneous sulphur dioxide and  
1142 infrared camera observations. *J Volcanol Geotherm Res*  
1143 <http://dx.doi.org/10.1016/j.jvolgeores.2014.10.003>

1144  
1145 Bear J (1972) Dynamics of fluids in porous media. Dover, New York  
1146  
1147 Belien IB, Cashman KV, Rempel AW (2010), Gas accumulation in particle-rich suspensions  
1148 and implications for bubble populations in crystal-rich magma. Earth Planet Sci Lett 297(1-  
1149 2):133-140. doi:10.1016/j.epsl.2010.06.014  
1150  
1151 Berlo K, Turner S (2010)  $^{210}\text{Pb}$ - $^{226}\text{Ra}$  disequilibria in volcanic rocks. Earth Planet Sci Lett  
1152 (Frontiers) 296:155-164  
1153  
1154 Berlo K, Blundy J, Turner S, Cashman K, Hawkesworth C, Black S (2004) Geochemical  
1155 precursors to volcanic activity at Mount St. Helens, USA. Science 306:1167-1169  
1156  
1157 Bernard B (2013) Home-made ashmeter: a low-cost, high-efficiency solution to improve  
1158 tephra field-data collection for contemporary explosive eruptions. J Appl Volcanol 2:1  
1159  
1160 Bernard ML, Zamora M, Geraud Y, Boudon G (2007) Transport properties of pyroclastic  
1161 rocks from Montagne Pele'e volcano (Martinique, Lesser Antilles). J Geophys Res  
1162 112:B05205.doi.org/10.1029/2006JB004385  
1163  
1164 Bindeman IN (2003) Crystal sizes in evolving silicic magma chambers. Geology 31:367-370  
1165  
1166 Bjornsson H, Magnusson S, Arason P and Petersen GN (2013) Velocities in the plume of the  
1167 2010 Eyjafjallajökull eruption. J Geophys Res Atmos 118:698–711 doi:10.1002/jgrd.50876  
1168  
1169 Blower JD (2001a) Factors controlling permeability-porosity relationships in magma. Bull  
1170 Volcanol 63:497–504  
1171  
1172 Blower JD (2001b) A three-dimensional network model of permeability in vesicular material.  
1173 Comp Geosci 27:115–119  
1174  
1175 Blower JD, Keating JP, Mader HM, Phillips JC (2001) Inferring volcanic degassing processes  
1176 from bubble size distributions. Geophys Res Lett 28(2):347–350  
1177

1178 Blower JD, Keating JP, Mader HM, Phillips JC (2002) The evolution of bubble size  
1179 distributions in volcanic eruptions. *J Volcanol Geother Res* 120:1–23.  
1180 [http://dx.doi.org/10.1016/S0377-0273\(02\)00404-3](http://dx.doi.org/10.1016/S0377-0273(02)00404-3)  
1181

1182 Blundy J, Cashman KV (2008) Petrologic reconstruction of magmatic system variables and  
1183 processes. *Rev Mineral Geochem* 69:179–239.  
1184

1185 Blundy J, Cashman K, Humphreys M (2006) Magma heating by decompression-driven  
1186 crystallization beneath andesite volcanoes. *Nature* 443:76-80  
1187

1188 Bombrun M, Barra V, Harris A (2014) Algorithm for particle detection and parameterization  
1189 in high-frame-rate thermal video. *J Appl Remote Sens* 8(1):083549.  
1190 [doi:10.1117/1.JRS.8.083549](https://doi.org/10.1117/1.JRS.8.083549)  
1191

1192 Bonadonna C, Costa A (2012) Estimating the volume of tephra deposits: A new simple  
1193 strategy. *Geology* 40 (5):415–418. [doi:10.1130/G32769.1](https://doi.org/10.1130/G32769.1)  
1194

1195 Bonadonna C, Ernst GGJ, Sparks RSJ (1998) Thickness variations and volume estimates of  
1196 tephra fall deposits: the importance of particle Reynolds number. *J Volcanol Geotherm Res*  
1197 81:173–187  
1198

1199 Bonadonna C, Genco R, Gouhier M, Pistolesi M, Cioni R, Alfano F, Hoskuldsson A, Ripepe  
1200 M (2011) Tephra sedimentation during the 2010 Eyjafjallajökull eruption (Iceland) from  
1201 deposit, radar, and satellite observations. *J Geophys Res* 116(B12202).  
1202 [doi:10.1029/2011JB008462](https://doi.org/10.1029/2011JB008462)  
1203

1204 Boorman S, Boudreau AE, Kruger FJ (2004) The lower zone–critical zone transition of the  
1205 Bushveld complex: a quantitative textural study. *J Petrol* 45:1209–1235  
1206

1207 Bouma AH (1969) *Methods for the study of sedimentary structures*. Jhon Wiley and Sons,  
1208 New York, p 458  
1209

1210 Bouvet de Maisonneuve C, Bachmann O, Burgisser A (2009) Characterization of juvenile  
1211 pyroclasts from the Kos Plateau Tuff (Aegean Arc): insights into the eruptive dynamics of a  
1212 large rhyolitic eruption. *Bull Volcanol* 71:643-658  
1213

1214 Braun T, Ripepe M (1993) Interaction of seismic and air waves as recorded at Stromboli  
1215 volcano. *Geophys Res Lett* 20(1):65–68  
1216

1217 Brodsky E, Kanamori H, Sturtevant B (1999) A seismically constrained mass discharge rate  
1218 for the initiation of the May 18, 1980 Mount St. Helens eruption. *J Geophys Res* 104:29,387–  
1219 29,400  
1220

1221 Bryon DN, Atherton MP, Hunter RH (1995) The interpretation of granitic textures from serial  
1222 thin sectioning, image analysis and three-dimensional reconstruction. *Miner Magaz* 59:203-  
1223 211  
1224

1225 Burbié T, Zinszner B (1985) Hydraulic and acoustic properties as a function of porosity in  
1226 Fontainebleau sandstone. *J Geophys Res* 90:11524–11532  
1227

1228 Burgisser A, Gardner JE (2005) Experimental constraints on degassing and permeability in  
1229 volcanic conduit flow. *Bull Volcanol* 67:42–56  
1230

1231 Burgisser A, Poussineau S, Arbaret L, Druitt TH, Giachetti T, Bourdier JL (2010) Pre-  
1232 explosive conduit conditions of the 1997 Vulcanian explosions at Soufrière Hills Volcano  
1233 (Montserrat): I. pressure and vesicularity distributions. *J Volcanol Geotherm Res* 194 (1–  
1234 3):27–41. doi:10.1016/j.jvolgeores.2010.01.008  
1235

1236 Burton MR, Mader HM, Polacci M (2007) The role of gas percolation in quiescent degassing  
1237 of persistently active volcanoes. *Earth Planet Sci Lett* 264:46–60.  
1238 doi:10.1016/j.epsl.2007.08.028  
1239

1240 Bustillos J, Mothes P (2010) Ash falls at Tungurahua volcano: implementation of systematic  
1241 ash collection for quantifying accumulated volumes, *Cities On Volcanoes abstract volume*,  
1242 Tenerife. Canary Island, Spain, May 31 – June 42010, 2.7-O-07  
1243

1244 Büttner R, Dellino P, Zimanowski B (1999) Identifying magma–water interaction from the  
1245 surface features of ash particles. *Nature* 401:688– 690  
1246

1247 Büttner R, Dellino P, La Volpe L, Lorenz V, Zimanowsky B (2002) Thermohydraulic  
1248 explosions in phreatomagmatic eruptions as evidenced by the comparison between pyroclasts  
1249 and products from Molten Fuel Interaction experiments. *J Geophys Res* 107 (B11):2277.  
1250 doi:10.1029/2001JB000511.  
1251

1252 Cadoux A, Scaillet B, Druitt TH, Deloule E (2014). Magma storage conditions of large  
1253 Plinian eruptions of Santorini Volcano (Greece). *J Petrology* 55(6):1129-1171.  
1254 doi:10.1093/petrology/egu021  
1255

1256 Caltabiano T, Roman R and Budetta G (1994) SO<sub>2</sub> flux measurements at Mount Etna (Sicily).  
1257 *J Geophys Res* 99:12 809 – 12 819  
1258

1259 Capaccioni B, Sarocchi D (1996) Computer-assisted image analysis on clast shape fabric from  
1260 the Orvieto-Bagnoregio ignimbrite (Vulsini District, central Italy): implications on the  
1261 emplacement mechanisms. *J Volcanol Geotherm Res* 70(1–2):75-90. doi: 10.1016/0377-  
1262 0273(95)00049-6  
1263

1264 Caracciolo C, Prodia F, Uijlenhoet R (2006) Comparison between Pludix and impact/optical  
1265 disdrometers during rainfall measurement campaigns. *Atmos Res* 82(1-2):137–163  
1266

1267 Carey RJ, Houghton BF, Thordarson T (2009) Abrupt shifts between wet and dry phases of  
1268 the 1875 eruption of Askja Volcano: microscopic evidence for macroscopic dynamics. *J*  
1269 *Volcanol Geotherm Res* 184:256–270  
1270

1271 Carey RJ, Manga M, Degruyter W, Swanson D, Houghton B, Orr T, Patrick M (2012)  
1272 Externally triggered renewed bubble nucleation in basaltic magma: The 12 October 2008  
1273 eruption at Halema‘uma‘u Overlook vent, Kīlauea, Hawai‘i, USA. *J Geophys Res*  
1274 117:B11202. doi:10.1029/2012JB009496  
1275

1276 Carey RJ, Manga M, Degruyter W, Gonnermann H, Swanson D, Houghton B, Orr T, Patrick  
1277 M (2013) Convection in a volcanic conduit recorded by bubbles. *Geology* 41(4):395–398

1278  
1279 Carey S, Sparks RSJ (1986) Quantitative models of the fallout and dispersal of tephra from  
1280 volcanic eruption columns. *Bull Volcanol* 48:109–125. doi:10.1007/BF01046546  
1281  
1282 Carey S, Maria A, Sigurdsson H (2000) Use of fractal analysis for discrimination of particles  
1283 from primary and reworked jökulhlaup deposits in SE Iceland. *J Volcanol Geotherm Res*  
1284 104:65–80  
1285  
1286 Carn SA, Krueger AJ, Bluth GJS, Schaefer SJ, Krotkov NA, Watson IM, Datta S (2003)  
1287 Volcanic eruption detection by the Total Ozone Mapping Spectrometer (TOMS) instruments:  
1288 a 22-year record of sulfur dioxide and ash emissions. In: *Volcanic Degassing* (eds. C  
1289 Oppenheimer, DM Pyle and J Barclay), Geological Society, London, Special Publications,  
1290 213, pp.177-202.  
1291  
1292 Carn SA, Strow LL, de Souza-Machado S, Edmonds Y, Hannon S (2005) Quantifying  
1293 tropospheric volcanic emissions with AIRS: the 2002 eruption of Mt. Etna (Italy). *Geophys*  
1294 *Res Lett* 32(2):L02301. doi:10.1029/2004GL021034  
1295  
1296 Cas RAF, Wright JV (1987) *Volcanic successions: modern and ancient*. Allen & Unwin,  
1297 London, 528p  
1298  
1299 Cashman KV (1988) Crystallization of Mount St. Helens 1980–1986 dacite: A quantitative  
1300 textural approach. *Bull Volcanol* 50(3):194-209. doi:10.1007/BF01079682  
1301  
1302 Cashman KV (1992) Groundmass crystallization of Mount St. Helens dacite, 1980-1986: A  
1303 tool for interpreting shallow magmatic processes. *Contrib Mineral Petrol* 109:431-449  
1304  
1305 Cashman KV (1993). Relationship between plagioclase crystallization and cooling rate in  
1306 basaltic melts. *Contrib Mineral Petr* 113:126-142  
1307  
1308 Cashman KV, Mangan MT (1994) Physical aspects of magmatic degassing II. Constraints on  
1309 vesiculation processes from textural studies of eruptive products. In: M. Carroll (Editor),  
1310 *Volatiles in Magmas*. Mineral Sot Am Washington, DC, pp. 447-478  
1311



1312 Cashman KV, Marsh BD (1988) Crystal size distribution (CSD) in rocks and the kinetics and  
1313 dynamics of crystallization II. Makaopuhi lava lake. *Contrib Mineral Petrol* 99:292–305  
1314

1315 Cashman KV, McConnell S (2005) Transitions from explosive to effusive activity – the  
1316 summer 1980 eruptions of Mount St. Helens. *Bull Volcanol* 68:57-75  
1317

1318 Cashman KV, Mangan MT, Newman S (1994) Surface degassing and modifications to vesicle  
1319 size distributions in Kilauea basalt. *J Volcanol Geotherm Res* 61:45-68  
1320

1321 Castro JM, Cashman KV, Manga M (2003) A technique for measuring 3D crystal-size  
1322 distributions of prismatic microlites in obsidian. *Am Mineral* 88:1230-1240  
1323

1324 Castro JM, Burgisser A, Shipper CI, Mancini S (2012) Mechanisms of bubble coalescence in  
1325 silicic magmas. *Bull Volcanol* 74:2339-2352  
1326

1327 Chakraborty S (2008) Diffusion in solid silicates: A tool to track timescales of processes  
1328 comes of age. *Annu Rev Earth Planet Sci* 36 (1):153-190  
1329

1330 Chen Y, Provost A, Schiano P, Cluzel N (2011) The rate of water loss from olivine-hosted  
1331 melt inclusions. *Contrib Mineral Petrol* 162:625-636  
1332

1333 Chen Y, Provost A, Schiano P, Cluzel N (2013) Magma ascent rate and initial water  
1334 concentration inferred from diffusive water loss from olivine-hosted melt inclusions. *Contrib*  
1335 *Mineral Petrol* 165:525-541  
1336

1337 Cheng HC, Lemlich R (1983) Errors in the measurement of bubble-size distribution in foam.  
1338 *Ind. Eng Chem Fundam* 22:105–109  
1339

1340 Chouet B, Hamisevicz N, McGetchin TR (1974) Photoballistics of volcanic jet activity at  
1341 Stromboli, Italy. *J Geophys Res* 79:4961–4976  
1342

1343 Cichy SB, Botcharnikov RE, Holtz F, Behrens H (2011) Vesiculation and microlite  
1344 crystallization induced by decompression: a case study of the 1991-1995 Mt Unzen eruption  
1345 (Japan). *J Petrol* 52:1469-1492  
1346

1347 Cigolini C, Laiolo M, Bertolino S (2008) Probing Stromboli volcano from the mantle to  
1348 paroxysmal eruptions. In: Annen C, Zellmer GF (eds) *Dynamics of crustal magma transfer,*  
1349 *storage and differentiation.* Geological Society, London, special publication, vol 304.  
1350 Geological Society, London, pp 33–70  
1351

1352 Cimarelli C, Di Traglia F, Taddeucci J (2010) Basaltic scoria textures from a zoned conduit as  
1353 precursors to violent Strombolian activity. *Geology* 38(5): 439-442  
1354

1355 Cioni R, D’Orlando C, Bertagnini A (2008) Fingerprinting ash deposits of small scale eruptions  
1356 by their physical and textural features. *J Volcanol Geotherm Res* 177:277–287  
1357

1358 Cioni R, Bertagnini A, Andronico D, Cole PD, Mundula F (2011) The 512 AD eruption of  
1359 Vesuvius: complex dynamics of a small scale subplinian event. *Bull Volcanol* 73 (7):789-810.  
1360 doi:10.1007/s00445-011-0454-3  
1361

1362 Clarke AB, Stephens S, Teasdale R, Sparks RSJ, Diller K (2007) Petrologic constraints on the  
1363 decompression history of magma prior to Vulcanian explosions at the Soufrière Hills volcano,  
1364 Montserrat. *J Volcanol Geotherm Res* 161:261-274  
1365

1366 Clarke AB, Phillips JC, Chojnicki KN (2009) An investigation of Vulcanian eruption  
1367 dynamics using laboratory analogue experiments and scaling analysis. In: *Studies in*  
1368 *Volcanology: The Legacy of George Walker,* Thordason T, Self S, Larsen G, Rowland SK,  
1369 Höskuldsson Á (eds) *IAVCEI Special Publications in Volcanology* 2: 155-166.  
1370

1371 Cluzel N, Laporte D, Provost A (2008) Kinetics of heterogeneous bubble nucleation in  
1372 rhyolitic melts: implications for the number density of bubbles in volcanic conduits and for  
1373 pumice textures. *Contrib Mineral Petrol* 156:745-763  
1374

1375 Colò L, Ripepe M, Baker DR, Polacci M (2010), Magma vesiculation and infrasonic activity  
1376 at Stromboli open conduit volcano. *Earth Planet Sc Lett* 292 (3–4)  
1377

1378 Colucci S, Palladino DM, Mulukutla GK, Proussevitch AA (2013) 3-D reconstruction of ash  
1379 vesicularity: Insight into the origin of ash-rich explosive eruptions. *J Volcanol Geotherm Res*  
1380 255:98-107  
1381

1382 Costa F, Cohmen R, Chakraborty S (2008) Time scales of magmatic processes from modeling  
1383 the zoning patterns of crystals. In Putirka KD, Tepley FJ (Eds) *Minerals, inclusions and*  
1384 *volcanic processes. Rev Mineral Geochem* 69:545-594  
1385

1386 Costantini L, Houghton BF, Bonadonna C (2010) Constraints on eruption dynamics of  
1387 basaltic explosive activity derived from chemical and microtextural study: the example of the  
1388 Fontana Lapilli Plinian eruption, Nicaragua. *J Volcanol Geother Res* 189 (3–4):207–224.  
1389 doi:10.1016/j.jvolgeores.2009.11.008  
1390

1391 Couch S, Sparks RSJ, Carroll MR (2003) The kinetics of degassing-induced crystallization at  
1392 Soufrière Hills Volcano, Montserrat. *J Petrol* 44(8):1477–1502  
1393

1394 De Campos CP, Dingwell DB, Perugini D, et al. (2008) Heterogeneities in magma chambers:  
1395 Insights from the behavior of major and minor elements during mixing experiments with  
1396 natural alkaline melts. *Chem Geol* 256:131–145. doi: 10.1016/j.chemgeo.2008.06.034  
1397

1398 De Keyser TL (1999) Digital scanning of thin sections and peels. *J Sedim Res* 69:962–964  
1399

1400 Degruyter W, Bachmann O, Burgisser A (2010a) Controls on magma permeability in the  
1401 volcanic conduit during the climactic phase of the Kos Plateau Tuff eruption (Aegean Arc).  
1402 *Bull Volcanol* 72:63–74. doi: 10.1007/s00445-009-0302-x  
1403

1404 Degruyter W, Burgisser A, Bachmann O, Malaspina O (2010b) Synchrotron X-ray  
1405 microtomography and lattice Boltzmann simulations of gas flow through volcanic pumices.  
1406 *Geosphere* 6:470–481  
1407

1408 Degruyter W, Bachmann O, Burgisser A, Manga M (2012) The effects of outgassing on the  
1409 transition between effusive and explosive silicic eruptions. *Earth Planet Sc Lett* 349-350:161-  
1410 170  
1411  
1412 Dehn J, Dean K, Engle K (2000) Thermal monitoring of North Pacific volcanoes from space.  
1413 *Geology* 28(8):755-758  
1414  
1415 Dehn J, Dean KG, Engle K, Izbekov P (2002) Thermal precursors in satellite images of the  
1416 1999 eruption of Shishaldin volcano. *Bull Volcanol* 64:525-545  
1417  
1418 Delle Donne D, Ripepe M (2012) High-frame rate thermal imagery of Strombolian  
1419 explosions: Implications for explosive and infrasonic source dynamics. *J Geophys Res*  
1420 117(B12). doi: 10.1029/2011JB008987  
1421  
1422 Dellino P, La Volpe L (1996a) Image processing analysis in reconstructing fragmentation and  
1423 transportation mechanisms of pyroclastic deposits. the case of Monte Pilato-Rocche Rosse  
1424 eruptions, Lipari (Aeolian Islands, Italy). *J Volcanol Geotherm Res* 71:13–29  
1425  
1426 Dellino P, La Volpe L (1996b) Cluster analysis on ash particles morphology features to  
1427 discriminate fragmentation dynamics in explosive eruptions. *Acta Vulcanologica* 1:31–39  
1428  
1429 Dellino P, Liotino G (2002) The fractal and multifractal dimension of volcanic ash particles  
1430 contour: a test study on the utility and volcanological relevance *J Volcanol Geotherm Res* 113  
1431 (1–2):1-18. doi:10.1016/S0377-0273(01)00247-5  
1432  
1433 Dellino P, Isaia R, La Volpe L, Orsi G (2001) Statistical analysis of textural data from  
1434 complex pyroclastic sequences: implications for fragmentation processes of the Agnano-  
1435 Monte Spina Tephra (4.1 ka), Phlegraean Fields, southern Italy. *Bull Volcanol* 63:443–461  
1436  
1437 Dellino P, Mele D, Bonasia R, Braia G, La Volpe L, Sulpizio R (2005) The analysis of the  
1438 influence of pumice shape on its terminal velocity. *J Geophys Res* 32:L21306.  
1439 doi:10.1029/2005GL023954  
1440

1441 Dellino P, Mele D, Sulpizio R, La Volpe L, Braia G (2012) A method for the calculation of  
1442 the impact parameters of dilute pyroclastic density currents based on deposit particle  
1443 characteristics. *J Geophys Res* 113 (B7). doi 10.1029/2007JB005365  
1444  
1445 Denniss AM, Harris AJL, Rothery DA, Francis PW, Carlton RW (1998) Satellite observations  
1446 of the April 1993 eruption of Lascar volcano. *Int J Remote Sensing* 19(5):801-821  
1447  
1448 Dixon JE (1997) Degassing of alkali basalts. *Am Min* 82:368-378  
1449  
1450 Dohmen R, Becker H-W, Chakraborty S (2007) Fe–Mg diffusion in olivine I: experimental  
1451 determination between 700 and 1,200°C as a function of composition, crystal orientation and  
1452 oxygen fugacity. *Phys Chem* 34:389–407. doi: 10.1007/s00269-007-0157-7  
1453  
1454 D’Oriano C, Poggianti E, Bertagnini A, Cioni R, Landi P, Polacci M, Rosi M (2005) Changes  
1455 in eruptive styles during the A.D. 1538 Monte Nuovo eruption (Phleagrean Fields, Italy): the  
1456 role of syneruptive crystallization. *Bull Volcanol* 67:601–621  
1457  
1458 D’Oriano C, Cioni R, Bertagnini A, Andronico D, Cole PD (2011a) Dynamics of ash-  
1459 dominated eruptions at Vesuvius: the post-512 AD AS1a event. *Bull Volcanol* 73 (6):699-  
1460 715. doi:10.1007/s00445-010-0432-1  
1461  
1462 D’Oriano C, Bertagnini A, Pompilio M (2011b) Ash erupted during normal activity at  
1463 Stromboli (Aeolian Islands, Italy) raises questions on how the feeding system works. *Bull*  
1464 *Volcanol* 73:471-477  
1465  
1466 D’Oriano C, Pompilio M, Bertagnini A, Cioni R, Pichavant M (2012) Effects of experimental  
1467 reheating of natural basaltic ash at different temperatures and redox conditions. *Contrib*  
1468 *Mineral Petrol*. doi: 10.1007/s00410-012-0839-0  
1469  
1470 Dubosclard G, Cordesses R, Allard P, Hervier C, Coltelli C, Kornprobst J (1999) First testing  
1471 of a volcano Doppler radar (Voldorad) at Mount Etna, Italy. *Geophys Rese Lett* 26(22):3389–  
1472 3392  
1473

1474 Eichelberger JC, Carrigan CR, Westrich HR, Price RH (1986) Non-explosive silicic  
1475 volcanism. *Nature* 323:598–602  
1476

1477 Engwell SL, Sparks RSJ, Aspinall WP (2013) Quantifying uncertainties in the measurement  
1478 of tephra fall thickness. *J Applied Volcanol* 2:5. doi:10.1186/2191-5040-2-5.  
1479

1480 Ersoy O, Chinga G, Aydar E, Gourgaud A, Cubuku HE, Ulusoy I (2006) Texture  
1481 discrimination of volcanic ashes from different fragmentation mechanisms: A case study,  
1482 Mount Nemrut stratovolcano, eastern Turkey. *Comput Geosci* 32:936-946  
1483

1484 Eychenne J, Le Pennec JL, Troncoso L, Gouhier M, Nedelec JM (2012) Causes and  
1485 consequences of bimodal grainsize distribution of tephra fall deposited during the August  
1486 2006 Tungurahua eruption (Ecuador). *Bull Volcanol* 74:187–205. doi: 10.1007/s00445-011-  
1487 0517-5  
1488

1489 Eychenne J, Le Pennec JL, Ramón P, Yepes H (2013) Dynamics of explosive paroxysms at  
1490 open-vent andesitic systems: High-resolution mass distribution analyses of the 2006  
1491 Tungurahua fall deposit (Ecuador). *Earth Planet Sci Lett* 361:343-355. doi: 10.10-  
1492 16/j.epsl.2012.11.002  
1493

1494 Eychenne J, Houghton BF, Swanson DA, Carey RJ, Swavely L (2015) Dynamics of an open  
1495 basaltic magma system: The 2008 activity of the Halema‘uma‘u Overlook vent, Kīlauea  
1496 Caldera. *Earth Planet Sci Lett* 409:49-60  
1497

1498 Fagents SA, Gregg TKP, Lopes RMC (2013) *Modeling Volcanic Processes. The Physics and*  
1499 *Mathematics of Volcanism*. Cambridge University Press  
1500

1501 Faure F, Troiliard G, Nicollet C, Montel J-M (2003) A developmental model of olivine  
1502 morphology as a function of the cooling rate and the degree of undercooling. *Contrib Mineral*  
1503 *Petrol* 145 (2):251–263. doi: 10.1007/s00410-003-0449-y  
1504

1505 Faure F, Schiano P, Troiliard G, Nicollet C, Soulestin B (2007) Textural evolution of  
1506 polyhedral olivine experiencing rapid cooling rates. *Contrib Mineral Petrol* 153:405-416  
1507

1508 Ferguson DJ; Plank TA; Hauri EH; Houghton BF; Gonnermann HM; Swanson DA; Blaser  
1509 AP (2013) Comparing eruptions of varying intensity at Kilauea via melt inclusion analysis.  
1510 American Geophysical Union, Fall Meeting 2013, abstract #V33F-07  
1511

1512 Fierstein J, Nathenson M (1992) Another look at the calculation of fallout tephra volumes.  
1513 Bull Volcanol 54:156–167  
1514

1515 Fierstein J, Houghton BF, Wilson CJN, Hildreth W (1997) Complexities of plinian fall  
1516 deposition at vent: an example from the 1912 Novarupta eruption (Alaska). J Volcanol  
1517 Geotherm Res 76:215–227  
1518

1519 Fischer TP (2008) Fluxes of volatiles (H<sub>2</sub>O, CO<sub>2</sub>, N<sub>2</sub>, Cl, F) from arc volcanoes. *Geochem J*  
1520 42:21–38. doi: 10.2343/geochemj.42.21  
1521

1522 Fisher RV, Schmincke H-U (1984) *Pyroclastic rocks*. Springer, Berlin Heidelberg New York  
1523

1524 Fiske RS, Rose TR, Swanson D, Champion D, McGeehin J (2009) Kulanaokuaiki Tephra (ca.  
1525 A.D. 400–1000): Newly recognized evidence for highly explosive eruptions at Kīlauea  
1526 Volcano, Hawai‘i." *GSA Bull* 121:712-728  
1527

1528 Formenti Y, Druitt TH (2003) Vesicle connectivity in pyroclasts and implications for the  
1529 fluidisation of fountain-collapse pyroclastic flows, Montserrat (West Indies). *Earth Planet Sci*  
1530 *Lett* 214:561–574  
1531

1532 Freundt A, Rosi M (1998) *From Magma to Tephra*. Elsevier, New York  
1533

1534 Friese K-I, Cichy SB, Wolter F-E, Botcharnikov RE (2013). Analysis of tomographic mineral  
1535 data using *YaDiV* – Overview and practical case study. *Comput Geosci* 56:92-103  
1536

1537 Gaonac’h H, Lovejoy S, Stix J, Schertzer D (1996a) A scaling growth model for bubbles in  
1538 basaltic flows. *Earth Planet Sci Lett* 139:395–409  
1539

1540 Gaonac’h H, Stix J, Lovejoy S (1996b) Scaling effects on vesicles shape, size and  
1541 heterogeneity of lavas from Mount Etna. *J Volcanol Geotherm Res* 74:131–153

1542  
1543 Gaonac'h H, Lovejoy S, Schertzer D (2003) Percolating magmas and explosive volcanism.  
1544 *Geophys Res Lett* 30. doi:10.1029/2002GL0116022  
1545  
1546 Gaonac'h H, Lovejoy S, Schertzer D (2005) Scaling vesicle distributions and volcanic  
1547 eruptions. *Bull Volcanol* 67(4):350–357  
1548  
1549 Gardner JE (2007) Heterogeneous bubble nucleation in highly viscous silicate melts during  
1550 instantaneous decompression from high pressure. *Chem Geol* 236:1-12  
1551  
1552 Gaudin D, Moroni M, Taddeucci J, Scarlato P, Shindler L. (2014a) Pyroclast Tracking  
1553 Velocimetry: A particle tracking velocimetry-based tool for the study of Strombolian  
1554 explosive eruptions. *J Geophys Res Solid Earth* 119:5369–5383. Doi:10.1002/2014JB011095  
1555  
1556 Gaudin D, Taddeucci J, Scarlato P, Moroni M, Freda C, Gaeta M, Palladino DM (2014b)  
1557 Pyroclast Tracking Velocimetry illuminates bomb ejection and explosion dynamics at  
1558 Stromboli (Italy) and Yasur (Vanuatu) volcanoes. *J Geophys Res Solid Earth* 119:5384–5397.  
1559 doi:10.1002/2014JB011096  
1560  
1561 Genareau K, Proussevitch AA, Durant AJ, Mulukutla GK, Sahagian DL (2012) Sizing up the  
1562 bubbles that produce very fine ash during explosive volcanic eruptions. *Geophys Res Lett*  
1563 39:(L15306).  
1564  
1565 Genareau K, Mulukutla GK, Proussevitch AA, Durant AJ, Rose WI, Sahagian DL (2013) The  
1566 size range of bubbles that produce ash during explosive volcanic eruptions. *J Appl Volcanol*  
1567 2:4. doi:10.1186/2191-5040-2-4  
1568  
1569 Genco R, Ripepe M (2010) Inflation-deflation cycles revealed by tilt and seismic records at  
1570 Stromboli volcano. *Geophys Res Lett* 37. doi: 10.1029/2010GL042925  
1571  
1572 Gerst A, Hort M, Aster RC, Johnson JB, Kyle PR (2013) The first second of volcanic  
1573 eruptions from the Erebus volcano lava lake, Antarctica—Energies, pressures, seismology,  
and infrasound. *J Geophys Res* 118:3318–3340. doi:10.1002/jgrb.50234



1574 Ghiorso MS, Sack RO (1995) Chemical mass transfer in magmatic processes. IV. A revised  
1575 and internally consistent thermodynamic model for the interpolation and extrapolation of  
1576 liquid-solid equilibria in magmatic systems at elevated temperatures and pressures. *Contrib*  
1577 *Mineral Petrol* 119:197–212  
1578  
1579 Giachetti T, Gonnermann HM (2013). Water in pumices: rehydration or incomplete degassing?  
1580 *Earth Planet Sci Lett* 369-370:317-332  
1581  
1582 Giachetti T, Druitt TH, Burgisser A, Arbaret L, Galven C (2010) Bubble nucleation and  
1583 growth during the 1997 Vulcanian explosions of Soufrière Hills Volcano, Montserrat. *J*  
1584 *Volcanol Geotherm Res* 193 (3–4):215–231. doi:10.1016/j.jvolgeores.2010.04.001  
1585  
1586 Giachetti T, Burgisser A, Arbaret L, Druitt TH, Kelfoun K (2011) Quantitative textural  
1587 analysis of Vulcanian pyroclasts (Montserrat) using multi-scale X-ray computed  
1588 microtomography: comparison with results from 2D image analysis. *Bull Volcanol* 73  
1589 (9):1295-1309. doi:10.1007/s00445-011-0472-1  
1590  
1591 Goldstein P, Chouet B (1994) Array measurements and modeling of sources of shallow  
1592 volcanic tremor at Kilauea Volcano, Hawaii. *J Geophys Res* 99(B2):2637–2652  
1593  
1594 Gonnermann HM, Houghton BF (2012) Magma degassing and fragmentation during the  
1595 Plinian eruption of Novarupta, Alaska, 1912. *Geochem Geophys Geosyst*13:Q10009. doi: 10  
1596 .1029 /2012GC004273  
1597  
1598 Gonnermann HM, Manga M (2013) Dynamics of magma ascent in the volcanic conduit. In  
1599 *Modelling volcanic processes: the physics and mathematics of volcanism*, ed. By S. Fagents,  
1600 T.K.P. Gregg, R.M.C. Lopes. Cambridge University Press, New York, pp. 55-84  
1601  
1602 Goodchild JS, Fueten F (1998) Edge detection in petrographic images using the rotating  
1603 polarizer stage. *Comput Geosci* 24:745–751  
1604  
1605 Gouhier M, Donnadiou F (2008) Mass estimations of ejecta from Strombolian explosions by  
1606 inversion of Doppler radar measurements. *J Geophys Res* 113:B10202.  
1607 doi:10.1029/2007JB005383

1608  
1609 Gouhier M, Donnadieu F (2011) Systematic retrieval of ejecta velocities and gas fluxes at  
1610 Etna volcano using L-Band Doppler radar. *Bull Volcanol* 73(9):1139-1145.  
1611 doi:10.1007/s00445-011-0500-1  
1612  
1613 Gualda GAR (2006) Crystal size distributions derived from 3D datasets: sample size versus  
1614 uncertainties. *J Petrol* 47(6):1245-1254  
1615  
1616 Gualda GAR, Rivers M (2006) Quantitative 3D petrography using X- ray tomography:  
1617 application to Bishop Tuff pumice clasts. *J Volcanol Geotherm Res* 154(1–2):48–62  
1618  
1619 Gualda GAR, Baker DR, Polacci M (2010a) Introduction: Advances in 3D imaging and  
1620 analysis of Geomaterials, *Geosphere*, special issue "Advances in 3D Imaging and Analysis of  
1621 Geomaterials" 6-5:468-469. doi:10.1130/GES00639.1  
1622  
1623 Gualda GAR, Pamukcu AS, Claiborne LL, Rivers ML (2010b) Quantitative 3D petrography  
1624 using X-ray tomography 3: documenting accessory phases with differential absorption  
1625 tomography. *Geosphere* 6(6):782–792  
1626  
1627 Gurioli L, Houghton B, Cashman K, Cioni R (2005) Complex changes in eruption dynamics  
1628 and the transition between Plinian and phreatomagmatic activity during the 79AD eruption of  
1629 Vesuvius. *Bull Volcanol* 67:144-159 doi: 10.1007/s00445-004-0368-4  
1630  
1631 Gurioli L, Harris AJL, Houghton BF, Polacci M, Ripepe M (2008) Textural and geophysical  
1632 characterization of explosive basaltic activity at Villarrica volcano. *J Geophys Res*  
1633 113:B08206. doi:10.1029/2007JB005328  
1634  
1635 Gurioli L, Harris AJL, Colò L, Bernard J, Favalli M, Ripepe M, Andronico D (2013)  
1636 Classification, landing distribution and associated flight parameters for a bomb field emplaced  
1637 during a single major explosion at Stromboli, Italy. *Geology* 41 (5):559–562. doi  
1638 10.1130/G33967.1  
1639

1640 Gurioli L, Colò L, Bollasina AJ, Harris AJL, Whittington A, Ripepe M (2014) Dynamics of  
1641 strombolian explosions: inferences from inferences from field and laboratory studies of  
1642 erupted bombs from Stromboli volcano. *J Geophys Res* 119. doi:10.1002/2013JB010355  
1643

1644 Hamada M, Laporte D, Cluzel N, Koga KT (2010) Simulating bubble number density of  
1645 rhyolitic pumices from Plinian eruptions: constraints from fast decompression experiments.  
1646 *Bull Volcanol* 72:735-746  
1647

1648 Hammer JE (2008). Experimental studies of the kinetics and energetics of magma  
1649 crystallization. *Rev Mineral Geochem* 69:9-59  
1650

1651 Hammer JE, Rutherford MJ (2002) An experimental study of the kinetics of decompression-  
1652 induced crystallization in silicic melt. *J Geophys Res* 107(B1). doi:10.1029/2001JB000281  
1653

1654 Hammer JE, Cashman KV, Hoblitt RP, Newman S (1999) Degassing and microlite  
1655 crystallization during pre-climactic events of the 1991 eruption of Mt. Pinatubo, Philippines.  
1656 *Bull Volcanol* 60:355–380  
1657

1658 Hammer JE, Sharp TG, Wessel P (2010) Heterogeneous nucleation and epitaxial crystal  
1659 growth of magmatic minerals. *Geology* 38: 367-370.  
1660

1661 Harris A (2013) *Thermal Remote Sensing of Active Volcanoes: A User's Manual*, Cambridge  
1662 University Press: 728 p.  
1663

1664 Harris AJL, Ripepe M (2007) Synergy of multiple geophysical approaches to unravel  
1665 explosive eruption conduit and source dynamics – A case study from Stromboli. *Chemie der*  
1666 *Erde* 67: 1-35.  
1667

1668 Harris AJL, Ripepe M, Hort M (2004) Foreward. *J Volcanol Geotherm Res* 137(1-3):vii– viii.  
1669 doi:10.1016/S0377-0273(04)00276-8  
1670

1671 Harris AJL, Ripepe M, Hughes EE (2012) Detailed analysis of particle launch velocities, size  
1672 distributions and gas densities during normal explosions at Stromboli. *J Volcanol Geotherm*  
1673 *Res* 231-232:109-131

1674  
1675 Harris AJL, Delle Donne D, Dehn J, Ripepe M, Worden K (2013a) Volcanic plume and bomb  
1676 field masses from thermal infrared camera imagery. *Earth Planet Sci Lett* 365:77-85. doi:  
1677 10.1016/j.epsl.2013.01.004  
1678  
1679 Harris AJL, Battaglia J, Donnadiou F, Gurioli L, Kelfoun K, Labazuy P, Sawyer G, Valade S,  
1680 Bombun M, Barra V, Delle Donne D, Lacanna G (2013b) Full bandwidth remote sensing for  
1681 total parameterization of volcanic plumes. *EOS* 94 (37):321-322  
1682  
1683 Heiken G and Pitts DE (1975) Identification of eruption clouds with the landsat satellites. *Bull*  
1684 *Volcanol* 39(2):255-265  
1685  
1686 Heiken G, Wohletz KH (1985) *Volcanic ash*, University of California Press, Berkeley, Ca,  
1687 USA  
1688  
1689 Heilbronner R (2000) Automatic grain boundary detection and grain size analysis using  
1690 polarization micrographs or orientation images. *J Struct Geol* 22:969–981  
1691  
1692 Herd R, Pinkerton H (1997) Bubble coalescence in basaltic lava: its impact on the evolution  
1693 of bubble populations. *J Volcanol Geotherm Res* 75:137–157  
1694  
1695 Higgins MD (2000) Measurement of crystal size distributions *Am Mineral* 85:1105–1116  
1696  
1697 Higgins MD (2002a) A crystal size-distribution study of the Kiglapait layered mafic intrusion,  
1698 Labrador, Canada: Evidence for textural coarsening. *Contrib Mineral Petr* 144:314-330  
1699  
1700 Higgins MD (2002b) Closure in crystal size distributions (CSD), verification of CSD  
1701 calculations, and the significance of CSD fans. *Am Mineral* 87:171-175  
1702  
1703 Higgins MD (2006) *Quantitative textural measurements in igneous and metamorphic*  
1704 *petrology*. Cambridge University Press, Cambridge  
1705  
1706 Higgins MD (2011) Textural coarsening in igneous rocks. *Int Geol Rev* 53:354–376  
1707

1708 Hoblitt RP, Harmon RS (1993) Bimodal density distribution of cryptodome dacite from the  
1709 1980 Mount St. Helens, Washington. *Bull Volcanol* 55:421– 437  
1710

1711 Holasek RE, Self S (1995) GOES weather satellite observations and measurements of the  
1712 May 18, 1980, Mount St. Helens eruption. *J Geophys Res* 100(B5):8469-8487  
1713

1714 Holasek RE, Self S, Woods AW (1996) Satellite observations and interpretation of the 1991  
1715 Mount Pinatubo eruption plumes. *J Geophys Res* 101(B12):27635-27655  
1716

1717 Holland ASP, Watson M, Phillips JC, Caricchi L, Dalton MP (2011) Degassing processes  
1718 during lava dome growth: Insights from Santiaguito lava dome, Guatemala. *J Volcanol*  
1719 *Geotherm Res* 202(1–2):153-166  
1720

1721 Hort M, Seyfried R, Vöge M (2003) Radar Doppler velocity of volcanic eruptions:  
1722 Theoretical considerations and quantitative documentation of changes in eruptive behaviour at  
1723 Stromboli volcano, Italy. *Geophys J Int* 154:515-532  
1724

1725 Hort M, Seyfried R (1998) Volcanic eruption velocities measured with a micro radar.  
1726 *Geophys Res Lett* 25:113–116  
1727

1728 Horton K, Williams-Jones G, Garbeil H, Elias T, Sutton AJ, Mougini-Mark P, Porter JN,  
1729 Clegg S (2005) Real-time measurement of volcanic SO<sub>2</sub> emissions: validation of a new UV  
1730 correlation spectrometer (FLYSPEC). *Bull Volcanol*: doi 10.1007/s00445-005-0014-9  
1731

1732 Houghton BF, Wilson CJN (1989) A vesicularity index for pyroclastic deposits. *Bull*  
1733 *Volcanol* 51:451–462. doi:10.1007/BF01078811  
1734

1735 Houghton BF, Carey RJ, Cashman KV, Wilson CJN, Hobden BJ, Hammer JE (2010) Diverse  
1736 patterns of ascent, degassing, and eruption of rhyolite magma during the 1.8 ka Taupo  
1737 eruption, New Zealand: Evidence from clast vesicularity, *J Volcanol Geotherm Res* 195:31–  
1738 47  
1739

1740 Houghton BF, Swanson DA, Rausch J, Carey RJ, Fagents SA, Orr TR (2013) Pushing the  
1741 Volcanic Explosivity Index to its limit and beyond: Constraints from exceptionally weak  
1742 explosive eruptions at Kilauea in 2008. *Geology* 41(6):627–630  
1743  
1744 Humphreys MCS, Menand T, Blundy JD, Klimm K (2008a) Magma ascent rates in explosive  
1745 eruptions: constraints from H<sub>2</sub>O diffusion in melt inclusions. *Earth Planet Sci Lett* 270:25-40  
1746  
1747 Humphreys MC, Blundy JD, Sparks RSJ (2008b) Shallow-level decompression crystallization  
1748 and deep magma supply at Shiveluch volcano. *Contrib Mineral Petrol* 155:45-61  
1749  
1750 Hurwitz S, Navon O (1994) Bubble nucleation in rhyolitic melts: experiments at high  
1751 pressure, temperature, and water content. *Earth Planet Sci Lett* 122:267-280  
1752  
1753 Iguchi M, Yakiwara H, Tameguri T, Hendrasto M, Hirabayashi J (2008) Mechanism of  
1754 explosive eruption revealed by geophysical observations at the Sakurajima, Suwanosejima  
1755 and Semeru volcanoes. *J Volcanol Geotherm Res* 178(1):1-9  
1756  
1757 Innocenti S, Andreastuti S, Furman T, del Marmol M-A, Voight B (2013) The pre-eruption  
1758 conditions for explosive eruptions at Merapi volcano as revealed by crystal texture and  
1759 mineralogy. *J Volcanol Geother Res* doi.org/10.1016/j.jvolgeores.2012.12.028  
1760  
1761 Ishibashi H, Sato H (2007) Viscosity measurements of subliquidus magmas: alkali olivine  
1762 basalt from the Higashi-Matsuura district, Southwest Japan. *J Volcanol Geotherm Res*  
1763 160:223–238  
1764  
1765 Jerram DA, Chedale MJ, Philpotts AR (2003) Quantifying the building blocks of igneous  
1766 rocks: are clustered crystal frameworks the foundation? *J Petrol* 44:2033–2051  
1767  
1768 Jouniaux L, Bernard ML, Zamora M, Pozzi JP (2000) Streaming potential in volcanic rocks  
1769 from Mount Pelée. *J Geophys Res* 105:8391–8401  
1770  
1771 Kahl M, Chakraborty S, Costa F, Pompilio M (2011) Dynamic plumbing system beneath  
1772 volcanoes revealed by kinetic modeling, and the connection to monitoring data: An example  
1773 from Mt. Etna. *Earth Planet Sc Lett* 308:11–22. doi: 10.1016/j.epsl.2011.05.008

1774  
1775 Kaneshima S, Kawakatsu H, Matsubayashi H, Sudo Y, Tsutsui T, Ohminato T, Ito H, Uhira  
1776 K, Yamasato H, Oikawa J, Takeo M, Iidaka T (1996) Mechanism of phreatic eruptions at Aso  
1777 Volcano inferred from near-field broadband seismic observations. *Science* 273(5275):643-645  
1778  
1779 Kennedy B, Spieler O, Scheu B, Kueppers U, Taddeucci J, Dingwell DB (2005) Conduit  
1780 implosion during Vulcanian eruptions. *Geology* 33:581-584. doi: 10.1130/G21488.1  
1781  
1782 Kent AJR (2008) Melt inclusions in basaltic and related volcanic rocks. *Rev Mineral*  
1783 *Geochem* 69: 273-331  
1784  
1785 Kent AJR, Blundy J, Cashman K, Cooper KM, Donnelly C. et al. (2007) Vapor transfer prior  
1786 to the October 2004 eruption of Mount St. Helens, Washington. *Geology* 35: 231–234  
1787  
1788 Ketcham RA (2005) Computational methods for quantitative analysis of three-dimensional  
1789 features in geological specimens. *Geosphere* 1:32-41  
1790  
1791 Ketcham RA, Carlson WD (2001) Acquisition, optimization and interpretation of X-ray  
1792 computed tomographic imagery: applications to the geosciences. *Comput Geosci* 27:381–400  
1793  
1794 Klawonn M, Houghton BF, Swanson DA, Fagents SA, Wessel P, Wolfe CJ (2014)  
1795 Constraining explosive volcanism: subjective choices during estimates of eruption magnitude.  
1796 *Bull Volcanol* 76:793. doi: 10.1007/s00445-013-0793-3  
1797  
1798 Klug C, Cashman KV (1994) Vesiculation of May 18, 1980, Mount St. Helens magma.  
1799 *Geology* 22:468–472  
1800  
1801 Klug C, Cashman KV (1996) Permeability development in vesiculating magmas: implications  
1802 for fragmentation. *Bull Volcanol* 58:87–100  
1803  
1804 Klug C, Cashman KV, Bacon CR (2002) Structure and physical characteristics of pumice  
1805 from the climatic eruption of Mount Mazama (Crater Lake), Oregon. *Bull Volcanol* 64:486–  
1806 501  
1807

1808 Koyaguchi T, Tokuno M (1993) Origin of the giant eruption cloud of Pinatubo, June 15,  
1809 1991. *J Volcanol Geotherm Res* 55:85-96  
1810

1811 Krueger AJ, Walter LS, Doiron SD (1990) TOMS measurement of sulfur dioxide emitted  
1812 during the 1985 Nevado del Ruiz eruptions. *J Volcanol Geotherm Res* 41:7-15  
1813

1814 Kueppers U, Scheu B, Spieler O, Dingwell DB (2005) Field-based density measurements as  
1815 tool to identify pre-eruption dome structure: set-up and first results from Unzen volcano,  
1816 Japan. *J Volcanol Geotherm Res* 141:65–75  
1817

1818 Kueppers U, Scheu B, Spieler O, Dingwell DB (2006) Fragmentation efficiency of explosive  
1819 volcanic eruptions: A study of experimentally generated pyroclasts. *J Volcanol Geotherm Res*  
1820 153(1–2):125-135  
1821

1822 Kyser TK, O’Neil JR (1984) Hydrogen isotope systematic of submarine basalts. *Geochim*  
1823 *Cosmochim Acta* 48:2123–2133  
1824

1825 Lak M, Néraudeau D, Nel A, Cloetens P, Perrichot V, Tafforeau P (2008) Phase contrast X-  
1826 ray synchrotron imaging: opening access to fossil inclusions in opaque amber. *Microsc*  
1827 *Microanal* 14(3):251–259  
1828

1829 Landi P, Marchetti E, La Felice S, Ripepe M, Rosi M (2011) Integrated petrochemical and  
1830 geophysical data reveals thermal distribution of the feeding conduits at Stromboli volcano,  
1831 Italy. *Geophys Res Lett* 38:L08305  
1832

1833 Lanza R, Meloni A (2006) *The Earth’s magnetism: an introduction for geologists*. 278 pp.  
1834 Berlin, Heidelberg, New York: Springer-Verlag  
1835

1836 Larsen JF (2008) Heterogeneous bubble nucleation and disequilibrium H<sub>2</sub>O exsolution in  
1837 Vesuvius K-phonolite melts. *J Volcanol Geotherm Res* 275:278–288  
1838

1839 Larsen JF, Gardner JE (2000) Experimental constraints on bubble interactions in rhyolite  
1840 melts: implications for vesicle size distributions. *Earth Planet Sci Lett* 180:201–214  
1841



1842 LaRue A, Baker DR, Polacci M, Allard P, Sodini N (2013), Can vesicle size distributions  
1843 assess eruption intensity during volcanic activity? *J Geophys Res-Solid Earth* 4:373–80.  
1844 doi:10.5194/se-4-373-2013  
1845

1846 Laumonier M, Arbaret L, Burgisser A, Champallier R (2011) Porosity redistribution enhanced  
1847 by strain localization in crystal-rich magmas. *Geology* 39:715–718.  
1848 <http://dx.doi.org/10.1130/G31803.1>  
1849

1850 Launeau P, Cruden AR (1998) Magmatic fabric acquisition mechanisms in a syenite: results  
1851 of a combined anisotropy of magnetic susceptibility and image analysis study. *J Geophys Res*  
1852 103:5067–5089  
1853

1854 Launeau P, Bouchez JL, Benn K (1990) Shape preferred orientation of object populations:  
1855 Automatic analysis of digitized images. *Tectonophysics* 180:201-211  
1856

1857 Launeau P, Cruden AR, Bouchez JL (1994) Mineral recognition in digital images of rocks: a  
1858 new approach using multichannel classification. *Can Mineral* 32:919–933  
1859

1860 Lautze NC, Houghton BF (2005) Physical mingling of magma and complex eruption  
1861 dynamics in the shallow conduit at Stromboli volcano, Italy. *Geology* 33:425–428.  
1862

1863 Lautze NC, Houghton BF (2007) Linking variable explosion style and magma textures during  
1864 2002 at Stromboli volcano, Italy. *Bull Volcanol* 69:445–460  
1865

1866 Lautze NC, Houghton BF (2008) Single explosions at Stromboli in 2002: use of clast  
1867 microtextures to map physical diversity across a fragmentation zone. *J Volcanol Geotherm*  
1868 *Res* 170:262–268  
1869

1870 Lautze N, Taddeucci J, Andronico D, Cannata C, Tornetta L, Scarlato P, Houghton B, Lo  
1871 Castro D (2012) SEM-based methods for the analysis of basaltic ash from weak explosive  
1872 activity at Etna in 2006 and the 2007 eruptive crisis at Stromboli. *Phys Chem Earth* 45–  
1873 46:113–127. doi:10.1016/j.pce.2011.02.001  
1874

1875 Lautze N, Taddeucci J, Andronico D, Houghton B, Niemeijer A, Scarlato P (2013) Insights  
1876 into explosion dynamics and the production of ash at Stromboli from samples collected in real  
1877 time, October 2009. *Geol S Am S* 498:125-139  
1878  
1879 Lavallée Y, Varley N, Alatorre-Ibargüengoitia MA, Hess KU, Mueller S, Richard D, Scheu  
1880 B, Spieler O, Dingwell DB (2012) Magmatic architecture of dome-building eruptions at  
1881 Volcán de Colima, Mexico. *Bull Volcanol* 74:249-260  
1882  
1883 Leduc L, Gurioli L, Harris AJL, Colò L, Rose-Koga E Dynamics of a gas-dominated  
1884 strombolian explosion. *Bull Volcanol* 77:8. doi: 10.1007/s00445-014-0888-5.  
1885  
1886 Le Losq C, Neuville DR, Moretti R, Roux J (2012) Determination of water content in silicate  
1887 glasses using Raman spectrometry: Implications for the study of explosive volcanism. *Am*  
1888 *Mineral* 97:779-790  
1889  
1890 Le Pennec JL, Hermitte D, Isya D, Pezard P, Coulon C, Cochemé J-J, Mulyadi E, Ollagnier  
1891 F, Revest C (2001). Electrical conductivity and pore-space topology of Merapi lavas:  
1892 implication for the degassing of porphyritic andesite magmas. *Geophys Res Lett*  
1893 28(22):4283–4286  
1894  
1895 Le Voyer M, Rose-Koga EF, Shimizu N, Grove TL, Schiano P (2010) Two contrasting H<sub>2</sub>O-  
1896 rich components in primary melt inclusions from Mount Shasta. *J Petrol* 5(7):1571–1595. doi:  
1897 10.1093/petrology/egq030  
1898  
1899 Lesne P, Kohn SC, Blundy J, Witham F, Botcharnikov RE, Behrens H. (2011). Experimental  
1900 simulation of closed-system degassing in the system basalt-H<sub>2</sub>O-CO<sub>2</sub>-S-Cl. *J Petrol* 52:1737-  
1901 1762  
1902  
1903 Liu Y, Anderson AT, Wilson CJN (2007) Melt pockets in phenocrysts and decompression  
1904 rates of silicic magmas before fragmentation. *J Geophys Res* 112. doi:10.1029/2006JB004500  
1905  
1906 Lovejoy S, Gaonac’h H, Schertzer D (2004) Bubble distributions, and dynamics: the  
1907 expansion-coalescence equation. *J Geophys Res* 109:B11203. doi:10.1029/2003JB002823  
1908

1909 Lumbreras F, Serrat J (1996) Segmentation of petrographical images of marbles. *Comput*  
1910 *Geosci* 22:547–558  
1911

1912 Magee C, O’Driscoll B, Chambers AD (2010) Crystallization and textural evolution of a  
1913 closed-system magma chamber: insights from a crystal size distribution study of the Lilloise  
1914 layered intrusion, east Greenland. *Geol Mag* 147:363–379  
1915

1916 Manga M. (1998) Orientation distribution of microlites in obsidian. *J Volcanol Geother Res*  
1917 86:107–115  
1918

1919 Mangan M (1990) Crystal size distribution systematics and the determination of magma  
1920 storage times: The 1959 eruption of Kilauea volcano, Hawaii. *J Volcanol Geother Res*  
1921 44:295–302  
1922

1923 Mangan MT, Cashman, KV (1996) The structure of basaltic scoria and reticulite and  
1924 inferences for vesiculation, foam formation, and fragmentation in lava fountains. *J Volcanol*  
1925 *Geotherm Res* 73:1-18  
1926

1927 Mangan M, Sisson T (2000) Delayed, disequilibrium degassing in rhyolite magma:  
1928 decompression experiments and implications for explosive volcanism. *Earth Planet Sci Lett*  
1929 183:441–55  
1930

1931 Mangan M, Sisson T (2005). Evolution of melt-vapor surface tension in silicic volcanic  
1932 systems: Experiments with hydrous melts. *J Geophys Res* 110:B01202. doi:  
1933 10.1029/2004JB003215  
1934

1935 Mangan MT, Cashman KV, Newman S (1993) Vesiculation of basaltic magma during  
1936 eruption. *Geology* 21:157–160  
1937

1938 Marchetti E, Ripepe M, Harris AJL, Delle Donne D (2009) Tracing the differences between  
1939 Vulcanian and Strombolian explosions using infrasonic and thermal radiation energy. *Earth*  
1940 *Planet Sci Lett* 279:273–281  
1941

1942 Marchetti E, Poggi P, Bonadonna C, Pistolesi M, Hoskuldsson A (2013) Towards real-time  
1943 measurements of tephra fallout grain-size distribution. MeMoVolc Meeting, Geneva  
1944 Switzerland, January 2014  
1945  
1946 Maria A, Carey S (2002) Using fractal analysis to quantitatively characterize the shapes of  
1947 volcanic particles. *J Geophys Res* 107:(B11):2283. doi:10.1029/2001JB000822  
1948  
1949 Maria A, Carey S (2007) Quantitative discrimination of magma fragmentation and pyroclastic  
1950 transport processes using the fractal spectrum technique. *J Volcanol Geotherm Res* 161:234–  
1951 246  
1952  
1953 Marsh BD (1988) Crystal size distribution (CSD) in rocks and the kinetics and dynamics of  
1954 crystallization: I. Theory. *Contrib Mineral Petrol* 99:277– 291  
1955  
1956 Marsh BD (1998) On the interpretation of crystal size distributions in magmatic systems. *J*  
1957 *Petrol* 39:553–599  
1958  
1959 Marsh BD (2007) Crystallization of silicate magmas deciphered using crystal size  
1960 distributions. *J Am Ceramic Society* 90:746-757  
1961  
1962 Marshall JR (1987) *Clastic particles: Scanning electron microscopy and shape analysis of*  
1963 *sedimentary and volcanic clasts*, Van Nostrand Reinhold Company, New York, 346 p.  
1964  
1965 Marschallinger R (1998a) A method for three-dimensional reconstruction of macroscopic  
1966 features in geological materials. *Comput Geosc* 24:875-883  
1967  
1968 Marschallinger R (1998b) Correction of geometric errors associated with the 3-D  
1969 reconstruction of geological materials by precision serial lapping. *Mineral Mag* 62:783-792  
1970  
1971 Marschallinger R (1998c) 3-D reconstruction and volume modelling of the grain fabric of  
1972 geological materials. *Phys Chem Earth* 23:267-271  
1973

1974 Martel C (2012) Eruption Dynamics inferred from microlite crystallization experiments:  
 1975 application to Plinian and dome-forming eruptions of Mt. Pelée (Martinique, Lesser Antilles).  
 1976 *J Petrol* 53:699-725  
 1977

1978 Martel C, Radadi Ali A, Poussineau S, Gourgaud A, Pichavant M (2006) Basalt-inherited  
 1979 microlites in silicic magmas: evidence from Mt. Pelée (Martinique, F.W.I.). *Geology* 34:905–  
 1980 908  
 1981

1982 Marti J, Soriano C, Dingwell DB (1999) Tube pumices as strain markers of the ductile-brittle  
 1983 transition during magma fragmentation. *Nature* 402(6762):650–653  
 1984

1985 Martí J, Castro A, Rodríguez C, Costa F, Carrasquilla S, Pedreira R, Bolos X (2013)  
 1986 Correlation of magma evolution and geophysical monitoring during the 2011–2012 El Hierro  
 1987 (Canary Islands) submarine eruption. *J Petrology* 54(7):1349-1373.  
 1988 doi:10.1093/petrology/egt014.  
 1989

1990 Mattsson HB (2010) Textural variation in juvenile pyroclasts from an emergent, Surteyan-  
 1991 type, volcanic eruption: The Capelas tuff cone, São Miguel (Azores). *J Volcanol Geoth Res*  
 1992 189:81–91  
 1993

1994 McNutt SR (1986) Observations and analysis of B-type earthquakes, explosions, and volcanic  
 1995 tremor at Pavlof Volcano, Alaska. *Bull Seis Soc Amer* 76:153-175  
 1996

1997 Mele D, Dellino P, Sulpizio R, Braia G (2011) A systematic investigation on the  
 1998 aerodynamics of ash particles, *J Volcanol Geotherm Res* 203:1–11.  
 1999 doi:10.1016/j.jvolgeores.2011.04.004  
 2000

2001 Melnik O, Sparks RSJ (2002) Dynamics of magma ascent and lava extrusion at Soufrière  
 2002 Hills Volcano, Montserrat. In: Druitt, T., Kokelaar, B. (Eds.), *The Eruption of Soufrière Hills*  
 2003 *Volcano, Montserrat, from 1995 to 1999*. The Geological Society of London, pp. 153–171.  
 2004

2005 Métrich N, Bertagnini A, Landi P, Rosi M (2001), Crystallization driven by decompression  
 2006 and water loss at Stromboli volcano (Aeolian Islands, Italy). *J Petrol* 42:1471–1490.  
 2007 doi:10.1093/petrology/42.8.1471

2008

2009 Métrich N, Wallace PJ (2008) Volatile abundances in basaltic magmas and their degassing  
2010 paths tracked by melt inclusions. In Putirka KD, Tepley FJ (Eds) Minerals, inclusions and  
2011 volcanic processes Rev Mineral Geochem 69:363-402

2012

2013 Métrich N, Bertagnini A, Di Muro A (2010) Conditions of magma storage, degassing and  
2014 ascent at Stromboli: new insights into the volcano plumbing system with inferences on the  
2015 eruptive dynamics. J Petrol 51(3):603-626

2016

2017 Miwa T, Toramaru A (2013) Conduit process in vulcanian eruptions at Sakurajima volcano,  
2018 Japan: Inference from comparison of volcanic ash with pressure wave and seismic data. Bull  
2019 Volcanol 75:685

2020

2021 Miwa T, Toramaru A, Iguchi M (2009) Correlations of volcanic ash texture with explosion  
2022 earthquakes from vulcanian eruptions at Sakurajima volcano, Japan. J Volcanol Geotherm  
2023 Res 184(3–4):473–486

2024

2025 Miwa T, Geshi N, Shinohara H (2013) Temporal variation in volcanic ash texture during a  
2026 vulcanian eruption at the Sakurajima volcano, Japan. J Volcanol Geotherm Res 260:80-89

2027

2028 Mock A, Jerram DA (2005) Crystal size distributions (CSD) in three dimensions: Insights  
2029 from the 3D reconstruction of a highly porphyritic rhyolite: J Petrol 46:1525–1541. doi:  
2030 10.1093/petrology/egi024

2031

2032 Mock A, Jerram DA, Breikreuz C (2003) Using quantitative textural analysis to understand  
2033 the emplacement of shallow-level rhyolitic laccoliths a case study from the Halle volcanic  
2034 complex, Germany. J Petrol 44:833-849

2035

2036 Moitra P, Gonnermann HM, Houghton BF, Giachetti T (2013) Relating vesicle shapes in  
2037 pyroclasts to eruption styles. Bull Volcanol 75:691. doi 10.1007/s00445-013-0691-8

2038

2039 Morgan DJ, Jerram DA, Chertkoff DG, Davidson JP, Pearson DG, Kronz A, Nowell GM  
2040 (2007) Combining CSD and isotopic microanalysis: magma supply and mixing processes at  
2041 Stromboli volcano, Aeolian islands, Italy. Earth Planet Sci Lett 260(3–4):419–431

2042

2043 Mori T, Burton M (2006) The SO<sub>2</sub> camera: a simple, fast and cheap method for groundbased  
2044 imaging of SO<sub>2</sub> in volcanic plumes. *Geophys Res Lett* 33(L24804):  
2045 doi:10.1029/2006GL027916

2046

2047 Mori T, Burton M (2009) Quantification of the gas mass emitted during single explosions on  
2048 Stromboli with the SO<sub>2</sub> imaging camera. *J Volcanol Geotherm Res* 188:395–400.  
2049 doi:10.1016/j.jvolgeores.2009.10.005

2050

2051 Mori J, Patia H, McKee C, Itikarai I, Lowenstein P, De Saint Ours P, Talai B (1989)  
2052 Seismicity associated with eruptive activity at Langila volcano, Papua New Guinea. *J*  
2053 *Volcanol Geotherm Res* 38(3–4):243-255

2054

2055 Mourtada-Bonnefoi CC, Laporte D (2002) Homogenous bubble nucleation in rhyolitic  
2056 magmas: An experimental study on the effect of H<sub>2</sub>O and CO<sub>2</sub>. *J Geophys Res* 107:B4. doi:  
2057 10.1029/2001JB000290

2058

2059 Mourtada-Bonnefoi CC, Laporte D (2004) Kinetics of bubble nucleation in a rhyolitic melt:  
2060 an experimental study of the effect of ascent rate. *Earth Planet Sci Lett* 218:521-537

2061

2062 Mueller S, Melnik O, Spieler O, Scheu B, Dingwell DB (2005) Permeability and degassing of  
2063 dome lavas undergoing rapid decompression: An experimental determination *Bull Volcanol*  
2064 67(6):526–538. doi:10.1007/s00445-004-0392-4

2065

2066 Mueller S, Scheu B, Spieler O, Dingwell DB (2008) Permeability control on magma  
2067 fragmentation. *Geology* 36(5):399–402. doi:10.1130/G24605A.1

2068

2069 Mueller S, Scheu B, Kueppers U, Spieker O, Richard D, Dingwell DB (2011) The porosity of  
2070 pyroclasts as an indicator of volcanic explosivity. *J Volcanol Geotherm Res* 203:168-174

2071

2072 Muir DD, Blundy JD, Rust AC (2012) Multiphase petrography of volcanic rocks using  
2073 element maps: a method applied to Mount St. Helens, 1980–2005 *Bull Volcanol* 74:1101–  
2074 1120

2075

2076 Murtagh RM, White JDL (2013) Pyroclast characteristics of a subaqueous to emergent  
2077 Surtseyan eruption, Black Point volcano, California. *J Volcanol Geotherm Res* 267:75-91  
2078

2079 Murtagh RM, White JDL, Sohn YK (2011) Pyroclast textures of the Ilchulbong ‘wet’ tuff  
2080 cone, Jeju Island, South Korea. *J Volcanol Geotherm Res* 201:385-396.  
2081

2082 Nakamura K (2006) Textures of plagioclase microlite and vesicles within volcanic products  
2083 of the 1914–1915 eruptions of Sakurajima Volcano, Kyushu, Japan. *J Mineral Petrol Sci*  
2084 101:178–198  
2085

2086 Nakamura M, Otaki K, Takeuchi S (2008) Permeability and pore-connectivity variation of  
2087 pumices from a single pyroclastic flow eruption: Implications for partial fragmentation. *J*  
2088 *Volcanol Geotherm Res* 176:302–314  
2089

2090 Németh K (2010) Volcanic glass textures, shape characteristics and compositions of  
2091 phreatomagmatic rock units from the Western Hungarian monogenetic volcanic fields and  
2092 their implications for magma fragmentation. *Cent Eur J Geosci* 2:399–419  
2093

2094 Neuberg J, Luckett R, Ripepe M, Braun T (1994) Highlights from a seismic broadband array  
2095 on Stromboli volcano. *Geophys Res Lett* 21:749–752  
2096

2097 Newman S, Lowenstern JB (2002) VolatileCalc: a silicate melt-H<sub>2</sub>O-CO<sub>2</sub> solution model  
2098 written in Visual Basic for Excel. *Computers and Geosciences* 28(5):597-604  
2099

2100 Newman S, Epstein S, Stolper E (1988) Water, carbon dioxide, and hydrogen isotopes in  
2101 glasses from the CA. 1340 A.D. eruption of the Mono Craters, California: constraints on  
2102 degassing phenomena and initial volatile content. *J Volcanol Geotherm Res* 35:75-96  
2103

2104 Nguyen CT, Gonnermann HM, Chen Y, Huber C, Maiorano AA, Gouldstone A, Dufek J  
2105 (2013) Film drainage and the lifetime of bubbles. *Geochem Geophys Geosyst* 14:3616–3631  
2106

2107 Nishimura T, McNutt SR (2008) Volcanic tremor during eruptions: temporal characteristics,  
2108 scaling and estimates of vent radius. *J Volcanol Geotherm Res* 178:10-18  
2109



2110 Noguchi S, Toramaru A, Shimano T (2006) Crystallization of microlites and degassing during  
2111 magma ascent: Constraints on the fluid mechanical behavior of magma during the Tenjo  
2112 Eruption on Kozu Island, Japan. *Bull Volcanol* 68:432–449. doi 10.1007/s00445-005-0019-4  
2113

2114 Noguchi S, Toramaru A, Nakada S (2008) Relation between microlite textures and discharge  
2115 rate during the 1991–1995 eruptions at Unzen, Japan. *J Volcanol Geotherm Res* 175(1–  
2116 2):141–155  
2117

2118 O’Driscoll B, Donaldson CH, Troll VR, Jerram DA, Emeleus CH (2007) An origin for  
2119 harrisitic and granular olivine in the rum layered suite, NW Scotland: a crystal size  
2120 distribution study. *J Petrol* 48(2):253–270  
2121

2122 Okumura S, Nakamura M, Tsuchiyama A (2006) Shear-induced bubble coalescence in  
2123 rhyolitic melts with low vesicularity. *Geophys Res Lett* 33:L20316.  
2124 doi:10.1029/2006GL027347  
2125

2126 Okumura S, Nakamura M, Tsuchiyama A, Nakano T, Uesugi K (2008) Evolution of bubble  
2127 microstructure in sheared rhyolite: Formation of a channel-like bubble network: *J Geophys*  
2128 *Res* 113:B07208. doi: 10.1029/2007JB005362  
2129

2130 Okumura S, Nakamura M, Uesugi K, Nakano T, Fujioka T (2013) Coupled effect of magma  
2131 degassing and rheology on silicic volcanism. *Earth Planet Sci Lett* 362:163–170  
2132

2133 Oppenheimer C, Scaillet B, Martin RS (2011) Sulfur degassing from volcanoes: source  
2134 conditions, surveillance, plume chemistry and impacts, *Rev Mineral Geochem* 73:363-421.  
2135 doi:10.2138/rmg.2011.73.13  
2136

2137 Palladino DM, Taddeucci J (1998) The basal ash deposit of the Sovana Eruption (Vulsini  
2138 Volcanoes, central Italy): the product of a dilute pyroclastic density current. *J Volcanol*  
2139 *Geotherm Res* 87:233–254  
2140

2141 Pamukcu AS, Gualda GAR (2010) Quantitative 3D petrography using X-ray tomography 2:  
2142 combining information at various resolutions. *Geosphere* 6:775–781.  
2143 doi.org/10.1130/GES00565.1

2144  
2145 Pamukcu AS, Gualda GAR, Anderson AT (2012) Crystallization stages of the Bishop Tuff  
2146 magma body recorded in crystal textures in pumice clasts. *J Petrol* 63:589–609  
2147  
2148 Pardo N et al (2014a) Perils in distinguishing phreatic from phreatomagmatic ash; insights  
2149 into the eruption mechanisms of the 6 August 2012 Mt. Tongariro eruption, New Zealand. *J*  
2150 *Volcanol Geotherm Res* <http://dx.doi.org/10.1016/j.jvolgeores.2014.05.001>  
2151  
2152 Pardo N, Cronin SJ, Wright HMN, Schipper IC, Smith I, Stewart B (2014b) Pyroclast textural  
2153 variation as an indicator of eruption column steadiness in andesitic Plinian eruptions at Mt.  
2154 Ruapehu. *Bull Volcanol* 76:822  
2155  
2156 Patrick MR (2007) Dynamics of Strombolian ash plumes from thermal video: motion,  
2157 morphology, and air entrainment. *J Geophys Res* 112:B06202. doi:10.1029/2006JB004387.  
2158  
2159 Perugini D, Poli G, Properini N (2002) Morphometric analysis of magmatic enclaves: a tool  
2160 for understanding magma vesiculation and ascent. *Lithos* 61:225–235  
2161  
2162 Perugini D, Valentini L, Poli G (2007) Insights into magma chamber processes from the  
2163 analysis of size distribution of enclaves in lava flows: a case study from Vulcano Island  
2164 (Southern Italy). *J Volcanol Geotherm Res* 166:193–203  
2165  
2166 Perugini D, Speziali A, Caricchi L, Kueppers U (2011) Application of fractal fragmentation  
2167 theory to natural pyroclastic deposits: Insights into volcanic explosivity of the Valentano  
2168 scoria cone (Italy). *J Volcanol Geotherm Res* 202(3-4):200-210  
2169  
2170 Pfeiffer T, Costa A, Macedonio G (2005) A model for the numerical simulation of tephra fall  
2171 deposits. *J Volcanol Geotherm Res* 140:273–294  
2172  
2173 Pickering G, Bull JM Sanderson DJ (1995) Sampling power-law distributions:  
2174 *Tectonophysics*. 248:1–20. doi:10.1016/0040-1951(95)00030-Q  
2175

2176 Pichavant M, Martel C, Bourdier JL, Scaillet B (2002) Physical conditions, structure, and  
2177 dynamics of a zoned magma chamber: Mount Pelée (Martinique, Lesser Antilles Arc). *J*  
2178 *Geophys Res* 107. doi:10.1029/2001JB000315  
2179  
2180 Pichavant M, Costa F, Burgisser A, et al. (2007) Equilibration scales in silicic to intermediate  
2181 magmas: implications for experimental studies. *J Petrol* 48:1955–1972. doi:  
2182 10.1093/petrology/egm045  
2183  
2184 Pichavant M, Carlo I, Rotolo SG, et al. (2013) Generation of CO<sub>2</sub>-rich melts during basalt  
2185 magma ascent and degassing. *Contrib Mineral Petr.* doi: 10.1007/s00410-013-0890-5  
2186  
2187 Piochi M, Mastrolorenzo G, Pappalardo L (2005) Magma ascent and eruptive processes from  
2188 textural and compositional features of Monte Nuovo pyroclastic products, Campi Flegrei,  
2189 Italy. *Bull Volcanol* 67:663–678  
2190  
2191 Piochi M, Polacci M, De Astis G, Zanetti A, Mangiacapra A, Vannucci R, Giordano D (2008)  
2192 Texture and composition from pumices and scoriae of the Campi Flegrei caldera (Italy):  
2193 Implications on the dynamics of explosive eruptions. *Geochem Geophys Geosyst* 9:Q03013.  
2194 doi:10.1029/2007GC001746  
2195  
2196 Pioli L, Erlund E, Johnson E, Cashman K, Wallace P, Rosi M, Delgado Granados H (2008)  
2197 Explosive dynamics of violent strombolian eruptions: the eruption of Parícutin volcano 1943–  
2198 1952 (Mexico). *Earth Planet Sci Lett* 271:359–368  
2199  
2200 Pioli L, Pistolesi M, Rosi M (2014) Transient explosions at open-vent volcanoes: the case of  
2201 Stromboli (Italy). *Geology* 42:863-866  
2202  
2203 Pistolesi M, Rosi M, Pioli L, Renzulli A, Bertagnini A, Andronico D (2008), The paroxysmal  
2204 explosion and its deposits, in *The Stromboli Volcano: An Integrated Study of the 2002–2003*  
2205 *Eruption*, *Geophys. Monogr. Ser.* vol. 182, edited by S. Calvari et al. pp. 317–329, AGU,  
2206 Washington, D. C. doi:10.1029/182GM26  
2207

2208 Pistolesi M, Delle Donne D, Pioli L, Rosi M, Ripepe M (2011) The 15 March 2007 explosive  
2209 crisis at Stromboli volcano, Italy: assessing physical parameters through a multidisciplinary  
2210 approach. *J Geophys Res* 116(B12). doi: 958 10.1029/2011JB008527  
2211

2212 Platz T, Cronin SJ, Cashman KV, Stewart RB, Smith IEM (2007) Transition from effusive to  
2213 explosive phases in andesite eruptions — A case-study from the AD1655 eruption of Mt.  
2214 Taranaki, New Zealand. *J Volcanol Geotherm Res* 161:15-34  
2215

2216 Polacci M, P Papale, M Rosi (2001) Textural heterogeneities in pumices from the climatic  
2217 eruption of Mount Pinatubo, 15 June 1991, and implications for magma ascent dynamics. *Bull*  
2218 *Volcanol* 63:83–97  
2219

2220 Polacci M, Pioli L, Rosi M (2003) The Plinian phase of the Campanian Ignimbrite eruption  
2221 (Phlegrean Fields, Italy): evidence from density measurements and textural characterization of  
2222 pumice. *Bull Volcanol* 65:418–432  
2223

2224 Polacci M, Corsaro R, Andronico D (2006a) Coupled textural and compositional  
2225 characterization of basaltic scoria: Insights into the transition from Strombolian to fire  
2226 fountain activity at Mount Etna, Italy. *Geology* 34(3):201–204. doi:10.1130/G223181.1  
2227

2228 Polacci M, Baker DR, Mancini L, Tromba G, Zanini F (2006b) Three-dimensional  
2229 investigation of volcanic textures by X-ray microtomography and implications for conduit  
2230 processes. *Geophys Res Lett* 33(13):L13312. doi:10.1029/2006GL026241  
2231

2232 Polacci M, Baker DR, Bai L, Mancini L (2008) Large vesicles record pathways of degassing  
2233 at basaltic volcanoes. *Bull Volcanol* 70:1023–1029. doi:10.1007/s00445-007-0184-8  
2234

2235 Polacci M, Baker DR, Mancini L, Favretto S, Hill RJ (2009a) Vesiculation in magmas from  
2236 Stromboli and implications for normal Strombolian activity and paroxysmal explosions in  
2237 basaltic systems. *J Geophys Res* 114:B01206. doi.org/10.1029/2008JB005672  
2238

2239 Polacci M, Burton MR, La Spina A, Murè F, Favretto S, Zanini F (2009b) The role of syn-  
2240 eruptive vesiculation on explosive basaltic activity at Mt. Etna, Italy. *J Volcanol Geotherm*  
2241 *Res* 179:265–269

2242  
2243 Polacci M, Mancini L, Baker DR (2010) The contribution of synchrotron X-ray computed  
2244 microtomography to understanding volcanic processes. *J Synchrotron Radiation* 17:215–221  
2245  
2246 Polacci M, Baker DR, La Rue A, Mancini L (2012) Degassing behaviour of vesiculated  
2247 basaltic magmas: an example from Ambrym volcano, Vanuatu Arc, and comparison to  
2248 Stromboli, Aeolian Islands, Italy. *J Volcanol Geotherm Res* 233-234:55-64. doi:  
2249 10.1016/j.jvolgeores.2012.04.019  
2250  
2251 Polacci M, Bouvet de Maisonneuve C, Giordano D, Piochi M, Mancini L, Degruyter W,  
2252 Bachmann O (2014) Permeability measurements of Campi Flegrei pyroclastic products: An  
2253 example from the Campanian Ignimbrite and Monte Nuovo eruptions. *J Volcanol Geotherm*  
2254 *Res* 272:16-22  
2255  
2256 Prata AJ (1989) Infrared radiative transfer calculations for volcanic ash clouds. *Geophys Res*  
2257 *Lett* 15(11):1293–1296  
2258  
2259 Prata AJ, Bernardo C (2009) Retrieval of volcanic ash particle size, mass and optical depth  
2260 from a ground-based thermal infrared camera. *J Volcanol Geotherm Res* 186:91–107  
2261  
2262 Prejean SG, Brodsky EE (2011) Volcanic plume height measured by seismic waves based on a  
2263 mechanical model. *J Geophys Res Solid Earth* 116(B1. doi:10.1029/2010JB007620  
2264  
2265 Prior DJ (1999) Problems in determining the orientations of crystal misorientation axes, for  
2266 small angular misorientations, using electron backscatter diffraction in the SEM. *J Microsc*  
2267 *195:217–225*  
2268  
2269 Prior DJ, Boyle AP, Brenker F, Cheadle MC, Day A, Lopez G, Peruzzo L, Potts GJ, Reddy S,  
2270 Spiess R, Timms NE, Trimby P, Wheeler J, Zetterström L (1999) The application of electron  
2271 backscatter diffraction and orientation contrast imaging in the SEM to textural problems in  
2272 rocks. *Am Mineral* 84:1741–1759  
2273

2274 Prodi F, Caracciolo D, Adderio LP, Gnuffi M, Lanzinger E (2011) Comparative investigation  
2275 of Pludix disdrometer capability as Present Weather Sensor (PWS) during the Wasserkuppe  
2276 campaign. *Atmos Res* 99(1):162–173  
2277

2278 Proussevitch AA, Sahagian DL, Tsentalovich EP (2007a) Statistical analysis of bubble and  
2279 crystal size distributions: formulations and procedures. *J Volcanol Geotherm Res* 164:95–111  
2280

2281 Proussevitch AA, Sahagian DL, Carlson W (2007b) Statistical analysis of bubble and crystal  
2282 size distributions: application to Colorado Plateau basalts. *J Volcanol Geotherm Res* 164:112–  
2283 126  
2284

2285 Proussevitch AA, Mulukutla GK, Sahagian DL (2011) A new 3D method of measuring bubble  
2286 size distributions from vesicle fragments preserved on surfaces of volcanic ash particles.  
2287 *Geosphere* 7:1–8  
2288

2289 Pyle M (1989) The thickness, volume and grainsize of tephra fall deposits. *Bull Volcanol*  
2290 51:1–15  
2291

2292 Pyle DM, Mather TA (2009) Halogens in igneous processes and their fluxes to the atmosphere  
2293 and oceans from volcanic activity: A review: *Chem Geol* 263(1-4):110–121. doi:  
2294 10.1016/j.chemgeo.2008.11.013  
2295

2296 Riley CM, Rose WI, Bluth GJS (2003) Quantitative shape measurements of distal volcanic  
2297 ash. *J Geophys Res* 108:B10. doi: 10.1029/2001JB000818  
2298

2299 Ripepe M, Braun T (1994) Air-wave phases in strombolian explosion-quake seismograms: a  
2300 possible indicator for the magma level? *Acta Vulcanol* 5:201–206  
2301

2302 Ripepe M, Marchetti E (2002) Array tracking of infrasonic sources at Stromboli volcano.  
2303 *Geophys Res Lett* 29 (22):2076  
2304

2305 Ripepe M, Ciliberto S, Della Schiava M (2001) Time constraints for modeling source  
2306 dynamics of volcanic explosions at Stromboli. *J Geophys Res* 106(B5):8713–8727  
2307

2308 Ripepe M, Harris AJL, Carniel R (2002). Thermal, seismic and infrasonic evidences of  
2309 variable degassing rates at Stromboli volcano. *J Volcanol Geotherm Res* 118:285–297  
2310

2311 Ripepe M, Poggi P, Braun T, Gordeev E (1996) Infrasonic waves and volcanic tremor at  
2312 Stromboli. *Geophys Res Lett* 23:181–184  
2313

2314 Ripepe M, Rossi M, Saccorotti G (1993) Image processing of explosive activity at Stromboli.  
2315 *J Volcanol Geotherm Res* 54:335–351  
2316

2317 Rix M, Valks P, Hao N, Loyola D, Schlager H, Huntrieser H, Flemming J, Koehler U,  
2318 Schumann U, Inness A (2012) Volcanic SO<sub>2</sub>, BrO and plume height estimations using  
2319 GOME-2 satellite measurements during the eruption of Eyjafjallajökull in May 2010. *J*  
2320 *Geophys Res* 117:D00U19. doi:10.1029/2011JD016718  
2321

2322 Robock A, Matson M (1982) Circumglobal transport of the El Chichon volcanic dust cloud.  
2323 *Science* 221:195-197  
2324

2325 Roggensack K, hervig RL, McKnight SB, Williams SN (1997) Explosive basaltic volcanism  
2326 from Cerro Negro volcano: influence of volatiles on eruptive style. *Science* 277:1639-1642  
2327

2328 Rose WI, Self S, Murrow PJ, Bonadonna C, Durant AJ, Ernst GGJ (2008) Nature and  
2329 significance of small volume fall deposits at composite volcanoes: Insights from the October  
2330 14, 1974 Fuego eruption, Guatemala. *Bull Volcanol* 70(9):1043–1067  
2331

2332 Rose-Koga EF, Koga K, Schiano P, Le Voyer M (2012) Mantle source heterogeneity for South  
2333 Tyrrhenian magmas revealed by Pb isotopes and halogen contents of olivine-hosted melt  
2334 inclusions. *Chem Geol* 334:266-279  
2335

2336 Rosseel JB, White JDL, Houghton BF (2006) Complex bombs of phreatomagmatic eruptions:  
2337 role of agglomeration and welding in vents of the 1886 Rotomahana eruption, Tarawera, New  
2338 Zealand. *J Geophys Res* 111:B12205. doi:10.1029/2005JB004073  
2339

2340 Rosi M, Bertagnini A, Harris AJL, Pioli L, Pistoiesi M, Ripepe M (2006) A case history of  
2341 paroxysmal explosion at Stromboli: Timing and dynamics of the April 5, 2003 event. *Earth*  
2342 *Planet Sci Lett* 243:594–606  
2343  
2344 Rotella MD, Wilson CJN, Barker SJ, Wright IC (2013) Novel origins of highly vesicular  
2345 pumice in a distinctive non-explosive submarine eruptive style. *Nature Geosci* 6:129–132  
2346  
2347 Rotella MD, Wilson CJN, Barker SJ, Cashman KV, Houghton BF, Wright IC (2013) Bubble  
2348 development in explosive silicic eruptions: insights from pyroclast vesicularity textures from  
2349 Raoul volcano (Kermadec arc). *Bull Volcanol* 76:826  
2350  
2351 Rust AC, Cashman KV (2004) Permeability of vesicular silicic magma: inertial and hysteresis  
2352 effects. *Earth Planet Sci Lett* 228:93–107, [http://dx.doi.org/ 10.1016/j.epsl.2004.09.025](http://dx.doi.org/10.1016/j.epsl.2004.09.025)  
2353  
2354 Rust AC, Cashman KV (2007) Multiple origins of pyroclastic obsidian and implications for  
2355 changes in the dynamics of the 1300 BP eruption of Newberry Volcano, OR. *Bull Volcanol*  
2356 69:825-845  
2357  
2358 Rust AC, Cashman KV (2011) Permeability controls on expansion and size distributions of  
2359 pyroclasts. *J Geophys Res* 116:B11202  
2360  
2361 Rust AC, Manga M, Cashman KV (2003) Determining flow type, shear rate and shear stress  
2362 in magmas from bubble shapes and orientations. *J Volcanol Geotherm Res* 122:111–132  
2363  
2364 Ruth D, Calder E (2014) Plate tephra: Preserved bubble walls from large slug bursts during  
2365 violent Strombolian eruptions. *Geology* 42(1):11–14, doi:10.1130/G34859.1  
2366  
2367 Rutherford MJ, Hill PM (1993) Magma ascent rates from amphibole breakdown: an  
2368 experimental study applied to the 1980–1986 Mount St. Helens eruptions. *J Geophys Res*  
2369 98:19667–19685  
2370  
2371 Rutherford MJ, Devine JD (2003) Magmatic conditions and magma ascent as indicated by  
2372 hornblende phase equilibria and reactions in the 1995-2002 Soufrière Hills magma. *J Petrol*  
2373 44:1433-1454



2374  
2375 Rutherford MJ, Sigurdsson H, Carey S, Davis A (1985) The May 18, 1980 eruption of Mount  
2376 St. Helens, 1. Melt compositions and experimental phase equilibria. *J Geophys Res* 90:2929-  
2377 2947  
2378  
2379 Saar MO, Manga M (1999) Permeability-porosity relationship in vesicular basalts. *Geophys*  
2380 *Res Lett* 26(1):111–114  
2381  
2382 Sable JE, Houghton BF, Del Carlo P, Coltelli M (2006) Changing conditions of magma ascent  
2383 and fragmentation during the Etna 122 BC basaltic Plinian eruption: evidence from clast  
2384 microtextures. *J Volcanol Geotherm Res* 158:333–354  
2385  
2386 Sable JE, Houghton BF, Wilson CJN, Carey RJ (2009) Eruption mechanisms during the  
2387 climax of the Tarawera 1886 basaltic Plinian eruption inferred from microtextural  
2388 characteristics of the deposits, in *Studies in Volcanology: The Legacy of George Walker*,  
2389 *Spec. Publ. IAVCEI*, vol. 2, pp. 129–154, Geol. Soc., London  
2390  
2391 Sahagian DL, Proussevitch AA (1998) 3D particle size distributions from 2D observations:  
2392 stereology for natural applications. *J Volcanol Geotherm Res* 84:173–196  
2393  
2394 Sahetapy-Engel ST, Harris AJL. (2009) Thermal-image-derived dynamics of vertical ash  
2395 plumes at Santiaguito volcano, Guatemala. *Bull Volcanol* 71:827-830. doi:10.1007/s00445-  
2396 009-0284-8  
2397  
2398 Salisbury MJ, Bohrson WA, Clynne MA, Ramos FC, Hoskin P (2008) Multiple plagioclase  
2399 crystal populations identified by crystal size distribution and in situ chemical data:  
2400 implications for timescales of magma chamber processes associated with the 1915 eruption of  
2401 Lassen Peak, CA. *J Petrol* 49:1755–1780  
2402  
2403 Saunders K, Blundy J, Dohmen R, Cashman (2012) Linking petrology and seismology at an  
2404 active volcano. *Science* 336(6084):1023-1027. doi:10.1126/science.1220066  
2405

2406 Scaillet B, Evans BW (1999) The 15 June 1991 eruption of Mount Pinatubo. I. Phase  
2407 equilibria and pre-eruption  $P$ - $T$ - $fO_2$ - $fH_2O$  conditions of the dacite magma. *J Petrol* 40(3):381-  
2408 411  
2409  
2410 Schiavi F, Kobayashi K, Moriguti T, et al. (2010) Degassing, crystallization and eruption  
2411 dynamics at Stromboli: trace element and lithium isotopic evidence from 2003 ashes. *Contrib*  
2412 *Mineral Petr* 159:541–561  
2413  
2414 Schiavi F, Kobayashi K, Nakamura E, et al. (2012) Trace element and Pb–B–Li isotope  
2415 systematics of olivine-hosted melt inclusions: insights into source metasomatism beneath  
2416 Stromboli (southern Italy). *Contrib Mineral Petrol* 163:1011-1031  
2417  
2418 Schipper CI, White JDL, Houghton BF (2010a) Syn- and post-fragmentation textures in  
2419 submarine pyroclasts from Loihi Seamount, Hawaii. *J Volcanol Geotherm Res* 191:93–106.  
2420 doi:10.1016/j.jvolgeores.2010.01.002  
2421  
2422 Schipper CI, White JDL, Houghton BF, Shimizu N, Stewart RB (2010b) Explosive submarine  
2423 eruptions driven by volatile-coupled degassing at Lo`ihi Seamount, Hawai`i. *Earth Planet Sci*  
2424 *Lett* 295(3-4):497-510  
2425  
2426 Schipper CI, White JDL, Houghton BF, Shimizu N, Stewart RB (2010c) "Poseidic" explosive  
2427 eruptions at Loihi Seamount, Hawaii. *Geology* 38(4):291-294  
2428  
2429 Schipper CI, White JDL, Houghton BF (2011) Textural, geochemical, and volatile evidence  
2430 for a Strombolian-like eruption sequence at Lo`ihi Seamount, Hawai`i. *J Volcanol Geotherm*  
2431 *Res* 207:16–32  
2432  
2433 Schipper CI, White JDL, Nichols ARL, Burgisser A, Hellebrand E, Murtagh RM (2012)  
2434 Incipient melt segregation as preserved in subaqueous pyroclasts. *Geology* 40(4):355-358  
2435  
2436 Schipper CI, Castro JM, Tuffen H, James MR, How P (2013) Shallow vent architecture during  
2437 hybrid explosive-effusive activity at Cordón Caulle (Chile, 2011-12): evidence from direct  
2438 observations and pyroclast textures. *J Volcanol Geotherm Res* 262:25–37  
2439

2440 Sciotto M, Cannata A, Di Grazia G, Gresta S, Privitera E, Spina L (2011) Seismoacoustic  
2441 investigations of paroxysmal activity at Mt. Etna volcano: New insights into the 16 November  
2442 2006 eruption. *J Geophys Res* 116. doi: 10.1029/2010JB008138  
2443  
2444 Shea T, Larsen JF, Gurioli L, Hammer JE, Houghton BF, Cioni R (2009) Leucite crystals:  
2445 surviving witnesses of magmatic processes preceding the 79 AD eruption at Vesuvius, Italy.  
2446 *Earth Planet Sci Lett* 281:88–98  
2447  
2448 Shea T, Houghton BF, Gurioli L, Cashman KV, Hammer JE, Hobden B (2010a) Textural  
2449 studies of vesicles in volcanic rocks: an integrated methodology. *J Volcanol Geotherm Res*  
2450 190:271–289  
2451  
2452 Shea T, Gurioli L, Larsen JF, Houghton BF, Hammer JE, Cashman KV (2010b) Linking  
2453 experimental and natural vesicle textures in Vesuvius 79 AD white pumice. *J Volcanol*  
2454 *Geotherm Res* 192:69–84  
2455  
2456 Shea T, Gurioli L, Houghton BF, Cashman KV, Cioni R (2011) Column collapse and  
2457 generation of pyroclastic density currents during the A.D. 79 eruption of Vesuvius: the role of  
2458 pyroclast density. *Geology* 39:695–698  
2459  
2460 Shea T, Gurioli L, Houghton BF (2012) Transitions between fall phases and pyroclastic  
2461 density currents during the AD 79 eruption at Vesuvius: building a transient conduit model  
2462 from the textural and volatile record. *Bull Volcanol* 74:2363–2381. doi 10.1007/s00445-012-  
2463 0668-z  
2464  
2465 Shea T, Hellebrand E, Gurioli L, Hugh T (2014) Conduit- to localized-scale degassing during  
2466 Plinian eruptions: Insights from major element and volatile (Cl and H<sub>2</sub>O) analysis within  
2467 Vesuvius AD79 pumice. *J Petrol.* doi:10.1093/petrology/egt069  
2468  
2469 Sheridan MF, Marshall JR (1983) Interpretation of pyroclast surface features using SEM  
2470 images. *J Volcanol Geotherm Res* 16:153–159  
2471  
2472 Sheridan MF, Marshall JR (1987) Comparative charts for quantitative analysis of grain-  
2473 textural elements on pyroclasts, in *Clastic Particles: Scanning Electron Microscopy And*

2474 Shape Analysis Of Sedimentary And Volcanic Particles, edited by J. R. Marshall, Van  
2475 Nostrand Reinhold Company, New York  
2476

2477 Shimano T, Nakada S (2006) Vesiculation path of ascending magma in the 1983 and the 2000  
2478 eruptions of Miyakejima volcano, Japan. Bull Volcanol 68:549–566. doi: 10.1007/s00445-  
2479 005-0029-2  
2480

2481 Shimano T, Nishimura T, Chiga N, Shibasaki Y, Iguchi M, Miki D and Yokoo A (2013)  
2482 Development of an automatic volcanic ash sampling apparatus for active volcanoes. Bull  
2483 Volcanol 75:73. doi: 10.1007/s00445-013-0773-7  
2484

2485 Shin H, Lindquist WB, Sahagian DL, Song S-R (2005) Analysis of the vesicular structure of  
2486 basalts. Comput Geosci 31(4):473–487. doi:10.1016/j.cageo.2004.10.013  
2487

2488 Simakin AG, Bindeman IN (2008). Evolution of crystal sizes in the series of dissolution and  
2489 precipitation events in open magma systems. J Volcanol Geotherm Res 17:997-1010  
2490

2491 Simkin T, Howard KA (1970) Caldera Collapse in the Galápagos Islands, 1968 The largest  
2492 known collapse since 1912 followed a flank eruption and explosive volcanism within the  
2493 caldera. Science 169(3944):429-437  
2494

2495 Sonder I, Graettinger A, Valentine G (2013) Large-scale blast experiments examine  
2496 subsurface explosions. EOS Trans AGU 94(39):337–338. doi:10.1002/2013EO390002  
2497

2498 Song SR, Jones KW, Lindquist WB, Dowd BA, Sahagian DL (2001) Synchrotron X-ray  
2499 computed microtomography: studies on vesiculated basaltic rocks. Bull Volcanol 63(4):252–  
2500 263. doi:10.1007/s004450100141  
2501

2502 Sottili G, Taddeucci J, Palladino DM, Gaeta M, Scarlato P, Ventura G (2009) Subsurface  
2503 dynamics and eruptive styles of maars in the Colli Albani Volcanic District, Central Italy. J  
2504 Volcanol Geotherm Res 180:189-202  
2505

2506 Sottili G, Taddeucci J, Palladino DM (2010) Constraints on magma–wall rock thermal  
2507 interaction during explosive eruptions from textural analysis of cored bombs. *J Volcanol*  
2508 *Geotherm Res* 192:27-34  
2509

2510 Sparks RSJ (1978) The dynamics of bubble formation and growth in magmas. *J Volcanol*  
2511 *Geotherm Res* 3:1–37. doi:10.1016/0377-0273(78)90002-1  
2512

2513 Sparks RSJ, Brazier S (1982) New evidence for degassing processes during explosive  
2514 eruptions. *Nature* 295:218–220  
2515

2516 Sparks RSJ, Burski MI, Carey SN, Gilbert JS, Glaze LS, Sigurdsson H, Woods AW (1997)  
2517 *Volcanic Plume*. John Wiley & Sons, New York  
2518

2519 Spillar V, Dolejs D (2013) Calculation of time-dependent nucleation and growth rates from  
2520 quantitative textural data: inversion of crystal size distribution. *J Petrol.*  
2521 doi:10.1093/petrology/egs091  
2522

2523 Stovall WK, Houghton BF, Gonnermann HM, Fagents S.A, Swanson DA (2011) Eruption  
2524 dynamics of Hawaiian-style fountains: The case study of episode 1 of the Kīlauea Iki 1959  
2525 eruption. *Bull Volcanol* 73:511–529. doi:10.1007/s00445-010-0426-z  
2526

2527 Stovall WK, Houghton BF, Hammer JE, Fagents SA, Swanson DA (2012) Vesiculation of  
2528 high fountaining Hawaiian eruptions: Episodes 15 and 16 of 1959 Kīlauea Iki. *Bull Volcanol*  
2529 74:441–455. doi:10.1007/s00445-011-0531-7  
2530

2531 Streck MJ (2008) Mineral textures and zoning as evidence for open system processes. In  
2532 Putirka KD, Tepley FJ (Eds) *Minerals, inclusions and volcanic processes*. *Rev Mineral*  
2533 *Geochem* 69:595-622  
2534

2535 Suzuki Y, Nakada S (2001) Timing of vesiculation and crystallization during magma ascent -  
2536 Example of the phreatomagmatic phase in Usu 2000 eruption. *Bull Earthq Res Inst* 76:253-  
2537 268  
2538

2539 Suzuki Y, Nakada S (2002) Vesiculation and magma ascent process in the Usu 2000 eruption,  
2540 inferred from texture and size distribution of bubbles. *Bull Volcanol Soc Japan* 47:675-688  
2541

2542 Swanson DA, Wooten K, Orr T (2009) Buckets of ash track tephra flux from Halema'uma'u  
2543 crater, Hawaii. *Eos Trans AGU* 90:427–428. doi:10.1029/2009EO460003  
2544

2545 Szramek L, Gardner JE, Larsen J. (2006) Degassing and microlite crystallization of basaltic  
2546 andesite magma erupting at Arenal Volcano, Costa Rica. *J Volcanol Geotherm Res* 157:182-  
2547 201  
2548

2549 Taddeucci J, Pompilio M, Scarlato P (2002) Monitoring the explosive activity of the July–  
2550 August 2001 eruption of Mt. Etna (Italy) by ash characterization. *Geophys Res Lett*  
2551 29(8):1029–1032. doi:10.1029/2001GL014372  
2552

2553 Taddeucci J, Pompilio M, Scarlato P (2004) Conduit processes during the July–August 2001  
2554 explosive activity of Mt. Etna (Italy): inferences from glass chemistry and crystal size  
2555 distribution of ash particles. *J Volcanol Geotherm Res* 137:33–54  
2556

2557 Taddeucci J, Scarlato P, Capponi A, Del Bello E, Cimarelli C, Palladino D, Kueppers U  
2558 (2012) High-speed imaging of Strombolian explosions: The ejection velocity of pyroclasts.  
2559 *Geophys Res Lett* 39(2)  
2560

2561 Takeuchi S, Nakashima S (2005) A new simple gas permeameter for permeability  
2562 measurement of small samples of volcanic eruptive material and experimental run products  
2563 (in Japanese with English abstract). *Bull Volcanol Soc Jpn* 50:1–8  
2564

2565 Takeuchi S, Nakashima S, Akihiko Tomiya A (2008) Permeability measurements of natural  
2566 and experimental volcanic materials with a simple permeameter: toward an understanding of  
2567 magmatic degassing processes. *J Volcanol Geotherm Res* 177:329–339.  
2568 <http://dx.doi.org/10.1016/j.jvolgeores.2008.05.010>.  
2569

2570 Tarquini S, Favalli M (2010) A microscopic information system (MIS) for petrographic  
2571 analysis. *Comput Geosci* 36:665–674  
2572

2573 Thomas N, Jaupart C, Vergnolle S (1994) On the vesicularity of pumice. *J Geophys Res*  
2574 99:15633–15644  
2575

2576 Thomas HE, Watson IM, Carn SA, Alfredo AJ, Prata F, Realmuto VJ (2011) A comparison of  
2577 AIRS, MODIS and OMI sulphur dioxide retrievals in volcanic clouds. *Geomatics, Nat*  
2578 *Hazards Risk* 2(3):217-232  
2579

2580 Thordarson T, Self S, Larsen G, Rowland SK, Hoskuldsson A (2009) *Studies in Volcanology:*  
2581 *the Legacy of George Walker*. *GSL Special Publication*  
2582

2583 Toramaru A (1989) Vesiculation process and bubble size distribution in ascending magmas  
2584 with constant velocities. *J Geophys Res* 94(1):523–17,542. doi:10.1029/JB094iB12p17523  
2585

2586 Toramaru A (1990) Measurement of bubble size distributions in vesiculated rocks with  
2587 implications for quantitative estimates of eruption processes. *J Volcanol Geotherm Res* 43:71–  
2588 90  
2589

2590 Toramaru A (2006) BND (bubble number density) decompression rate meter for explosive  
2591 volcanic eruptions *J Volcanol Geotherm Res* 154:303-316  
2592

2593 Toramaru A, Noguchi S, Oyoshihara S, Tsune A (2008) MND (microlite number density)  
2594 water exsolution rate meter. *J Volcanol Geotherm Res* 175(1–2):156–167  
2595

2596 Tsukui M, Suzuki Y (1995) Vesiculation of basaltic magma: magmatic versus  
2597 phreatomagmatic eruption in 1983 eruption of Miyakejima. *Bull Volcanol Soc Jpn* 40, 395–  
2598 399  
2599

2600 Valade S, Donnadieu F (2011) Ballistics and ash plumes discriminated by Doppler radar.  
2601 *Geophys Res Lett* 38:L22301. doi:10.1029/2011GL049415  
2602

2603 Valade SA, Harris AJL, Cerminara M (2014) Plume Ascent Tracker: Interactive Matlab  
2604 software for analysis of ascending plumes in image data. *Comput Geosci* 66:132–144. doi:  
2605 10.1016/j.cageo.2013.12.015  
2606

2607 Villemant B, Boudon G (1998) Transition between dome-forming and plinian eruptive styles:  
2608 H<sub>2</sub>O and CL degassing behaviour. *Nature* 392:65-69  
2609

2610 Vinkler AP, Cashman K, Giordano G, Gropelli G (2012) Evolution of the mafic Villa Senni  
2611 caldera-forming eruption at Colli Albani volcano, Italy, indicated by textural analysis of  
2612 juvenile fragments. *J Volcanol Geotherm Res* 235-236:37–54  
2613

2614 Vlastélic I, Staudacher T, Bachèlery P, Télouk P, Neuville D, Benbakkar M (2011) lithium  
2615 isotope fractionation during magma degassing: constraints from silicic differentiates and  
2616 natural gas condensates from Piton de la Fournaise volcano (Réunion Island). *Chem Geol*  
2617 284:26-34  
2618

2619 Voltolini M, Zandomeneghi D, Mancini L, Polacci M (2011) Texture analysis of volcanic rock  
2620 samples: Quantitative study of crystals and vesicles shape preferred orientation from X-ray  
2621 microtomography data. *J Volcanol Geot Res* 202:83–95  
2622

2623 Vöge M, Hort M, Seyfried R (2005) Monitoring volcano eruptions and lava domes with  
2624 Doppler radar. *EOS Trans AGU* 86:537-541  
2625

2626 Walker JC, Carboni E, Dudhia A, Grainger RG (2012) Improved detection of sulphur dioxide  
2627 in volcanic plumes using satellite-based hyperspectral infrared measurements: Application to  
2628 the Eyjafjallajökull 2010 eruption. *J Geophys Res* 117:D00U16. doi:10.1029/2011JD016810  
2629

2630 Wallace PJ (2001) Volcanic SO<sub>2</sub> emissions and the abundance and distribution of exsolved gas  
2631 in magma bodies. *J Volcanol Geotherm Res* 108:85-106  
2632

2633 Wallace PJ (2005) Volatiles in subduction zone magmas: concentrations and fluxes based on  
2634 melt inclusion and volcanic gas data. *J Volcanol Geotherm Res* 140:217-240  
2635

2636 Watson IM, Realmuto VJ, Rose WI, Prata AJ, Bluth GJS, Gu Y, Bader CE, Yu T (2004)  
2637 Thermal infrared remote sensing of volcanic emissions using the moderate resolution imaging  
2638 spectroradiometer. *J Volcanol Geotherm Res* 135:75–89  
2639



2640 Wen S, Rose WI (1994) Retrieval of sizes and total masses of particles in volcanic clouds  
2641 using AVHRR bands 4 and 5. *J Geophys Res: Atmospheres* 99(D3):5421–5431  
2642

2643 White JDL, Houghton BF (2006) Primary volcanoclastic rocks. *Geology* 34:677-680.  
2644 doi:10.1130/G22346.1  
2645

2646 Whitham AG, Sparks RSJ (1986) Pumice. *Bull Volcanol* 48:209–223  
2647

2648 Wilhelm S, Worner, G (1996) Crystal size distribution in Jurassic Ferrar flows and sills  
2649 (Victoria Land, Antarctica): Evidence for processes of cooling, nucleation, and crystallisation.  
2650 *Contrib Mineral Petr* 125:1-15  
2651

2652 Williams-Jones G, Stix J, Hickson C (2008) The COSPEC cookbook. IAVCEI: Methods in  
2653 Volcanology I: 233 p.  
2654

2655 Wilson L, Huang TC (1979) The influence of shape on the atmospheric settling velocity of  
2656 volcanic ash particles. *Earth Planet Sci Lett* 44:311–324  
2657

2658 Wilson L, Self S (1980) Volcanic explosion clouds: density, temperature and particle content  
2659 estimates from cloud motion. *J Geophys Res* 85:2567-2572  
2660

2661 Wright HMN, Weinberg R (2009) Strain localization in vesicular magma: Implications for  
2662 rheology and fragmentation. *Geology* 37:1023–1026. doi:10.1130/G30199A.1  
2663

2664 Wright HMN, Cashman KV (2014) Compaction and gas loss in welded pyroclastic deposits  
2665 as revealed by porosity, permeability, and electrical conductivity measurements of the Shevlin  
2666 Park Tuff. *GSA Bulletin* 126(1/2):234–247. doi: 10.1130/B30668.1  
2667

2668 Wright HMN, Roberts JJ, Cashman KV (2006) Permeability of anisotropic tube pumice:  
2669 model calculations and measurements. *Geophys Res Lett* 33:L17316.  
2670 doi.org/10.1016/j.epsl.2009.01.023  
2671

2672 Wright HMN, Cashman KV, Rosi M, Cioni R (2007) Breadcrust bombs as indicators of  
2673 Vulcanian eruption dynamics at Guagua Pichincha volcano. Ecuador. *Bull Volcanol* 69: 281–  
2674 300  
2675  
2676 Wright HMN, Cashman KV, Gottesfeld EH, Roberts JJ (2009) Pore structure of volcanic  
2677 clasts: Measurements of permeability and electrical conductivity. *Earth Planet Sci Lett*  
2678 280:93–104. doi.org/10.1016/j.epsl.2009.01.023  
2679  
2680 Wright HMN, Folkes CB, Cas RAF, Cashman KV (2011) Heterogeneous pumice populations  
2681 in the 2.08-Ma Cerro Galán Ignimbrite: implications for magma recharge and ascent  
2682 preceding a large-volume silicic eruption. *Bull Volcanol* 73:1513–1533  
2683  
2684 Wright HMN, Cashman KV, Mothes PA, Hall ML, Ruiz AG, Le Pennec J-L (2012) Estimating  
2685 rates of decompression from textures of erupted ash particles produced by 1999-2006  
2686 eruptions of Tungurahua Volcano, Ecuador. *Geology* 40:619-622. doi:10.1130/G32948  
2687  
2688 Wohletz K (1983) Mechanisms of hydrovolcanic pyroclast formation: grainsize, scanning  
2689 electron microscopy, and experimental studies. *J Volcanol Geother Res* 17:31–63  
2690  
2691 Wohletz K (1986) Explosive magma–water interactions: thermodynamics, explosion  
2692 mechanisms, and field studies. *Bull Volcanol* 48:245–264  
2693  
2694 Wohletz K (1987) Chemical and textural surface features of pyroclasts from hydrovolcanic  
2695 eruption sequences. In: Marsall, J.R. (Ed.), *Clastic Particles*. Van Nostrand Reinhold Co, New  
2696 York, N.Y., pp. 79–97  
2697  
2698 Yang K, Krotkov NA, Krueger AJ, Carn SA, Bhartia PK, Levelt PF (2007) Retrieval of large  
2699 volcanic SO<sub>2</sub> columns from the Aura Ozone Monitoring Instrument (OMI): comparison and  
2700 limitations. *J Geophys Res* 112:D24S43. doi:10.1029/2007JD008825  
2701  
2702 Yamada K, Emori H, Nakazawa K (2008) Time-evolution of bubble formation in a viscous  
2703 liquid. *Earth Planets Space* 60:1–19  
2704

2705 Yokoyama T, Takeuchi S (2009) Porosimetry of vesicular volcanic products by a water-  
2706 expulsion method and the relationship of pore characteristics to permeability. *J Geophys Res*  
2707 114:B02201. <http://dx.doi.org/10.1029/2008JB005758>.

2708

2709 Yoshimoto M, Shimano T, Nakada S, Koyama E, Tsuji H, Iida A, Kurokawa M, Okayama Y,  
2710 Nonaka M, Kaneko T, Hoshizumi H, Ishizuka Y, Furukawa R, Nogami K, Onizawa S, Niihori  
2711 K, Sugimoto T, Nagai M (2005) Mass estimation and characteristics of ejecta from the 2004  
2712 eruption of Asama volcano. *Bull Volcanol, Soc Jpn* 50:519–533 (In Japanese with English  
2713 abstract)

2714

2715 Zandomeneghi D, Voltolini M, Mancini L, F. Brun, D. Dreossi, M. Polacci (2010)  
2716 Quantitative analysis of X-ray microtomography images of geomaterials: Application to  
2717 volcanic rocks, *Geosphere*, special issue "Advances in 3D Imaging and Analysis of  
2718 Geomaterials" 6:793-804. doi:10.1130/GES00561.1.

2719

2720 Zakšek K, Hort M, Zaletelj J, Langmann B (2013) Monitoring volcanic ash cloud top height  
2721 through simultaneous retrieval of optical data from polar orbiting and geostationary satellites.  
2722 *Atmos Chem Phys* 13(5):2589-2606

2723

2724 Zimanowski B, Wohletz K, Dellino P, Buttner R (2003) The volcanic ash problem *J. Volcanol.*  
2725 *Geotherm. Res.* 122:1-5

2726

2727 Zobin VM, Santiago-Jiménez H, Ramírez-Ruiz JJ, Reyes-Dávila GA, Bretón-González M,  
2728 Navarro-Ochoa C (2007) Quantification of volcanic explosions from tilt records: Volcán de  
2729 Colima, México. *J Volcanol Geotherm Res* 166(2):117-124

2730

## 2731 **Figure captions**

2732

2733 **Figure 1** Diagrammatic illustration showing a volcanic strombolian conduit (modified from  
2734 Harris and Ripepe 2007), and the list of a few parameters that can be measured through the  
2735 deposit (D), the texture of the pyroclasts (T), the geochemistry (G) and the geophysics (G)  
2736 methods for small, magmatic explosions.

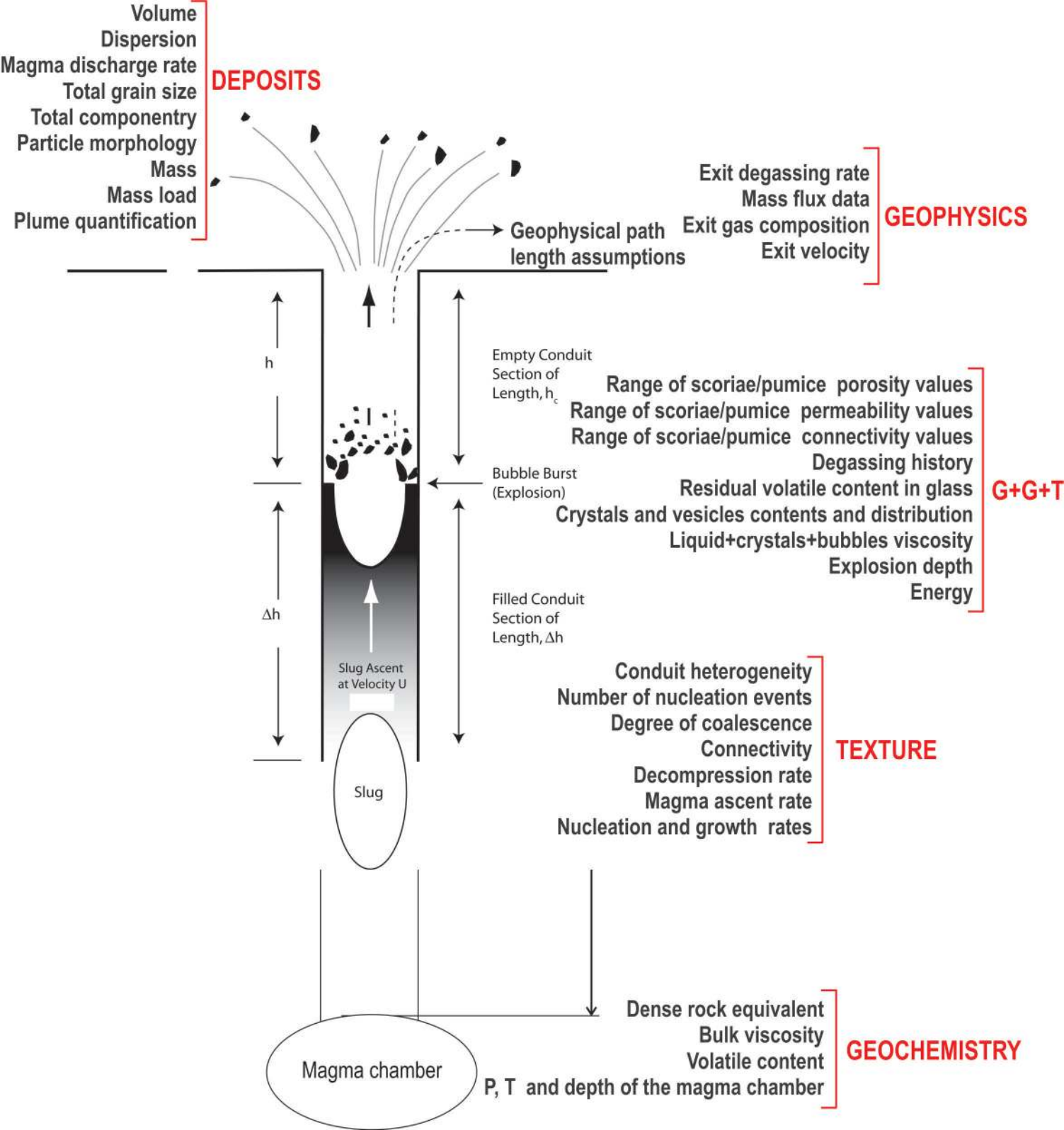


**Table 1** Quantification of explosive dynamics from textural parameters of the pyroclast components

<i>Textural parameters</i>	<i>Quantification</i>		<i>References</i>
Clast shape, morphology and size	Discriminate between different fragmentation mechanisms		Wohletz 1983; 1986; 1987; Heiken and Wohletz 1985; Sheridan and Marshall 1983; 1987; Dellino and La Volpe 1996a; b; Palladino and Taddeucci 1998; Büttner et al. 1999; 2002; Kueppers et al. 2006; Dellino et al. 2001; 2012; Zimanowski et al. 2003 Németh 2010 Pardo et al. 2014a
	Conduit stratigraphy and processes		Taddeucci et al. 2002; D’Oriano et al. 2005; Cioni et al. 2011; Perugini et al. 2011; Andronico et al. 2009b; 2013a; Lautze et al. 2012; 2013; Perugini et al. 2002;2007
	State of the magma at the fragmentation		Carey et al. 2000; Dellino and Liotino 2002; Maria and Carey 2002; 2007; D’Oriano et al. 2011; Ruth and Calder 2014
	Link between vesicularity and particle morphology, and particle morphology with cloud dispersal and sedimentation		Wilson and Huang 1979; Dellino et al. 2005; Mattsson 2010 Alfano et al. 2011; Mele et al. 2011
Clast density and vesicularity	Lateral variability of magma within the conduit		Houghton and Wilson 1989; Kennedy et al. 2005; Kueppers et al. 2005; Mueller et al. 2011; Barker et al. 2012
	Dense juvenile	Presence of outgassed magma	Sable et al. 2006; Lautze and Houghton 2005; 2007; 2008; Polacci et al. 2008; 2009a; b; 2012; Gurioli et al. 2005; 2014; Shea et al. 2011; 2012; 2014; Cimarelli et al. 2010
		Presence of a plug	Hoblitt and Harmon 1993; D’Oriano et al. 2005; Sable et al. 2009; Adams et al. 2006a; 2006b; Giachetti et al. 2010; Barker et al. 2012; Lavallée et al. 2012
Clast permeability and connectivity	Degassing history experienced by the magma		Eichelberger et al. 1986; Klug and Cashman 1996; Saar and Manga 1999; Jouniaux et al. 2000; Blower 2001a, b; Klug et al. 2002; Melnik and Sparks 2002; Rust and Cashman 2004; 2011; Mueller et al. 2005; 2008; Wright et al. 2006; 2007; 2009; Plats et al. 2007; Bernard et al. 2007; Takeuchi et al. 2008; Nakamura et al. 2008; Bouvet de Maisonneuve et al. 2009; Yokoyama and Takeuchi 2009; Bai et al. 2010; 2011; Degruyter et al. 2010a; 2010b; 2012

		Vinkler et al. 2012; Polacci et al. 2012; 2014; Nguyen et al. 2014; Pioli et al. 2008; Formenti and Druitt 2003; Giachetti et al. 2010; Shea et al. 2011; 2012
Clast conductivity	Input parameters for numerical percolation simulations	Le Pennec et al; 2001; Bernard et al. 2007; Wright et al. 2009; Wright et Cashman 2014
Vesicle shape and size	Bubble coalescence, ripening or collapse signatures	Klug and Cashman 1996; Mangan and Cashmann 1996; Gurioli et al. 2005; Shin et al. 2005; Sable et al. 2006; Polacci et al. 2008; Castro et al. 2012
	Shear conditions in the conduit Convection in the conduit	Marti et al. 1999; Polacci et al. 2001; 2003; Rust et al. 2003; Okumura et al. 2006; 2008; Bouvet de Maisonneuve et al. 2009; Wright and Weinberg 2009; Laumonier et al. 2011; Shea et al. 2011; 2012 Carey et al. 2013
	Eruptive style	Moitra et al. 2013
Vesicle size distributions (VSDs)	Vesicle nucleation processes and growth in magmas	Klug and Cashman 1994; Shea et al 2010a; LaRue et al. 2013, and references therein
	Total number of nucleation, coalescence or ripening events	Gaonac'h et al. 1996a; b Klug and Cashman 1996; Herd and Pinkerton 1997; Blower et al. 2001; 2002; Gaonac'h et al. 2003; 2005; Lovejoy et al. 2004, Yamada et al. 2008; Bai et al. 2008; Costantini et al. 2010
	Post-fragmentation evolution as indicator of : i) fountaining mechanisms ii) transportation and dispersal of the pyroclasts in submarine environment	Polacci et al; 2006a; Gurioli et al; 2008; Stovall et al. 2011; 2012; Schipper et al. 2010a, b, c; 2011; 2012; Rotella et al. 2013; 2014
Vesicle Number density (N <sub>v</sub> )	Link with magma mass eruption rate (MER), link with column height	Polacci et al. 2006b; Toramaru 2006; Gurioli et al. 2008; Carey et al. 2009; Houghton et al. 2010; Rust and Cashman 2011; Alfano et al. 2012
	Magma decompression rate	Mangan and Sisson 2000; Suzuki and Nakada 2001; 2002; Toramaru 2006; Cluzel et al. 2008; Shea et al. 2010b; 2011; 2012; Wright et al. 2012
	Phreatomagmatic fragmentation	Tsukui and Suzuki 1995; Suzuki, Nakada 2001, 2002; Shimano and Nakada 2006; Mattsson 2010; Murtagh et al. 2011; Murtagh and White 2013
	Link vesicularity with external trigger mechanisms (crystallinity, pressure changes)	Belien et al. 2010; Carey et al. 2012; Gurioli et al. 2014

Crystal size distribution (CSD)	Crystal size (mean, modal, and maximum crystal size), crystallization kinetics (nucleation and growth rates), annealing, crystal accumulation, and fractionation	Cashman and Marsh, 1988; Marsh 1988; 1998; 2007; Cashman 1993; Armienti et al. 1994; Higgins 2000; 2002a;b; 2006; 2011; Wilhelm and Wörner, 1996; Bindeman 2003; Gualda 2006; Gualda and Rivers 2006; Mock et al. 2003; Simakin and Bindeman, 2008; Spillar and Dolejs 2013
	Magma ascent rate	Cashman 1992; Rutherford and Hill 1993; Rutherford and Devine 2003; Noguchi et al. 2008; D’Oriano et al. 2011
	Pre-eruptive decompression paths	Hammer et al. 1999; Szramek et al. 2006; Clarke et al. 2007; Innocenti et al. 2013
	Magma storage conditions prior to eruption and residence times	Mangan 1990; O’Driscoll et al. 2007; Cigolini et al. 2008; Simakin and Bindeman 2008; Magee et al. 2010; Shea et al. 2009
	Water exsolution rate meter	Toramaru et al. 2008
	Magma mixing	Morgan et al. 2007; Jerram et al. 2003
Crystal+Vesicle size and percentage	Three phases magma rheology, fluid mechanical behavior of magma	Gurioli et al. 2014; Noguchi et al. 2006